

Biophysical characterization of the N-terminal region of Dengue virus NS4A protein

Inaugural-Dissertation

zur Erlangung des Doktorgrades
der Mathematisch-Naturwissenschaftlichen Fakultät
der Heinrich-Heine-Universität Düsseldorf

vorgelegt von

Yu-Fu Hung

aus Chiayi, Taiwan

Düsseldorf, September 2013

aus dem Institut für Physikalische Biologie
der Heinrich-Heine Universität Düsseldorf

Gedruckt mit der Genehmigung der
Mathematisch-Naturwissenschaftlichen Fakultät der
Heinrich-Heine-Universität Düsseldorf

Referent: Prof. Dr. Dieter Willbold
Korreferent: Priv.-Doz. Dr. Bernd König

Tag der mündlichen Prüfung: 15.10.2013

Content

Table of contents	I
List of figures	III
List of tables	IV
List of abbreviations	V
1 Introduction	1
1.1 Dengue virus	1
1.1.1 Dengue virus infection cycle	2
1.1.2 Virus genome and protein functions	2
1.1.3 Non-structural protein 4A of DENV	3
1.1.4 Viruses and cellular membranes	4
1.2 Biophysical analysis of membrane-associated proteins	6
1.2.1 Membrane proteins	6
1.2.2 Membrane mimetics for biophysical analysis	7
1.2.3 Solution NMR spectroscopy of membrane proteins	8
1.2.4 Protein-lipid interaction study by surface plasmon resonance	10
1.2.5 Circular dichroism (CD) spectroscopy	11
2 Aims	12
3 Scientific publications	13
3.1 An N-terminal amphipathic helix in dengue virus nonstructural protein 4A mediates oligomerization and is essential for replication	15
3.2 Recombinant production of the amino terminal cytoplasmic region of dengue virus non-structural protein 4A for structural studies	23
3.3 Dengue virus NS4A cytoplasmic domain binding to liposomes stabilizes membrane curvature	35
Summary	59
Zusammenfassung	60

A Appendix

A.1 Material	61
A.1.1 Chemicals, enzymes, detergents and lipids	61
A.1.2 Bacterial strains	62
A.1.3 Vectors	63
A.1.4 Primers	63
A.1.5 Kits	64
A.1.6 Gel electrophoresis markers	64
A.1.7 Laboratory equipment	65
A.1.8 Software and databases	65
A.2 Methods	67
A.2.1 Bacterial cultures	67
A.2.2 DNA preparation methods	68
A.2.2.1 Plasmid DNA isolation	68
A.2.2.2 Concentration determination of DNA samples	68
A.2.2.3 DNA agarose gel electrophoresis	68
A.2.2.4 Polymerase chain reaction (PCR)	69
A.2.2.5 Construction of pGEX-GB1-NS4A(1-48)/(1-48, L6E;M10E)	69
A.2.3 NS4A(1-48) fusion protein preparations	70
A.2.3.1 Expression and purification of GST-GB1-NS4A(1-48) fusion proteins.	70
A.2.3.2 Protein gel electrophoresis	71
A.2.3.3 Protein concentration determination	72
A.2.4 Liposome preparation	72
A.2.4.1 Preparation of extruded liposomes	73
A.2.4.2 Preparation of sonicated liposomes	73
A.2.5 SPR analysis of NS4A peptide binding to liposomes	73
A.2.5.1 Liposome immobilization on L1 chip	73
A.2.5.2 SPR experiments	74
A.2.6 Circular dichroism (CD) experiments	74
A.2.7 NMR spectroscopy experiments	75
A.2.7.1 Sample preparation of NS4A(1-48) proteins	75
A.2.7.2 NMR experiments	75
A.2.7.3 NMR resonance assignment	76
A.2.7.4 Secondary structure and backbone dynamics analysis	76
Bibliography	77
Acknowledgements	87

List of figures

Figure 1: Schematic representation of the open reading frame of DENV genome and the encoded proteins	3
Figure 2: Model of the membrane topology of Dengue virus NS4A	4
Figure 3: Schematic drawing an SPR method	11

List of tables

Table 1: Chemicals and enzymes	61
Table 2: Detergents	62
Table 3: Lipids	62
Table 4: Bacterial strains and genotype	62
Table 5: Vectors	63
Table 6: Primers used for cloning of NS4A(1-48) vectors	63
Table 7: Commercial kits	64
Table 8: Molecular weight markers used for this work	64
Table 9: Instruments, equipment and consumables	65
Table 10: Software used for NMR data analysis	66
Table 11: PCR reaction components in a 0.2 ml PCR tube	69
Table 12: PCR reaction condition	69
Table 13: NMR experiments performed on NS4A(1-48) and selected acquisition parameters	75
Table 14: NMR experiments performed on NS4A(1-48, L6E;M10E) and selected acquisition parameters	76

List of abbreviations

2D	Two-dimensional
3D	Three-dimensional
AH	Amphipathic α -helix
ANN	Artificial neural network
APS	Ammoniumperoxodisulfate
BSA	Bovine serum albumin
BVDV	Bovine viral diarrhea virus
CA	Cardiolipin
CD	Circular dichroism
CMC	Critical micelle concentration
CTAB	Cetyltrimethylammonium bromide
CV	Column volume
Da	Dalton (molecular mass unit for biopolymers)
DAGK	Diacylglycerol kinase
DDM	n-Dodecyl- β -D-Maltopyranoside
DENV	Dengue virus
DLS	Dynamic light scattering
DNA	Desoxyribonucleic acid
dNTP	Deoxynucleotide triphosphate
DOPS	1,2-dioleoyl- <i>sn</i> -glycero-3-phospho-L-serine
DPC	n-Dodecylphosphocholine
DSS	4,4-dimethyl-4-silapentane-1-sulfonic acid
DTT	Dithiothreitol
<i>E.coli</i>	<i>Escherichia coli</i>
EDTA	Ethylenediaminetetraacetic acid
E _F	FRET efficiency
ER	Endoplasmic reticulum
FRET	Fluorescence resonance energy transfer
g	Gravitational acceleration
GB1	Immunoglobulin-binding domain of streptococcal protein G
GSH	Glutathione
GST	Glutathione S-transferase
HCV	Hepatitis C virus
HSQC	Heteronuclear single quantum coherence
IFN	Interferon
IMP	Integral membrane protein
IPTG	Isopropyl-beta-D-thiogalactoside
LB	Lysogeny broth
LDAO	n-Dodecyl-N,N-Dimethylamine-N-Oxide
LTE	Liver Total Lipid Extract
M9	Minimal growth medium for bacterial cultures
MSP	Membrane scaffold protein
MWCO	Molecular weight cut off
Ni-NTA	Nickel nitrilotriacetic acid
NLPs	Nanolipoprotein particles

NMR	Nuclear magnetic resonance
NOE	Nuclear Overhauser effect
NS	Non-structural protein
OD600	Optical density at a wavelength of 600 nm
ORF	Open reading frame
PA	L- α -phosphatidic acid
PAGE	Polyacrylamide gel electrophoresis
PCR	Polymerase chain reaction
PFG	Pulsed field gradient
PI	L- α -phosphatidylinositol
POPC	1-palmitoyl-2-oleoyl-sn-glycero-3-phosphocholine
POPE	1-palmitoyl-2-oleoyl-sn-glycero-3-phosphoethanolamine
POPG	1-palmitoyl-2-oleoyl-sn-glycero-3-phosphatidylglycerol
ppm	Parts per million
PTFE	Polytetrafluorethylene
pTMDs	Predicted transmembrane domains
R _h	Hydrodynamic radius
RC	Replication complex
RCI	Random coil index
RDC	Residual dipolar coupling
rGPCRs	Rhodopsin-like G-protein-coupled receptors
RLU	Relative light units
RNA	ribonucleic acid
ROI	Region of interest
RU	Response units
SAP	Shrimp alkaline phosphatase
SDS	Sodium dodecyl sulfate
SDS-d25	Sodium dodecyl sulfate, perdeuterated
SEC	Size exclusion chromatography
SM	Sphingomyelin
SPR	Surface plasmon resonance
SS	Secondary structure
SUV	Small unilamellar vesicles
TALOS-N	Torsion angle likelihood obtained from NMR chemical shifts with artificial neural network
TEV	Tobacco etch virus
TMD	Transmembrane domain
Tris	Tris(hydroxymethyl)-aminomethane
TROSY	Transverse relaxation optimized spectroscopy
U	unit
[U- ¹⁵ N], [U- ¹³ C]	Uniform isotope labeling with ¹⁵ N and ¹³ C, respectively
UTR	Untranslated region
UV	Ultraviolet
v/v	Volume per volume
VDAC	Voltage-dependent anion channel
w/v	Weight per volume
WHO	World Health Organization
YFP	Yellow fluorescent protein

Chapter 1

Introduction

1.1. Dengue virus

Dengue virus (DENV) is the pathogen of dengue disease and is transmitted by mosquitoes of *Aedes* genus as vectors. The first severe cases of dengue disease were reported in the years 1953 to 1954 during dengue epidemics in Manila, Philippines, followed by Thailand in 1958, and Malaysia, Singapore and Vietnam in the 1960s [1]. According to the estimation of the publication “Dengue guidelines for diagnosis, treatment, prevention and control” (World Health Organization, 2009), the incidence of dengue has increased 30-fold over the last 50 years. Up to 50-100 million infections occur annually in over 100 endemic countries. However, a very recent study estimates that up to 390 million dengue infections occur worldwide per year, of which only 96 million are apparent [2]. DENV has spread mainly in tropical and subtropical regions, in particular in Southeast Asia, Africa and Latin America for several decades. There are 3.6 billion people, more than half the population of the world, living in areas at risk for DENV transmission [3]. Due to the international trade and the high temperature tolerance of *Aedes albopictus*, DENV has started to spread to Europe. Local transmission of dengue virus was reported for the first time in France and Croatia in 2010 [4]. Travel-associated dengue fever cases in Germany also increased significantly in 2010 [5].

DENV is an enveloped positive-strand RNA virus, which comprises four antigenically distinct DENV serotypes (DENV 1-4) and belongs to the *Flavivirus* genus of the *Flaviviridae* family. The flaviviruses cause various diseases, including Dengue fever, Yellow fever, Japanese encephalitis, Tick-borne encephalitis and West Nile fever [6]. The response of DENV-infected patients can be asymptomatic or symptomatic. Symptoms range from self-limited febrile illness, called dengue fever, to the severe and often fatal Dengue hemorrhagic fever and Dengue shock syndrome [7]. The risk factors for the latter two severe forms include viral strain virulence as well as host age, genetics and immune status [8]. The severe incidences predominantly occur in patients with secondary heterologous DENV infections [9] and the death rate is about 5% of the severe manifestations of the disease [10]. The absence of a suitable animal model presents a serious obstacle for the development of vaccines against DENV infection and for research studies on dengue disease pathogenesis [11].

1.1.1. Dengue virus infection cycle

DENV is transmitted between humans by a bite of a female infected mosquito. The virus particle is injected into the blood stream of the host together with saliva, which prevents the blood from clotting [12]. The majority of published studies support the view, that DENV enters host cells via receptor-mediated endocytosis. The viral envelope protein can bind to several candidate receptors and/or attachment factors on the target cell [13, 14] thereby triggering the clathrin-dependent endocytosis [15]. Similar internalization pathways are also known from other members of the flaviviridae family [6, 16, 17]. However, newer data indicate that the mode of infective entry into the host cell may depend on DENV serotype and/or host cell type. In particular, a non-classical, clathrin-independent endocytic pathway was observed for entry of DENV-2 into Vero cells [18]. After endocytotic virus internalization into the host cell, the viral particles traffic into the endosomal compartment. The acidic environment in the endosome induces a conformational change of the envelope protein and triggers the fusion of the viral and endosomal membranes [19, 20]. Then, the viral RNA genome is released into the cytoplasm. After initial translation of the viral replicase gene, the newly produced replicase protein, host factors and the [+] RNA-template assemble into the membrane-associated replication complex (RC), located at virus-induced vesicles attached to the endoplasmic reticulum (ER) membrane [21]. The virions then assemble at the ER membrane and bud out [22]. Virion maturation takes place during trafficking of the virions through the Golgi network [23] and includes glycosylation of the viral membrane proteins and proteolytic cleavage of the precursor of mature protein M by the cellular serine protease furin. Infectious, mature progeny virus particles are then released into the extracellular space [24].

1.1.2. Virus genome and protein functions

The DENV genome is a single positive-strand RNA of approximately 11 kb, and consists of a 5' untranslated region (UTR), a 3' UTR and a single open reading frame (ORF). The ORF is translated into a polyprotein, which is co- and post-translationally cleaved by cellular and viral proteases to produce three structural proteins (capsid protein C, membrane protein M and envelope protein E, the last two as precursors) and seven non-structural (NS) proteins (NS1, NS2A, NS2B, NS3, NS4A, NS4B and NS5) (Figure 1).

The structural proteins are components for the assembly of the mature virus. The three-dimensional structure of the viral envelope and capsid proteins as well as that of its RNA-dependent RNA polymerase catalytic domain have been solved by cryo-electron microscopy and X-ray diffraction [19, 25, 26]. Present results on the network of NS proteins have revealed that the interaction of NS1 and NS4A is required for replicase function [27]. NS2B is a cofactor for the NS2B-NS3 serine protease complex, which is involved in processing of the viral polyprotein [28]. NS3 also contains RNA helicase and nucleotide triphosphatase activity [29]. NS5 is a multifunctional protein with RNA-capping,

methyltransferase and RNA-dependent RNA polymerase activities [30, 31]. NS2A, NS4A and NS4B can block the interferon (IFN) signaling [32]. It was suggested, that NS4A plays a role in the rearrangement of host cell ER membranes leading to formation of viral RC [21]. The NS proteins associate with the RC membranes through membrane association determinants and protein-protein interactions among the NS proteins themselves or with yet unknown host factors [8]. It was shown, that the integral membrane protein (IMP) NS4A is part of the viral RC complex and colocalizes with other viral proteins and RNA [21]. A recent study revealed the complex architecture of virus-induced convoluted and vesicular membrane structures in DENV-infected cells, that are part of one ER-derived network and very likely contain the virus replication and assembly sites, i.e., the RC [22]. The authors further identified several DENV NS proteins, including NS4A, in those membrane structures [22].

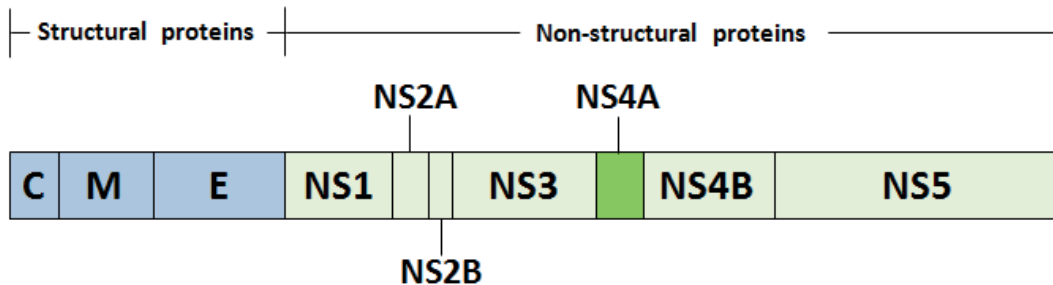


Figure 1. Schematic representation of the open reading frame of DENV genome and the encoded proteins.

1.1.3. Non-structural protein 4A of DENV

NS4A is an ER-localized, 16 kDa transmembrane protein component of the viral RC. While the exact function of NS4A is still unclear, it was shown to down-regulate interferon-stimulated gene expression allowing the virus to evade the host immune response [33, 34]. Recent research also indicates that NS4A induces autophagy in epithelial cells [35]. The localization of NS4A to the RC suggests that it has additional functions. Indeed, the results of studies on NS4A membrane topology and the observation of DENV-induced vesicles support the hypothesis that NS4A is involved in inducing host membrane alterations resembling the virus-induced membrane structures [21, 22]. As shown in figure 2, NS4A consists of a cytoplasm-exposed amino terminal region (amino acid residues 1-50) and three internal hydrophobic regions (amino acid residues 50-73, 76-99, and 101-122) which are predicted to form transmembrane domains (pTMDs) [21]. However, experimental results suggest that pTMD2 is deeply embedded in the ER-luminal lipid monolayer of the membrane and might not actually span it [21]. Perhaps, pTMD2 is involved in inducing membrane alterations that lead to formation of the RC by generating pressure on the ER membrane to bend toward the cytosol [21]. A very recent molecular dynamics simulation study shows that a U-shaped structure of NS4A,

consisting of two membrane spanning α -helices (pTMD1 and pTMD3) linked together by a membrane surface-attached helical domain (pTMD2), has a strong capacity to induce membrane curvature and thereby supports membrane undulation [36]. However, involvement of additional motifs of NS4A in this process cannot be excluded. Previous analysis of NS4A-specific antibodies of DENV infected patients revealed that all the identified epitopes map to the amino terminal region of NS4A. In combination with the topology prediction of NS4A shown in Figure 2 this indicates that the amino terminal region of NS4A is localized in the cytoplasm [37]. Recent results obtained with NS3 and NS4A domains of the related West Nile virus showed that the hydrophilic amino terminal region of NS4A, i.e., amino acids 1 to 50, is essential for the optimal performance of NS3 as a helicase [38]. In particular, the highly conserved acidic EELPD motif at the C-terminus of the hydrophilic N-terminal NS4A domain is required for regulating the ATPase activity within the helicase domain of NS3 [38]. However, the exact mechanism of how the amino terminal region of DENV NS4A is involved in DENV replication remains to be recovered. A more detailed understanding of the mechanisms that mediate the membrane rearrangement as well as a deeper knowledge of the viral and cellular factors involved in the viral replication cycle could provide crucial information for the development of new antiviral strategies.

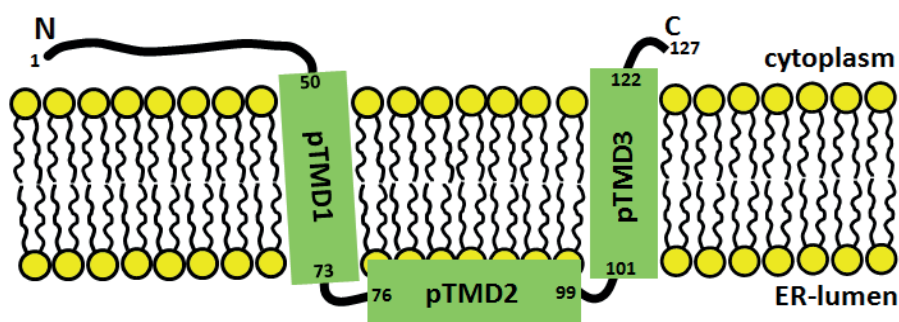


Figure 2. Model of the membrane topology of Dengue virus NS4A. Sequence position and location of the helices is based on [21].

1.1.4. Viruses and cellular membranes

Interactions of viral proteins with host cell membranes can be found during all stages of the viral life cycle starting with the internalization of the virus into the cell and ending with its budding from the host cell. Replication of the viral genome and production of infectious progeny is dependent on host cell resources. Plus-stranded RNA viruses, including members of Flaviviridae, Picornaviridae, Togaviridae, Coronaviridae, Arteriviridae families and many insect and plant viruses are well known to replicate in association with cytoplasmic membranes of the infected cells [6].

The virus-induced membrane structures may help the virus to evade certain host defense mechanisms and they may provide a scaffold for the viral RC. The concentration of the components necessary for viral replication could be reached in these local platforms [39, 40]. The observed membrane alterations could be induced by individual viral proteins, but additional cellular factors might also play a role in the formation of these platforms. The NS4B proteins of hepatitis C virus (HCV) and the NS4A of Dengue, Kunjin and West Nile viruses have been shown to be involved in the membrane rearrangements [21, 41, 42].

A number of mechanisms have been proposed that could induce the required change in membrane curvature [40]. Different cellular proteins may be involved in these processes: The lipid composition and asymmetry of the membrane could be modified by lipases or flippases. Curvature of the membrane may also change due to integration of transmembrane proteins with conical shape or membrane protein oligomerization on only one side of the membrane. Other options are scaffolding by peripheral proteins and preferential insertion of amphipathic helices (AHs) in one monolayer of the membrane. AHs are α -helical stretches of amino acids of proteins in which one face of the helix is hydrophobic while the opposite face is hydrophilic. In contrast to transmembrane domains (TMDs) that span the membrane bilayer, AHs have been proposed to serve as in-plane membrane anchors [43]. AHs are frequently unstructured until they insert into membranes, where the helices are predicted to sit flat on the membrane surface with the hydrophobic side chains extending into the hydrophobic core of the membrane [44]. Notably, AHs in proteins of several positive-strand RNA viruses were shown to be essential for their viral life cycle. Among these are the polio virus 2C protein [45], the Semliki forest virus nsP1 [46], and HCV NS4B [47] and NS5A [48]. In addition to serving as membrane anchors, AHs can induce membrane curvature and thus might participate in inducing the membrane alterations on which the viral RC resides [21]. If the AH is inserted into one leaflet of the membrane only, it can act like a wedge, displacing membrane lipid head groups and reorienting lipid acyl chains. Such a geometry should result in lipid bilayer curvature [49].

As already mentioned above, another mechanism contributing to membrane curvature is oligomerization of membrane associated proteins [50]. HCV NS4B was shown to form oligomers and interestingly, its second amino terminal AH (AH2) was found to be important for this activity [51]. Recently, the AHs in the HCV proteins NS4B and NS5A were found to be amenable to pharmacological inhibition [52, 53] indicating that AH domains could serve as novel antiviral drug targets.

1.2 Biophysical analysis of membrane-associated proteins

In 1985, Johann Deisenhofer and Hartmut Michel solved the first atomic resolution structure of the photosynthetic reaction center of *Rhodospseudomonas viridis* by x-ray diffraction [54]. This initiated a new age of membrane protein structure determination and functional characterization. According to the “Membrane Proteins of Known 3D Structure” website, which is part of the Structural Biology Knowledgebase, (<http://blanco.biomol.uci.edu/mpstruc/>) there were 417 unique 3D structures of membrane proteins in the database as of September 3rd, 2013. High resolution membrane protein structures can provide crucial molecular details required for an ultimate understanding of membrane protein function within a living cell, for unraveling mechanisms, molecular networks and biological pathways. However, a comprehensive understanding of membrane protein function requires additional knowledge beyond structure determination. Protein dynamics on various timescales, strength, stoichiometry and specificity of interactions with other biomolecules (proteins, lipids, nucleic acids, etc.) or molecular assemblies (protein complexes, membrane particles, etc.) as well as quantitative indicators of membrane protein function are of tremendous interest for a detailed understanding of biomolecular function. A multitude of biophysical and biochemical tools and methods have been developed in order to address such questions. In the following sections, the biophysical methods used for the characterization of membrane proteins in this doctoral thesis are briefly introduced.

1.2.1. Membrane proteins

Biological membranes are mainly composed of phospholipids, glycolipids, proteins and cholesterol [55]. Functionally, lipids form the matrix of cellular membranes, store energy (via lipid droplets) and also act as one source of second messengers in signal transduction and molecular recognition processes [56]. Membrane proteins have been estimated to comprise 30% of all proteins encoded by the human genome [57]. Membrane proteins function as signal receptors, transporters, ion channels and enzymes that are vital to cellular regulation, metabolism and homeostasis. Many drug targets are membrane proteins. Examples include rhodopsin-like G-protein-coupled receptors (rGPCRs), nuclear receptors, and ligand-gated ion channels [58]. Membrane proteins can be classified into two categories, integral and peripheral, depending on how the membrane proteins associate with the lipid bilayer [55]. Integral membrane proteins (IMP) have a portion of their mass embedded in the lipid bilayer. IMPs are subdivided into two subclasses. Transmembrane proteins traverse the lipid bilayer of the membrane. Members of the other IMP subclass, referred to as membrane-anchored IMPs, do not span the lipid bilayer of the membrane.

They are anchored to one of the membrane leaflets with AHs or fatty acid modifications. All IMPs are in general tightly associated with the membrane and can be separated from the membrane only by treatment with detergents or chaotropic agents, i.e., by destroying the integrity of the membrane [59]. Peripheral membrane proteins do not interact with the hydrophobic core of the membrane and are subdivided into associated and skeletal membrane proteins [59]. Members of the first subclass associate with the lipid polar head groups or with IMPs via polar or ionic interactions. Membrane proteins often assemble in lipid-protein complexes for correct insertion, folding, structural integrity and full functionality. Therefore the correct lipid composition of the membrane is vital to the function of many membrane proteins [60, 61].

The preparation of sufficient amounts of pure and functionally active membrane protein is a major bottleneck for membrane protein studies. A number of different approaches and specific systems have been developed for protein overexpression, including prokaryotic, eukaryotic and cell-free expression systems. The most common and often most cost-efficient method is the recombinant protein expression in *E.coli* cells. However, the expression level, correct folding and stability of the target protein may be difficult to optimize, especially for non-bacterial proteins. Therefore, when applying an *E.coli*-based expression system, it is crucial to screen promoters, fusion tags and bacterial strains in a systematic manner in order to optimize the protein expression level [62]. Since membrane proteins contain hydrophobic lipid-interacting regions it might also be difficult to establish a suitable purification procedure. Isolation of the membrane protein with a suitable detergent that allows to accommodate the hydrophobic protein regions while maintaining the correct fold of the solubilized membrane protein is the key to success.

1.2.2. Membrane mimetics for biophysical analysis

Even though there have been several structural and functional studies on membrane proteins, the analysis of membrane proteins remains very challenging. This is mainly due to the fact that the structure and function of membrane proteins are heavily influenced by their membrane environments. However, the majority of biophysical techniques for protein studies have been designed and optimized for soluble proteins. Therefore, studies on membrane proteins require appropriate membrane-mimicking systems which support the biological activity and at the same time make the membrane protein amenable to the available biophysical methods.

The most frequently used membrane-mimicking or model membrane systems are detergent micelles, amphipols, liposomes, bicelles, and nanodiscs [63]. Because detergents can efficiently solubilize membrane proteins from membrane bilayers, they are a very popular

membrane mimic for membrane protein studies. Detergent molecules contain a polar head group and a hydrophobic chain, and spontaneously form micelles when the detergent concentration is above the critical micelle concentration (CMC). Detergents are generally classified as ionic, zwitterionic, and nonionic. A suitable detergent must maintain the structure and the function of the target protein. Detergents have been used in various membrane protein studies by NMR, as outlined in recent review articles [64, 65]. However, the detergent micelles may affect the overall activity and stability of the membrane protein [63, 66].

Amphipols represent an alternative membrane mimicking medium. Amphipols are a special class of short amphipathic polymers designed as a substitute for detergents. They stabilize the integral membrane proteins in solution by adsorbing to hydrophobic and normally lipid-exposed protein surface regions [67]. Phospholipids are the major natural components of the membrane bilayer and therefore have been utilized to develop model membranes like liposomes, bicelles and nanodiscs. Liposomes and proteoliposomes (composed of lipids and IMPs) can be obtained by freeze-thawing and extrusion of lipid/protein suspensions, which results in relatively uniform, small unilamellar vesicles (SUV). Extruded proteoliposomes have been used for functional assays of membrane proteins [68, 69]. However, the relatively large size of extruded liposomes (> 30 nm in diameter) prevents their use in solution NMR studies of membrane proteins. Bicelles are composed of long-chain phospholipids in the central, presumably planar bilayer part, which is surrounded by a rim of either detergent or short-chain phospholipids to seal the hydrophobic edge from energetically unfavorable contact with water. The bicelles are a useful medium for structure determination of detergent-sensitive membrane proteins [70, 71]. Soluble nanodiscs or nanolipoprotein particles (NLPs) contain a nanometer-sized lipid bilayer fragment surrounded by two copies of an amphipathic helical apolipoprotein, termed membrane scaffold protein (MSP) [72]. The size of a nanodisc is relatively small, 7-10 nm in diameter, and depends on the type and length of the specific MSP used. Nanodiscs have been shown to be suitable for solution NMR experiments [73, 74]. A variety of membrane proteins have been successfully reconstituted into nanodiscs for structural and functional investigations [75, 76].

1.2.3. Solution NMR spectroscopy of membrane proteins

Solution NMR spectroscopy is a widely used method for determination of atomically resolved information on structure, dynamics and molecular interactions of proteins or small protein complexes in aqueous buffer. An NMR spectrum displays the resonance frequencies of magnetically active nuclei of the studied molecules in the strong and extremely homogeneous B_0 field that is present in the center of the NMR magnet. The exact resonance

frequency of a given nucleus depends on the effective magnetic field strength at the position of the nucleus. Therefore, it reflects the local chemical environment of the observed nucleus and is referred to as “chemical shift”. The measured chemical shifts of certain protein backbone nuclei are sensitive indicators of the local protein secondary structure [77]. More elaborate NMR experiments can be used to determine large numbers of ^1H - ^1H distances in a folded protein based on the nuclear Overhauser effect [78], to estimate the distance of a nucleus from a paramagnetic center [79], to measure scalar couplings that are sensitive to backbone torsion angles [80], or to determine residual dipolar couplings (RDCs) which contain useful information on the orientation of bond vectors with respect to a common coordinate frame of the folded protein [81]. All these NMR-based geometric restraints on protein structure can be subsequently used to derive the high resolution protein structure by employing restrained molecular dynamics and simulated annealing protocols [82, 83]. Fourier transform NMR methodology in combination with ultra-high magnetic field strength and multidimensional NMR experiments are crucial for achieving sufficient spectral resolution and sensitivity for protein studies. Modern triple-resonance NMR methods usually employ ^1H , ^{13}C and ^{15}N spins, which requires uniform or specific isotope labeling of the studied protein with non-radioactive ^{15}N and ^{13}C or even ^2H nuclei. Isotope labeling is normally accomplished by using appropriately labeled growth media for recombinant protein production.

Assignment of the experimentally detected resonance frequencies to the corresponding nuclei in the protein of interest presents the first milestone in an NMR study of a protein. Information on the secondary structure of the protein can be derived already from selected backbone chemical shifts. This can be accomplished by comparison of the measured chemical shifts with tabulated, amino acid type-specific random coil shifts that must, perhaps, be corrected for amino acid sequence effects [84-86]. Following empirical rules, referred to as chemical shift index method, the local secondary structure can be predicted as a function of sequence position [87, 88]. Alternatively, experimental chemical shift data, the protein amino acid sequence and data base knowledge reflecting the complex relationship between chemical shifts, backbone torsion angles and protein sequence can be used to predict torsion angles and local secondary structure in the studied protein. The latter approach has been implemented in the software program TALOS-N [89, 90] and is available via the internet (<http://spin.niddk.nih.gov/bax/software/TALOS-N/>).

The solubilization of a membrane protein in a suitable and NMR-compatible membrane mimicking environment is a critical requirement for solution NMR studies on membrane proteins. Detergent micelles are the most frequently used medium for this purpose. However, the size of the membrane protein-micelle complex may exceed the limit of

~30 kDa that applies to many standard solution NMR experiments. In such cases, transverse relaxation-optimized spectroscopy (TROSY) based methods have been applied for studies of membrane proteins in micelles [91]. Partial deuteration and selective labeling strategies also improve the spectral quality and in particular the signal-to-noise level [92]. A sizable number of successful solution NMR studies on membrane protein structure and dynamics have been published. For example, the structures of a voltage-dependent anion channel (VDAC) and of *Escherichia coli* diacylglycerol kinase (DAGK) were successfully solved in n-Dodecyl-N,N-Dimethylamine-N-Oxide (LDAO) and n-Dodecylphosphocholine (DPC) micelles [93, 94]. Solution NMR spectroscopy on membrane proteins in detergent micelles has also been used to study the interaction of the membrane protein with soluble ligands or to gain insight into the association of the membrane protein with lipid membranes. For example, solution NMR data revealed a ligand-regulated conformational change of the extracellular surface of a G protein-coupled receptor [95]. Further, the interaction between amphipathic helices of NS5A of HCV and of bovine viral diarrhea virus (BVDV), respectively, and the membrane mimicking detergent micelle was explored by solution NMR experiments [96, 97]. Attachment of paramagnetic probes to the detergent or the protein, respectively, enabled the use of paramagnetic relaxation enhancement experiments for determination of the amino acid residues of the protein that are involved in membrane binding [98, 99].

1.2.4. Protein-lipid interaction study by surface plasmon resonance

Surface plasmon resonance (SPR) is a well-established method for studying protein-protein and protein-ligand interactions. Typically the SPR system (Figure 3 a) contains a light source, a detector for reflected light, and a sensor chip, comprising a specifically coated sensor surface suitable for the desired immobilization strategy. The target molecule, referred to as ligand, will be immobilized on the sensor chip. The soluble potential interaction partner, referred to as analyte, will pass over the sensor surface in the predefined flow path. An incident light beam will pass through a prism before getting reflected on the sensor chip surface and finally reaching the detector. The intensity of the reflected light is angle-dependent. The angular position of the minimum of the reflection curve reports on the relative amount of organic material absorbed onto the sensor chip surface within a thin layer of approximately 150 nm. The change of the position of this minimum will be reported as response units (RU). A plot of the detected RU values versus time is referred to as a sensorgram and contains important information on the binding interaction (Figure 3 b) [100].

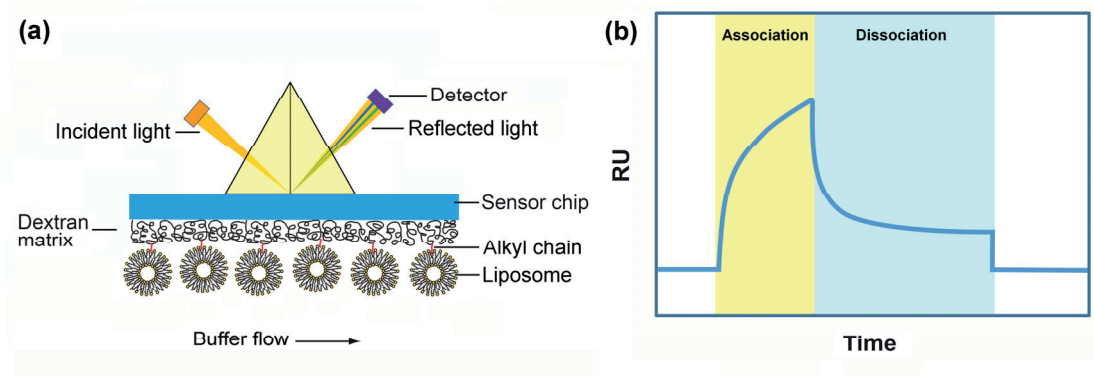


Figure 3. (a) SPR optical unit with liposomes immobilized on the L1 sensor chip. The angle of the reflected light beam will change during the association and dissociation phases, reflecting the adsorption of analyte to and the desorption of analyte from the immobilized liposomes, respectively. (b) The result is reported as a sensorgram, i.e., RU versus time.

For protein-membrane interaction analysis, there are various chip surfaces available. In this study, an L1 sensor chip was used. The L1 surface is composed of a dextran matrix including lipophilic anchor molecules (alkyl chains) and thereby enables the immobilization of liposomes (Figure 3 a) [101]. The L1 sensor surface can stably and reproducibly capture liposomes and supports experiments under various conditions such as different temperature, pH and liposome composition [102-104]. SPR experiments are quick, allow real time monitoring of binding with unlabeled analyte molecules and require only low amounts of sample. This efficient method has been utilized previously for the analysis of membrane binding of pore-forming toxins [105], of peripheral membrane proteins and peptides [102, 106].

1.2.5. Circular dichroism (CD) spectroscopy

Circular dichroism (CD) spectroscopy is the measurement of the difference in absorbance of left- and right-hand circularly polarized light [107]. CD spectroscopy is widely used for structure analysis of proteins. The near-UV CD spectrum (260-320 nm) is sensitive to the tertiary structure of proteins. The far-UV CD spectrum (240 nm and below) can be used to characterize the secondary structure of proteins. For CD spectroscopic analysis, the protein sample is prepared in aqueous buffer and requires only sub-milligram amounts of protein. CD spectroscopy is a convenient method for protein structural analysis in different buffers. CD spectroscopy can be utilized for screening different detergent containing buffers for their ability to solubilize the protein of interest in a folded conformation. CD spectroscopy has also been used for studying conformational changes of membrane proteins in different detergent or lipid containing buffers [108, 109].

Chapter 2

Aims

The exact function of the DENV non-structural protein 4A (NS4A) is still unclear. However, a crucial role of NS4A has been suggested for host membrane alterations implicated in the formation of the viral replication complex. This work is based on the hypothesis that the amino terminal region of NS4A contains structural elements that are essential for DENV replication. Secondary structure prediction indicates a prevalence of α -helices in this region which are in addition highly amphipathic. However, there has been no experimental structural characterization of the amino terminal region of DENV NS4A until now. Also, it is not known, if the amino terminal region directly interacts with cellular membranes.

Aim of this thesis is the experimental structural investigation of the putative amphipathic helical stretches in the amino terminal region of NS4A both in the presence and absence of model membranes. Further, biophysical techniques will be used to verify or disprove a direct interaction of the amino terminus of NS4A with lipid bilayer membranes.

For these purposes, a procedure needs to be established for production of i) the wild-type peptide NS4A(1-48) resembling this NS4A domain, as well as of ii) a peptide corresponding to the same region in a replication-deficient virus containing the NS4A mutant NS4A(L6E;M10E). In order to determine the influence of membranes on the 3D structure of these two peptides, the recombinant peptides will be investigated both in the absence and presence of various membrane mimicking environments.

Solution nuclear magnetic resonance (NMR) and circular dichroism (CD) spectroscopy will be used to collect structural information on the peptides. The membrane association properties of the two peptides will be studied by surface plasmon resonance (SPR) experiments using liposomes of different lipid compositions.

Chapter 3

Scientific publications

The following publications arose during the work on this thesis. My personal contribution to each of these manuscripts is specified below:

3.1 An N-terminal amphipathic helix in dengue virus nonstructural protein 4A mediates oligomerization and is essential for replication

Omer Stern, Yu-Fu Hung*, Olga Valdau*, Yakey Yaffe, Eva Harris, Silke Hoffmann, Dieter Willbold and Ella H. Sklan

J. Virol. 2013, 87(7):4080-4085; Impact factor 5.08 (2012)

* These authors contributed equally

Designed cloning and purification strategy for the two studied NS4A peptides. Executed recombinant production of the peptides used in this manuscript. Performed the CD and SPR experiments and evaluated the data. Contributed to the writing of the manuscript (20%).

3.2 Recombinant production of the amino terminal cytoplasmic region of dengue virus non-structural protein 4A for structural studies

Yu-Fu Hung, Olga Valdau, Sven Schünke, Omer Stern, Bernd W. Koenig, Dieter Willbold, Silke Hoffmann

PLoS One. Jan 23;9(1):e86482; Impact factor 3.73 (2012)

Designed and experimentally verified a new cloning and purification strategy for efficient recombinant production of amphipathic NS4A peptides. Contributed to the writing of the manuscript (80 %).

3.3 Dengue virus NS4A cytoplasmic domain binding to liposomes stabilizes membrane curvature

Yu-Fu Hung, Melanie Schwarten, Sven Schünke, Pallavi Thiagarajan-Rosenkranz, Silke Hoffmann, Ella H. Sklan, Dieter Willbold, Bernd W. Koenig

Manuscript under review at BBA-Biomembranes; Impact factor 3.39 (2012)

Conducted all experiments (protein production, NMR spectroscopy, CD, SPR) and analyzed the data (NMR signal assignment). Contributed to the writing of the manuscript (80 %).

3.1 An N-terminal amphipathic helix in dengue virus nonstructural protein 4A mediates oligomerization and is essential for replication

An N-Terminal Amphipathic Helix in Dengue Virus Nonstructural Protein 4A Mediates Oligomerization and Is Essential for Replication

Omer Stern,^a Yu-Fu Hung,^b Olga Valdau,^c Yakey Yaffe,^d Eva Harris,^e Silke Hoffmann,^c Dieter Willbold,^{b,c} Ella H. Sklan^a

Department of Clinical Microbiology and Immunology, Sackler School of Medicine, Tel Aviv University, Tel Aviv, Israel^a; Institut für Physikalische Biologie, Heinrich-Heine-Universität, Düsseldorf, Germany^b; Institute of Complex Systems (ICS-6), Forschungszentrum Jülich, Jülich, Germany^c; Department of Pathology, Sackler School of Medicine, Tel Aviv University, Tel Aviv, Israel^d; Division of Infectious Diseases, School of Public Health, University of California, Berkeley, Berkeley, California, USA^e

Dengue virus (DENV) causes dengue fever, a major health concern worldwide. We identified an amphipathic helix (AH) in the N-terminal region of the viral nonstructural protein 4A (NS4A). Disruption of its amphipathic nature using mutagenesis reduced homo-oligomerization and abolished viral replication. These data emphasize the significance of NS4A in the life cycle of the dengue virus and demarcate it as a target for the design of novel antiviral therapy.

Dengue virus (DENV) infection is a growing public health threat, with more than one-third of the world population at risk (1). DENV is a positive single-strand RNA virus. Its genome is translated into a single polypeptide, which is cleaved to produce structural (components of the mature virus) and nonstructural (NS) proteins. In addition, the NS proteins generate the viral replication complexes (RC) (2). DENV replicates its RNA genome in association with modified intracellular membranes; the details of the assembly of these complexes are incompletely understood.

NS4A, a transmembrane endoplasmic reticulum (ER) resident protein, is thought to induce the host membrane modifications that harbor the viral RC (3). A similar function for NS4A was reported in other flaviviruses (4, 5). To further understand the role of NS4A, we analyzed its cytosolic N-terminal region (amino acids 1 to 48) using sequence alignment of the four DENV serotypes. Within this sequence, amino acids that differed in their identity maintained their biochemical properties, suggesting the presence of a conserved structural motif with a potential functional significance (Fig. 1A). Secondary structure algorithms (6) indicated that this segment is predicted to fold into an α -helix (Fig. 1B). Helical wheel projections of amino acids 3 to 20 indicated a conserved polar-nonpolar asymmetry indicative of an amphipathic helix (AH) (Fig. 1C). To experimentally examine the conformation of the NS4A N terminus, a recombinant peptide comprising amino acids 1 to 48 was prepared. Codon-optimized DENV2 NS4A 1-48 was cloned into pGEV2 (7) with an N-terminal fusion to the immunoglobulin binding domain of streptococcal protein G (GB1). A tobacco etch virus (TEV) protease cleavage site (ENLYFQ) was introduced into the beginning of the NS4A coding sequence. Due to difficulties in separating NS4A from GB1 after TEV protease cleavage, an N-terminal glutathione S-transferase (GST) affinity tag was added to GB1-TEV-NS4A(1-48) by cloning it into pGEX4T-2. Protein expression and purification of the GST-GB1-NS4A(1-48) fusion were performed as described previously (8), except that an on-column cleavage was performed by adding TEV protease. The flowthrough was concentrated and subjected to size exclusion chromatography (HiLoad 16/60 Superdex 75) yielding pure NS4A(1-48). The resulting peptide was characterized using far-UV circular dichroism (CD) (Fig. 1D). In aqueous buffer, NS4A(1-48) showed limited solubility and a CD spectrum typical of a random coil conformation with an α -helix content below 10%. Addition of various membrane-mimicking,

micelle-forming detergents significantly increased the amount of α -helical content. This α -helical content varied from 30 to 40% in the presence of charged micelles (cetyl trimethylammonium bromide [CTAB], sodium dodecyl sulfate [SDS], and dodecyl phosphocholine [DPC]). In the presence of uncharged detergent (*n*-dodecyl- β -D-maltoside [DDM]) micelles, the helix content was significantly increased compared to detergent-free buffer, but was lower than other micelles. Together, these data support the existence of a conserved AH in the N terminus of NS4A.

To test the relevance of this AH to the life cycle of DENV, the hydrophobic face of the helix was genetically disrupted by introduction of charged amino acids (L6E, M10E, or a combination designated L6E;M10E) (Fig. 2A) into the nonpolar face of the helix. A Western blot with comparable expression levels of full-length NS4A (in its mature form lacking the 2K signal sequence) (3, 9) and the L6E;M10E mutant is shown in Fig. 2B. A recombinant NS4A(1-48, L6E;M10E) mutant peptide was prepared using the plasmid described above and tail-to-tail mutagenesis to insert the L6E;M10E mutations (10). A CD analysis of the mutant peptide in the presence of charged micelles (SDS, DPC, and CTAB) did not lead to significant changes of the α -helix content compared to the wild-type peptide (Fig. 2C). In contrast to the wild type, the NS4A(1-48, L6E;M10E) mutant has lost its helix-forming capability in the presence of uncharged detergent (DDM) micelles (Fig. 2C). This result indicates that although the mutations did not change the helix propensity of NS4A(1-48), the wild-type and mutant peptides differ in their properties. The mutations were inserted into a luciferase reporter replicon of DENV2 (DRrep strain 16681) (11). RNA from mutated replicons was transcribed *in vitro* and transfected into BHK21 cells. Luciferase activity was measured as shown in Fig. 2E. DRrep with a lethal mutation (GVD) (12) in the RNA-dependent RNA polymerase served as a negative control. All of the AH mutants showed a

Received 21 July 2012 Accepted 27 December 2012

Published ahead of print 16 January 2013

Address correspondence to Ella H. Sklan, sklan@post.tau.ac.il.

Y.-F.H. and O.V. contributed equally to this article.

Copyright © 2013, American Society for Microbiology. All Rights Reserved.

doi:10.1128/JVI.01900-12

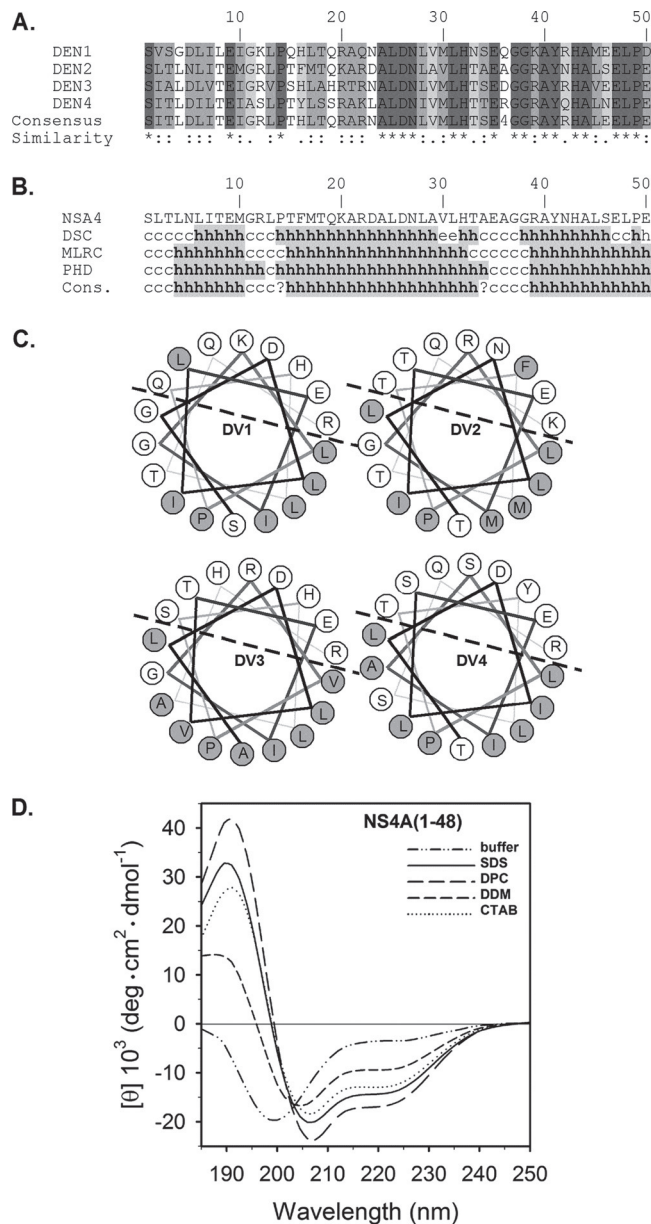


FIG 1 Secondary structure analysis of the N-terminal of NS4A. (A) ClustalW (23) multiple alignments of NS4A from the 4 DENV serotypes (accession numbers NP733810, NP739588, YP001531173, and NP740322). Similarities are shown as follows: asterisk, invariant amino acids; colon, highly similar; and period, different amino acids that are somewhat similar. The degree of similarity is also color coded in a gradient of gray color where the darkest gray is the most similar. (B) Secondary structure prediction (6). Structures are shown as helical (h), extended (e), turn (t), or undetermined (c, coil). (C) A helical wheel plot of NS4A amino acids 3 to 20. Hydrophilic residues are labeled in gray. Dashed line separates the putative polar and nonpolar faces of the helix. (D) Far-UV CD analysis of recombinant wild-type NS4A(1–48) peptide in 50 mM sodium phosphate buffer (pH 7.0) (dashed dotted line) and in the presence of 100 mM sodium dodecyl sulfate (SDS; solid line), *n*-dodecyl phosphocholine (DPC; long dashed line), *n*-dodecyl- β -D-maltoside (DDM; short dashed line), respectively, or in the presence of 1 mM cetyl trimethylammonium bromide (CTAB; dotted line). Spectra were recorded on a Jasco J810 spectrometer (Jasco, Groß-Umstadt, Germany) at 298 K in a 0.1-cm path-length quartz cuvette (Hellma) with 30 μ M peptide. Data collection was done at 260 to 185 nm, with a 0.5-increment and a bandwidth of 1 nm. Spectra were baseline corrected and smoothed by a local smoothing technique with bisquare weighting and polynomial regression (SigmaPlot 11; Systat Software, Inc.).

severe replication defect displaying low levels of luciferase activity comparable to the GVD negative control. This result indicated that NS4A AH is essential for DENV replication. As a control for the mutagenesis experiment, we prepared two additional mutants, K20R and M10A; these replacements had no apparent effect on viral replication (Fig. 2E). Nevertheless, mutation of P14 to alanine abolished viral replication, indicating that this proline has a critical role in viral replication (Fig. 2E). AHs are typically known to associate with membranes, where their polar side faces the aqueous phase and the hydrophobic face is immersed in the membrane (13). Membrane binding of the AH was studied using surface plasmon resonance (SPR) (Fig. 3A and B). NS4A(1–48) and mutant NS4A(1–48, L6E;M10E) peptides were tested for their ability to bind to a 1-palmitoyl-2-oleoyl-sn-glycero-3-phosphocholine (POPC) bilayer or to a negatively charged POPC/1-palmitoyl-2-oleoyl-sn-glycero-3-phosphatidylglycerol (POPG; 4:1) bilayer. The sensogram in Fig. 3A shows that NS4A(1–48) binds strongly to chips coated with both bilayer types. Interestingly, the signal does not return to baseline levels during buffer washes. Moreover, repeated pulses of 100 mM sodium hydroxide or hydrochloric acid were not sufficient to restore the signal to the baseline (data not shown). This result indicates that once bound, the peptide remains tightly bound to the membranes, particularly to the negatively charged POPC/POPG bilayer. In contrast, injection of the NS4A(1–48, L6E;M10E) mutant resulted in a considerably low signal. Moreover, the mutant curve returned to baseline (POPC) or close to the baseline levels (POPC/POPG) following the termination of the peptide injection. These results indicate that the AH of NS4A has a high affinity for membranes *in vitro* and that the hydrophobic patch necessary for this membrane binding ability is disrupted in the L6E;M10E mutant.

NS4A was previously implicated in the induction of the membrane domains that harbor the viral RCs (3). To create these rearrangements, NS4A most likely induces membrane curvature by an unknown mechanism (3). Oligomerization of membrane proteins can form a scaffold that can locally bend the membrane (14–16). A similar mechanism is thought to mediate membrane alterations induced by HCV NS4B (17, 18). To this end, we analyzed the effect of the above-mentioned mutations on the intracellular localization of NS4A.

Figure 3C shows live U2OS cells expressing the yellow fluorescent protein (YFP)-tagged full-length NS4A wild type or the L6E;M10E NS4A mutant and the β -subunit of the ER resident signal recognition particle (SRP) receptor (SR β) fused to cyan fluorescent protein (CFP). Both NS4A proteins demonstrated localization to ER membranes and widely spread bright foci across the cell. Interestingly, although these NS4A-induced foci were previously shown to colocalize with a different ER marker (calreticulin) (3), SR β was generally excluded from these foci. Photobleaching experiments demonstrated that NS4A was dynamically exchanged between ER membranes and the foci, which possibly represent densely packed, high-curvature membranes (data not shown). Both the wild-type and mutant NS4A YFP fusions showed similar expression levels (Fig. 3D).

Units are given as the mean residue ellipticity ($[\theta]$) by using peptide concentrations based on UV light absorption at 280 nm. The α -helical content was estimated with various deconvolution methods by the use of CDPPro software (<http://lamar.colostate.edu/~sreeram/CDPro/main.html>).

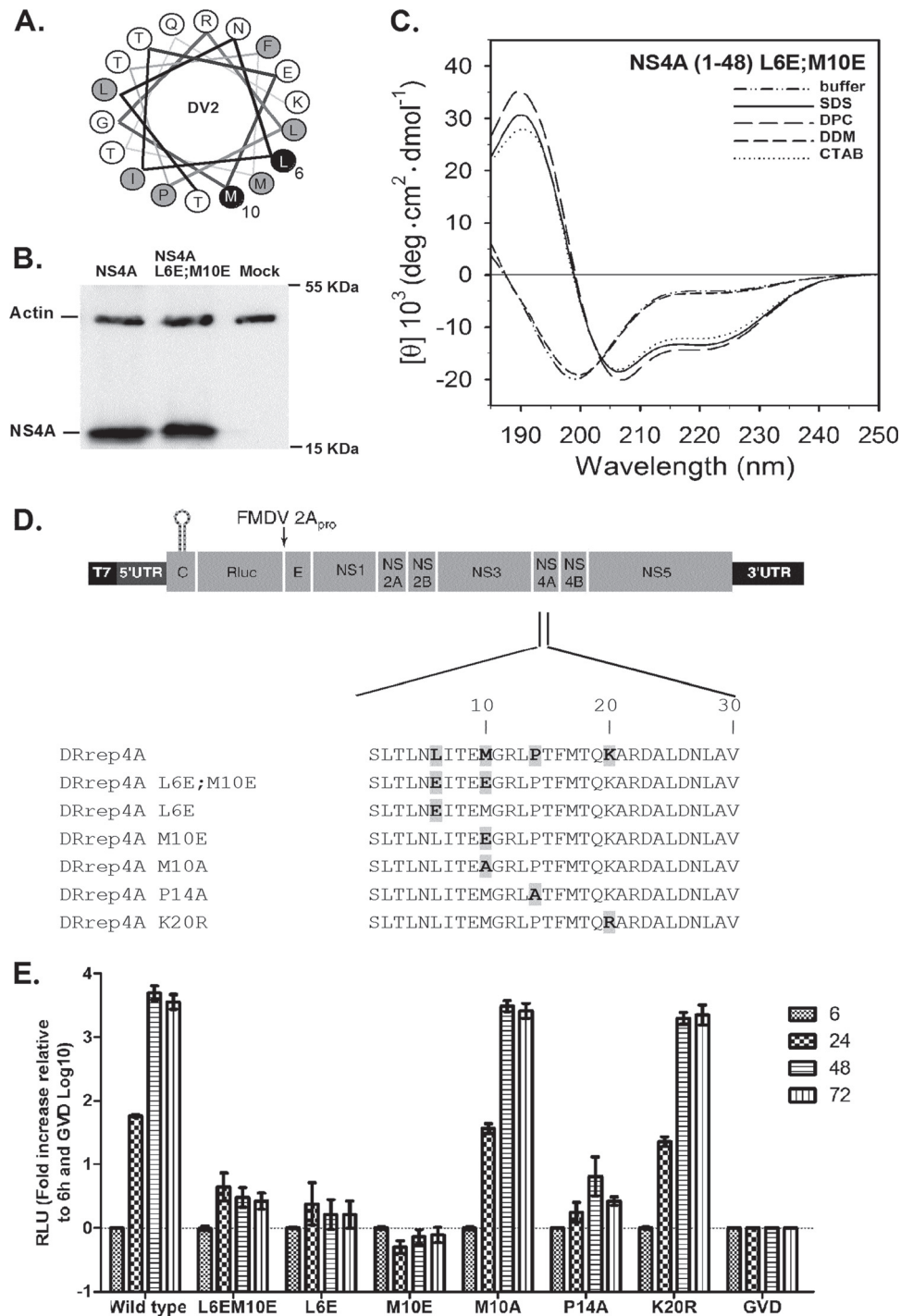


FIG 2 An intact N-terminal NS4A AH is required for DENV replication. (A) A helical wheel plot of NS4A amino acids 3 to 20 showing the location of the inserted mutations (black, L6E and M10E). (B) Comparable expression levels of full-length wild-type and L6E;M10E mutant NS4A as determined by Western blot analysis of FLAG-tagged wild-type or mutant NS4A expression levels using an anti-FLAG antibody. Monoclonal mouse anti-actin antibody was used as a loading control. (C) Spectra of the purified mutant peptide was recorded in 10 mM sodium phosphate buffer (pH 7.0) (dashed dotted line) or in the presence of 100 mM sodium dodecyl sulfate (SDS; solid line), *n*-dodecyl phosphocholine (DPC; long dashed line), *n*-dodecyl- β -D-maltoside (DDM; short dashed line), or 1 mM cetyl trimethylammonium bromide (CTAB; dotted line). (D) Schematic diagram of the DENV2 luciferase reporter replicon (pDRrep) used (11). Amino acids 1 to 30 of NS4A containing the AH region are shown for the wild-type and mutant replicons. Amino acid changes are in bold. (E) Replication assay for NS4A-AH mutated dengue replicons. Wild-type and mutated replicons were transfected into BHK21 cells. Luciferase activity was measured at 6, 24, 48, and 72 h posttransfection. Luciferase activity (relative light units [RLU]) is plotted for each time point. The data were normalized to the 6-h values that reflect transfection efficiency and to luciferase levels in replicon with a mutated polymerase. The mean values of at least two independent experiments performed in triplicates are shown. Error bars indicate standard errors of the means.

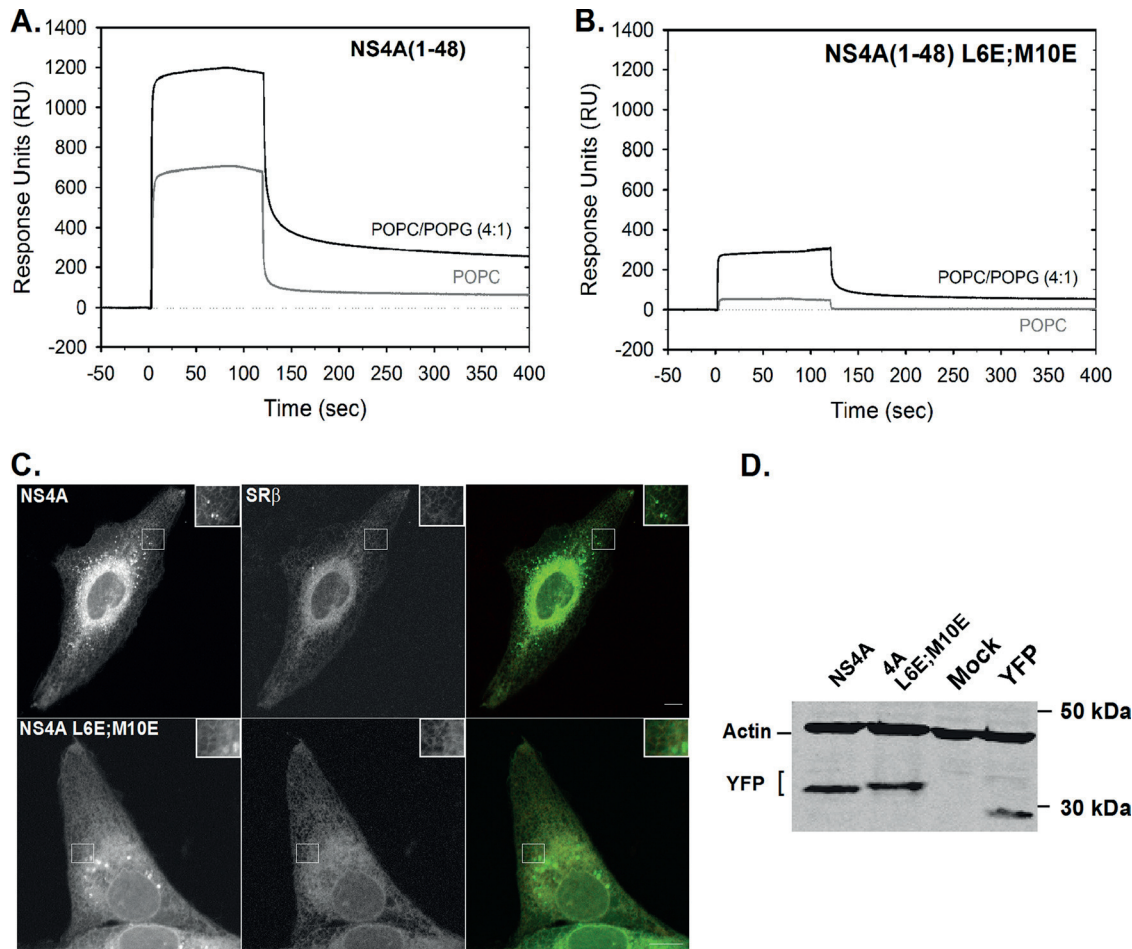


FIG 3 The N-terminal NS4A AH binds membranes *in vitro*. (A) Binding of recombinant wild-type NS4A(1–48) peptide to lipid bilayers. Association of NS4A(1–48) to an L1 chip (GE Healthcare, Piscataway, NJ) covered with a POPC bilayer (gray) or a negatively charged bilayer containing 20% of POPG and 80% of POPC [POPC/POPG (4:1), black], prepared as described elsewhere (24). Sensograms were recorded with a Biacore X device (GE Healthcare) using a flow rate of 20 μ l/min, an injection time of 1 min, and a peptide concentration of 50 μ M. (B) Binding behavior of mutant NS4A(1–48, L6E;M10E) to lipid bilayers. Conditions are as in panel A, and the data shown are representative of three independent experiments. (C) Subcellular localization of NS4A-YFP fusion constructs. U2OS cells were cotransfected with wild-type NS4A-YFP or a similar construct with the AH mutations (M6E;M10E; see Fig. 2 for details) and SR β -CFP. Images were captured 24 h posttransfection using a confocal microscope. Insets show an enlarged portion of the cell (white square). Bar = 10 μ m. (D) Comparable expression levels of the constructs shown in panel C as determined by Western blotting using an anti-GFP antibody. Monoclonal mouse anti-actin antibody was used as a loading control.

To test if NS4A can self-oligomerize, immunoprecipitation was performed. A modified vaccinia virus expressing T7 polymerase (19) was used to obtain increased levels of NS4A expression. Cells were infected with the recombinant vaccinia virus and cotransfected with full-length wild-type or mutant NS4A, each with a C-terminal FLAG or hemagglutinin (HA) tag. Cells coexpressing NS4A and HCV NS4B were used as a negative control. Lysates from cells expressing all combinations of these plasmids were subjected to immunoprecipitation using FLAG beads. Figure 4A shows that NS4A forms oligomers (lane 1). The ability of NS4A to form oligomers was not dramatically changed by the presence of the AH mutations (lanes 2 to 4). Since immunoprecipitation tests protein interactions in solubilized membranes, we verified NS4A self-association using an experimental approach that allows analysis of the proteins in their native intact membranes. On this premise, we analyzed the fluorescence resonance energy transfer (FRET) using acceptor photobleaching (20). Full-length NS4A or NS4A with AH mutants were fused to CFP or YFP which were

coexpressed in U2OS cells. The cells were fixed 24 h posttransfection, and the NS4A-YFP (acceptor) was repeatedly bleached in a region of interest (ROI). The changes in NS4A-CFP (donor) and photobleached acceptor fluorescence were measured. FRET efficiency (E_F) from at least 10 different cells was calculated using the equation $E_F = (D_{\text{post}} - D_{\text{pre}})/D_{\text{post}}$, where D_{post} is the fluorescence intensity of the donor after acceptor photobleaching and D_{pre} is the fluorescence intensity of the donor before acceptor photobleaching. Figure 4B shows typical cells coexpressing CFP and YFP fusions of wild-type NS4A or NS4A mutants before (top panel) and after (bottom panel) photobleaching of the acceptor within the ROI (white square). Images are pseudocolored for fluorescence intensity; colors reflect the fluorescence intensity from lowest (black) to highest (red). The increase in donor fluorescence after acceptor photobleaching can be observed in the cell coexpressing a pair of wild-type NS4A (Fig. 4B). Figure 4C shows quantification of the fluorescence intensities within the labeled ROI. FRET was observed in cells coexpressing YFP- and CFP-

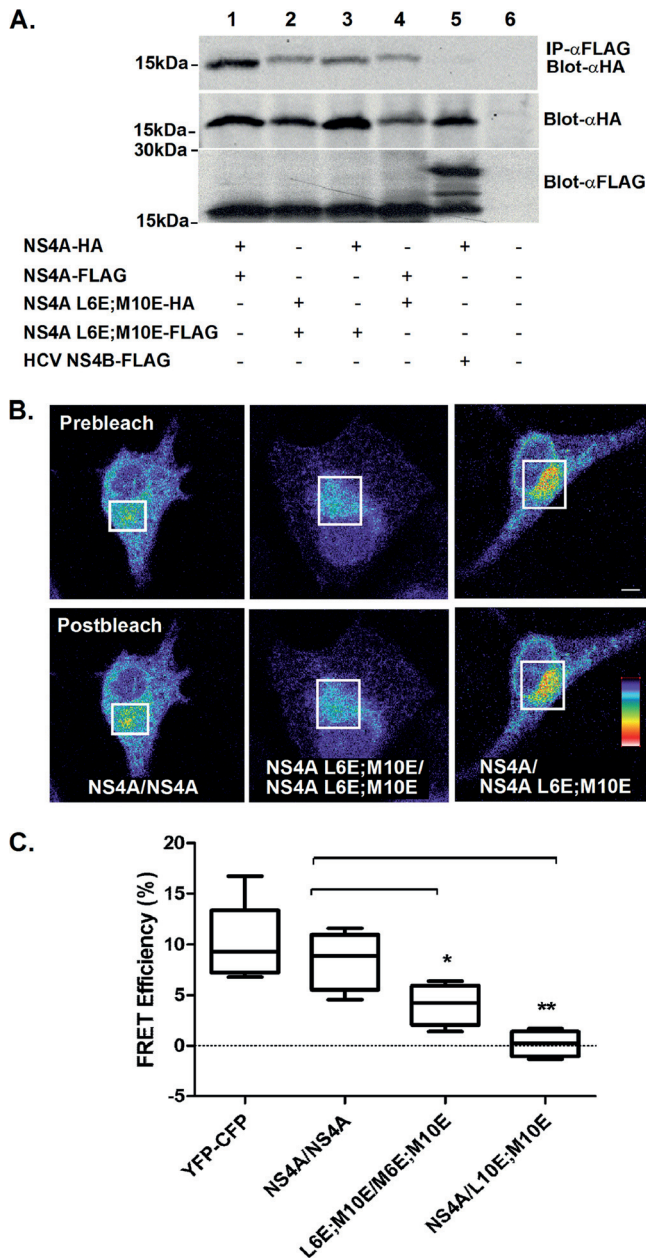


FIG 4 NS4A forms AH-dependent oligomers. (A) Immunoprecipitation of wild-type NS4A and AH mutants. HEK293T cells were cotransfected with the indicated combinations. The cells were lysed 24 h posttransfection and subjected to immunoprecipitation using anti-FLAG beads followed by Western blotting with an anti-HA antibody. Direct Western blotting of the cell lysates with anti-FLAG and anti-HA antibodies are shown in the lower panels. Molecular mass markers are indicated on the left. (B) NS4A CFP and YFP fusion constructs and AH mutants thereof were transfected into U2OS cells as indicated. FRET was determined using acceptor photobleaching. Fluorescence of donor and acceptor was measured as a function of time during acceptor photobleaching. Intensities within the labeled (white square) region of interest were analyzed and are plotted in the graphs. Bar = 5 μ m. Asterisks denote statistical significance in an up-paired Student *t* test. **, *P* < 0.05; ***, *P* < 0.005.

tagged wild-type NS4A (mean E_F , 8.5% \pm 2.9%). Intermediate FRET efficiency was detected in cells coexpressing the AH mutants. FRET was not observed in cells (mean E_F , 4% \pm 2%) coexpressing both the wild type and the AH mutant. These results

indicate that the AH has an important role in the self-oligomerization of NS4A. The intermediate FRET efficiency of the mutant pair might imply that additional elements within NS4A are required for oligomerization. The lack of FRET in the mixed wild-type-mutant pair might result from the alteration of the mutant's membrane binding capabilities; this may, in turn, induce a conformational change that dissociates the mutant NS4A from the wild type.

To summarize, we identified an N-terminal AH within NS4A that has a critical role in the DENV life cycle. As AHs were previously found to be amenable to pharmacological inhibition (21, 22), the data here merit consideration of the NS4A AH as a target for anti-DENV drugs. A more detailed study to investigate the exact structure of the AH in diverse membrane model systems and the role(s) of this motif in DENV replication is under way.

ACKNOWLEDGMENTS

This work was supported by a grant from the Sackler Faculty of Medicine V. Schreiber Fund (to E.H.S.) and by a grant from the Jürgen Manchot Foundation, Molecules of Infection Graduate School (to Y.-F.H.).

We thank Julian M. Glück for help with the SPR measurements and Simone König (Integrated Functional Genomics, University of Münster, Germany) for mass spectrometric analysis. Special thanks go to Koret Hirschberg (Tel Aviv University) and Bernd W. Koenig for critical reading of the manuscript and to Menashe Elazar (Stanford University) for helpful discussions.

REFERENCES

1. Deen JL, Harris E, Wills B, Balmaseda A, Hammond SN, Rocha C, Dung NM, Hung NT, Hien TT, Farrar JJ. 2006. The WHO dengue classification and case definitions: time for a reassessment. *Lancet* 368: 170–173.
2. Lindénbach BD, Rice CM, Thiel HJ. 2007. Flaviviridae: the viruses and their replication, p 1101–1152. In Knipe DM, Howley PM (ed), *Fields virology*, 5th ed. Lippincott, Williams & Wilkins, Philadelphia, PA.
3. Miller S, Kastner S, Krijnse-Locker J, Buhler S, Bartenschlager R. 2007. The non-structural protein 4A of dengue virus is an integral membrane protein inducing membrane alterations in a 2K-regulated manner. *J. Biol. Chem.* 282:8873–8882.
4. Mackenzie JM, Khromykh AA, Jones MK, Westaway EG. 1998. Subcellular localization and some biochemical properties of the flavivirus Kunjin nonstructural proteins NS2A and NS4A. *Virology* 245:203–215.
5. Roosaendaal J, Westaway EG, Khromykh A, Mackenzie JM. 2006. Regulated cleavages at the West Nile virus NS4A-2K-NS4B junctions play a major role in rearranging cytoplasmic membranes and Golgi trafficking of the NS4A protein. *J. Virol.* 80:4623–4632.
6. Combet C, Blanchet C, Geourjon C, Deléage G. 2000. NPS@: network protein sequence analysis. *Trends Biochem. Sci.* 25:147–150.
7. Huth JR, Bewley CA, Jackson BM, Hinnebusch AG, Clore GM, Gronenborn AM. 1997. Design of an expression system for detecting folded protein domains and mapping macromolecular interactions by NMR. *Protein Sci.* 6:2359–2364.
8. Feuerstein S, Solyom Z, Aladağ A, Hoffmann S, Willbold D, Brutscher B. 2011. 1H, 13C, and 15N resonance assignment of a 179 residue fragment of hepatitis C virus non-structural protein 5A. *Biomol. NMR Assign.* 5:241–243.
9. Lin C, Amberg SM, Chambers TJ, Rice CM. 1993. Cleavage at a novel site in the NS4A region by the yellow fever virus NS2B-3 proteinase is a prerequisite for processing at the downstream 4A/4B signalase site. *J. Virol.* 67:2327–2335.
10. Hemsley A, Arnheim N, Toney MD, Cortopassi G, Galas DJ. 1989. A simple method for site-directed mutagenesis using the polymerase chain reaction. *Nucleic Acids Res.* 17:6545–6551.
11. Clyde K, Barrera J, Harris E. 2008. The capsid-coding region hairpin element (cHP) is a critical determinant of dengue virus and West Nile virus RNA synthesis. *Virology* 379:314–323.
12. Guyatt KJ, Westaway EG, Khromykh AA. 2001. Expression and purifi-

- cation of enzymatically active recombinant RNA-dependent RNA polymerase (NS5) of the flavivirus Kunjin. *J. Virol. Methods* 92:37–44.
13. Rees DC, DeAntonio L, Eisenberg D. 1989. Hydrophobic organization of membrane proteins. *Science* 245:510–513.
 14. McMahon HT, Gallop JL. 2005. Membrane curvature and mechanisms of dynamic cell membrane remodelling. *Nature* 438:590–596.
 15. Miller S, Krijnse-Locker J. 2008. Modification of intracellular membrane structures for virus replication. *Nat. Rev. Microbiol.* 6:363–374.
 16. Yaffe Y, Shepshelovitch J, Nevo-Yassaf I, Yeheskel A, Shmerling H, Kwiatek JM, Gaus K, Pasmanik-Chor M, Hirschberg K. 2012. The MARVEL transmembrane motif of occludin mediates oligomerization and targeting to the basolateral surface in epithelia. *J. Cell Sci.* 125:3545–3556.
 17. Gouttenoire J, Roingeard P, Penin F, Moradpour D. 2010. Amphipathic alpha-helix AH2 is a major determinant for the oligomerization of hepatitis C virus nonstructural protein 4B. *J. Virol.* 84:12529–12537.
 18. Yu G-Y, Lee K-J, Gao L, Lai MMC. 2006. Palmitoylation and polymerization of hepatitis C virus NS4B protein. *J. Virol.* 80:6013–6023.
 19. Wyatt LS, Moss B, Rozenblatt S. 1995. Replication-deficient vaccinia virus encoding bacteriophage T7 RNA polymerase for transient gene expression in mammalian cells. *Virology* 210:202–205.
 20. Kenworthy AK. 2001. Imaging protein-protein interactions using fluorescence resonance energy transfer microscopy. *Methods* 24:289–296.
 21. Cho NJ, Dvory-Sobol H, Lee C, Cho SJ, Bryson P, Masek M, Elazar M, Frank CW, Glenn JS. 2010. Identification of a class of HCV inhibitors directed against the nonstructural protein NS4B. *Sci. Transl. Med.* 2:15ra16.
 22. Elazar M, Cheong KH, Liu P, Greenberg HB, Rice CM, Glenn JS. 2003. Amphipathic helix-dependent localization of NS5A mediates hepatitis C virus RNA replication. *J. Virol.* 77:6055–6061.
 23. Thompson JD, Higgins DG, Gibson TJ. 1994. CLUSTAL W: improving the sensitivity of progressive multiple sequence alignment through sequence weighting, position-specific gap penalties and weight matrix choice. *Nucleic Acids Res.* 22:4673–4680.
 24. Cooper MA, Hansson A, Lofas S, Williams DH. 2000. A vesicle capture sensor chip for kinetic analysis of interactions with membrane-bound receptors. *Anal. Biochem.* 277:196–205.

3.2 Recombinant production of the amino terminal cytoplasmic region of dengue virus non- structural protein 4A for structural studies

Recombinant Production of the Amino Terminal Cytoplasmic Region of Dengue Virus Non-Structural Protein 4A for Structural Studies

Yu-Fu Hung², Olga Valda¹, Sven Schünke¹, Omer Stern³, Bernd W. Koenig^{1,2}, Dieter Willbold^{1,2}, Silke Hoffmann^{1*}

1 Institute of Complex Systems, Structural Biochemistry (ICS-6), Forschungszentrum Jülich, Jülich, Germany, **2** Institut für Physikalische Biologie, Heinrich-Heine-Universität, Düsseldorf, Germany, **3** Department Clinical Microbiology and Immunology, Sackler School of Medicine, Tel Aviv University, Tel Aviv, Israel

Abstract

Background: Dengue virus (DENV) is a mosquito-transmitted positive single strand RNA virus belonging to the Flaviviridae family. DENV causes dengue fever, currently the world's fastest-spreading tropical disease. Severe forms of the disease like dengue hemorrhagic fever and dengue shock syndrome are life-threatening. There is no specific treatment and no anti-DENV vaccines. Our recent data suggests that the amino terminal cytoplasmic region of the dengue virus non-structural protein 4A (NS4A) comprising amino acid residues 1 to 48 forms an amphipathic helix in the presence of membranes. Its amphipathic character was shown to be essential for viral replication. NMR-based structure-function analysis of the NS4A amino terminal region depends on its milligram-scale production and labeling with NMR active isotopes.

Methodology/Principal Findings: This report describes the optimization of a uniform procedure for the expression and purification of the wild type NS4A(1-48) peptide and a peptide derived from a replication-deficient mutant NS4A(1-48; L6E, M10E) with disrupted amphipathic nature. A codon-optimized, synthetic gene for NS4A(1-48) was expressed as a fusion with a GST-GB1 dual tag in *E. coli*. Tobacco etch virus (TEV) protease mediated cleavage generated NS4A(1-48) peptides without any artificial overhang. Using the described protocol up to 4 milligrams of the wild type or up to 5 milligrams of the mutant peptide were obtained from a one-liter culture. Isotopic labeling of the peptides was achieved and initial NMR spectra were recorded.

Conclusions/Significance: Small molecules targeting amphipathic helices in the related Hepatitis C virus were shown to inhibit viral replication, representing a new class of antiviral drugs. These findings highlight the need for an efficient procedure that provides large quantities of the amphipathic helix containing NS4A peptides. The double tag strategy presented in this manuscript answers these needs yielding amounts that are sufficient for comprehensive biophysical and structural studies, which might reveal new drug targets.

Citation: Hung Y-F, Valda O, Schünke S, Stern O, Koenig BW, et al. (2014) Recombinant Production of the Amino Terminal Cytoplasmic Region of Dengue Virus Non-Structural Protein 4A for Structural Studies. PLoS ONE 9(1): e86482. doi:10.1371/journal.pone.0086482

Editor: Cheryl A. Stoddart, University of California, San Francisco, United States of America

Received: August 29, 2013; **Accepted:** December 9, 2013; **Published:** January 23, 2014

Copyright: © 2014 Hung et al. This is an open-access article distributed under the terms of the Creative Commons Attribution License, which permits unrestricted use, distribution, and reproduction in any medium, provided the original author and source are credited.

Funding: This work was supported by a grant from the Jürgen Manchot Foundation, Molecules of Infection Graduate School to YFH and DW (<http://www.moi.hhu.de/en.html>). The funders had no role in study design, data collection and analysis, decision to publish, or preparation of the manuscript.

Competing Interests: The authors have declared that no competing interests exist.

* E-mail: si.hoffmann@fz-juelich.de

Introduction

Dengue fever is currently the fastest-spreading tropical disease in the world, with more than 2.5 billion people at risk. Dengue virus (DENV), the causative agent of this disease, is estimated to infect 390 million people across all continents each year [1]. DENV is transmitted by the bite of female mosquitoes. DENV causes flu-like symptoms in most of the infected patients, but severe forms of the disease like dengue hemorrhagic fever and dengue shock syndrome are life-threatening. There is no specific treatment and no anti-DENV vaccines.

DENV is a positive single strand RNA virus of the *Flaviviridae* family. Its genome is translated into a single polypeptide, which is subsequently cleaved into three structural and seven non-structural (NS) proteins. DENV replicates its RNA genome in replication

complexes (RCs), which are associated with modified intracellular membranes [2]. While the viral structural proteins compose the mature virion, the NS proteins together with the viral RNA and host factors generate the viral RC. NS4A is an endoplasmic reticulum (ER)-localized, 16 kDa transmembrane protein, which is an essential component of the viral RC. NS4A has been suggested to be involved in inducing host membrane alterations that resemble the virus-induced membrane structures [3]. A membrane remodeling function of NS4A was also reported in other flaviviruses [4,5].

Recently, we identified a conserved amphipathic helix (AH) in the cytoplasmic, amino terminal region of NS4A (amino acid residues 1–48) that is essential for viral replication [6]. AHs are α helical protein regions in which one face of the helix is hydrophobic while the opposite face is hydrophilic [8]. In contrast

to transmembrane domains that span the membrane bilayer, AHs often serve as in-plane membrane anchors [7]. Peptides that are predicted to form amphipathic helices are frequently unstructured in buffer devoid of membranes but adopt a helical conformation upon association with membranes or in a membrane mimicking environment. In addition AHs can contribute to membrane curvature [8–10] or mediate protein-protein-interactions. AHs in proteins of several positive strand RNA viruses were shown to be essential for the viral life cycle [11–16].

The use of direct acting antivirals is one of the most important new therapeutic approaches for treating infections with hepatitis C virus (HCV), a close relative of DENV. Notably, AHs in HCV NS4B and NS5A were found to be amenable to pharmacological inhibition [11,17] indicating that AHs could serve as novel antiviral targets. Our recent data emphasizes the significance of the amino terminal AH of NS4A in the DENV life cycle and demarcate it as potential target for the design of novel antiviral therapy [6]. In this report, we describe a novel protocol for recombinant production of a peptide comprising the first 48 amino acids of NS4A, NS4A(1–48), and containing the above mentioned AH. Production of milligram amounts of NS4A(1–48) is a crucial prerequisite for biophysical and in particular NMR experiments on NS4A(1–48). Such studies are urgently needed as a starting point for the rational design of new strategies to inhibit the activity of this NS4A region in the virus life cycle.

It is a common strategy to express short peptides as a fusion with another protein in order to avoid the well-known degradation of short peptides in bacterial cells. However, expression of fusion proteins is complex and does not always follow predictions. Hence, it is necessary to test several fusion strategies in search for a highly efficient protocol that works for a given peptide. Several different proteins have been described in the literature as fusion tags for peptide production [18,19]. We tested glutathion S-transferase (GST), the immunoglobulin-binding domain of streptococcal protein G (GB1), and yeast ubiquitin as fusion partners of NS4A(1–48) in our quest for an effective production strategy of this peptide in *E. coli*. For DENV NS4A(1–48) a dual fusion tag in combination with a tobacco etch virus (TEV) protease cleavage site revealed the highest peptide yields. Our aim was to establish a general protocol for production and purification of decent amounts of wild type NS4A(1–48) as well as of various mutated forms of the peptide. Such mutants are quite useful in an in-depth structure-function-analysis of proteins.

Materials and Methods

Materials

E. coli Mach 1 cells obtained from Life Technologies GmbH (Darmstadt, Germany) were used for cloning purposes. *E. coli* BL21-(DE3) (Agilent Technologies, Inc., Santa Clara, CA, USA) or *E. coli* BL21 (GE Healthcare, Freiburg, Germany) strains were used for peptide expression. All enzymes used for cloning were obtained from MBI Fermentas (St. Leon-Rot, Germany) if not stated otherwise. Synthetic oligonucleotides were from BioTez (Berlin, Germany). Plasmid pGEX-4T-2 was obtained from GE Healthcare. The plasmid pTKK19ubi was a kind gift from Toshiyuki Kohno (Mitsubishi Kagaku Institute of Life Sciences (MITILS), Machida, Tokyo, Japan) [20] and pRK793 (plasmid #8827) was obtained from the Addgene plasmid depository (<http://addgene.org>). PCR purification kit, gel extraction kit (QIAquick), miniprep kit (QIAprep spin) and Ni-NTA agarose were all from Qiagen (Hilden, Germany). Difco LB broth was purchased from BD Biosciences (Heidelberg, Germany). Ampicillin and kanamycin were from AppliChem (Darmstadt, Germany),

Isopropyl β -D-1-thiogalactopyranoside (IPTG) was from Boehringer (Mannheim, Germany). [^{15}N] ammonium chloride and [$^{13}\text{C}_6$]-glucose were from Euriso-top (Saarbrücken, Germany). Protein standards were obtained from MBI Fermentas and Sigma-Aldrich (Munich, Germany). Glutathion-sepharose 4B was purchased from GE Healthcare. All other chemicals were from Sigma-Aldrich, Roth (Karlsruhe, Germany) or Merck (Darmstadt, Germany) unless stated otherwise.

Construction of NS4A(1–48) expression vectors

NS4A(1–48) plasmid constructs with a single fusion tag. We first cloned NS4A(1–48) into a modified pTKK19ubi vector (see below), which codes for an amino terminal yeast ubiquitin fusion. The peptide bond between ubiquitin and a defined peptide insert in the expressed fusion protein can be cleaved by yeast ubiquitin hydrolase. This strategy enables the production of a NS4A(1–48) peptide without any artificial overhangs. In order to simplify cloning of inserts into pTKK19ubi vector [20], we modified the original pTKK19ubi by introducing silent mutations that generate a unique *SacII* endonuclease cleavage site at the carboxy-terminal end of the ubiquitin coding sequence. In detail, the original codons for Leu 73, Arg 74 and Gly 75 in the ubiquitin coding sequence of pTKK19ubi are substituted with ctc, cgc, and ggc, respectively, in the new pTKK19ubi/*SacII*. Plasmid pUbi-NS4A(1–48) was obtained by cloning an optimized sequence coding for amino acids 1 to 48 of NS4A from dengue virus type 2 (GenBank: NP739588) into pTKKubi/*SacII*. Gene optimization was performed using the GeneOptimizer® software provided by GeneArt® [21]. To construct the plasmid, four complementary synthetic oligonucleotides (sequences 1 to 4, table 1) were annealed, ligated and subjected to a PCR-amplification with two shorter primers (9 and 10, table 1) containing the restriction sites for *SacII* and *SalI*. The purified fragment was cut by *SacII* and *SalI* and then ligated into dephosphorylated pTKK19Ubi/*SacII*.

Second, a plasmid for expression of the NS4A peptide as protein fusion with the immunoglobulin-binding domain of streptococcal protein G (GB1) at the amino terminus was obtained by cloning the optimized sequence coding for NS4A(1–48) into the vector pGEV2 [22] using the four synthetic oligonucleotides 1 to 4 (table 1). PCR amplification was performed with different primers (5 and 6) in order to introduce a nucleotide sequence that codes for the first six residues of a tobacco etch virus (TEV) protease cleavage site (ENLYFQ) in front of the NS4A coding sequence. The primers contained *BamHI* and *XhoI* restrictions sites at their 5' and 3' ends, respectively. This fragment was ligated into dephosphorylated pGEV2 to yield pGEV-NS4A(1–48). As TEV protease recognizes E-X-X-Y-X-Q↓(G/S), and the first amino acid of the NS4A peptide is serine, a NS4A(1–48) peptide without any artificial overhang can be produced with this vector as well.

Third, we engineered a plasmid for expression of NS4A(1–48) as protein fusion with an amino terminal glutathion-S-transferase (GST) following the strategy described above for pGEV-NS4A(1–48). The insert coding for NS4A(1–48) was ligated into a dephosphorylated pGEX-4T-2 vector. The resulting construct was named pGEX-TEV-NS4A(1–48).

NS4A(1–48) plasmid construct with a dual fusion tag. Efficient separation of NS4A(1–48) from GB1 after TEV protease cleavage was impossible when utilizing pGEV-NS4A(1–48). In order to avoid this problem we extended the GB1-NS4A(1–48) fusion by an amino terminal GST affinity tag. For this purpose the GB1-NS4A(1–48) sequence was amplified with a 5'-primer containing an *EcoRI* site (7, table 1) and a commercially available T7-terminator primer (8, table 1). The restricted insert was cloned

Table 1. Primers used for amplification of NS4A (1–48).

Oligo	Sequence (5'–3')
1	agcctgaccctgaatctgattaccgaaatgggtcgtgccgacctttatgaccagaaagcacgtgatgcactggataatctgg
2	cagtctgcataccgctgaagccgggtggtcgtgcataatcatgcactgagcgaaactgtaag
3	tgctttctgggtcataaaggctcgacgacgacccatttcggaatcagattcagggtcaggct
4	gacgttacagtcgctcagtcgcatgattatgacgacaccggcttcagcggtatgcagaactgccagattccagtcgcatcac
5	ggaggaggagccgaaacctgtatttcagagcctgacccctgaatctgattacc <i>Bam</i> HI
6	ggaggagtcgacctcgagttacagttcgtcgtcagtc <i>Xho</i> I
7	gctggaattcagtaacaagcttgcctgaacgg <i>Eco</i> RI
8	gctagtattgctcagcgg (T7-Terminator-Primer; Novagen #69337-3)
9	ggaggaccgcccggtagcctgacccctgaatctga <i>Sac</i> II
10	ggaggagtcgacctcgagttacagttcgtcgtcagtc <i>Sal</i> I
11	gaaattaccgaagagggtcgtcgtccgac
12	attcagggtcaggctctgaaatacaggtt

Note: The sequences of the restriction sites used for cloning are underlined, the name of the enzyme is given below.
doi:10.1371/journal.pone.0086482.t001

into the pGEX4T-2 vector using the *Eco*RI and *Xho*I sites. The obtained vector pGEX-GB1-NS4A(1–48) was used to produce the GST-GB1-NS4A fusion protein in *E. coli*.

Tail-to-tail mutagenesis was used to obtain the mutant NS4A peptide carrying L6E and M10E substitutions (pGEX-GB1-NS4A(1–48; L6E, M10E) [23] using kappa HiFi DNA polymerase (Kapa Biosystems Cambridge, MA, USA). The forward primer (11, table 1) carried the mutations while the reverse primer (12, table 1) annealed to the opposite strand, with their 5'-ends adjacent to each other. Subcloning into pGEX4T-2 was performed as described for the wild type peptide. The correct sequence of all constructs was verified using DNA sequencing (SeqLab, Göttingen, Germany).

Expression of NS4A(1–48) fusion proteins

BL21 cells were transformed with pGEX-TEV-NS4A(1–48), pGEX-GB1-NS4A(1–48) or the mutant plasmid pGEX-GB1-NS4A(1–48; L6E, M10E). BL31(DE3) cells were used for pUbi-NS4A(1–48) and pGEV-NS4A(1–48), respectively. Recombinant protein was produced in LB medium supplemented with the appropriate antibiotics (ampicillin or kanamycin, 100 µg/ml). Uniformly [¹⁵N] or [¹³C, ¹⁵N] isotope-labeled NS4A(1–48) was expressed at 37°C in M9 medium containing [¹³C₆] or [¹²C₆] glucose and [¹⁵N] ammonium chloride as the sole carbon and nitrogen sources, respectively. Each 1 L expression medium was inoculated with an aliquot of a 50 ml overnight culture to an optical density of 0.1 at 600 nm (OD₆₀₀). Gene expression was induced at an OD₆₀₀ of 0.8 by addition of an IPTG stock to a final IPTG concentration of 1 mM. Cells were incubated under gentle agitation (150 rpm) and harvested 5 hours after induction by centrifugation (5000 × g, 4°C, 30 min). Cell pellets were washed once in PBS buffer, spun down and stored at –20°C. Protein expression was verified using SDS-PAGE with Coomassie staining.

Purification of GST-GB1-NS4A(1–48) fusion proteins and their proteolytic cleavage

Pellets of pGEX-GB1-NS4A(1–48) or pGEX-GB1-NS4A(1–48; L6E, M10E) transformed cells harvested from 1 L expression culture, respectively, were thawed and resuspended on ice in 25 ml lysis buffer (50 mM Tris-HCl pH 8.0, 150 mM NaCl, 1 mM DTT, 0.5 mM EDTA) supplemented with protease inhibitors (Complete mini, Roche, Penzberg, Germany). Cells were lysed using 4–5 cycles in a Microfluidizer M-100P (Microfluidics, Worcestershire, UK). The crude lysate was clarified by centrifugation (50000 × g, 4°C, 30 min). Subsequent purification steps were performed at 22°C. The supernatant was applied onto a gravity flow column (column volume (CV) of 5 ml) packed with GSH sepharose 4B (GE Healthcare) and pre-equilibrated with lysis buffer. Unbound material was removed by washing with 10 CV of lysis buffer. When utilizing the mutant plasmid, on column cleavage of the GST-GB1-NS4A(1–48; L6E, M10E) fusion protein with 10 µM TEV protease (corresponding to a peptide to TEV ratio of about 100) was performed in standard buffer at 22°C overnight. The flow-through as well as the wash fractions (5 CVs) containing the free NS4A(1–48; L6E, M10E) peptide and TEV protease were pooled and concentrated to 5 ml using a Vivaspin 20 centrifugal concentrator (MWCO: 3 kDa, Sartorius, Göttingen, Germany). Separation of TEV protease from NS4A mutant peptide was accomplished with a HiLoad 16/60 Superdex 75 prep grade column (GE Healthcare) on an ÄKTA purifier system at 22°C with a flow rate of 1 ml/min. Interestingly, the GST-GB1-NS4A(1–48) wild type fusion protein could not reliably be digested under these standard conditions. Here, cell lysis had to be performed in lysis buffer supplemented with 0.5 M urea. GSH-binding and on column cleavage had to be done in the presence of 0.5 M urea and at a higher TEV concentration (50 µM, peptide to TEV ratio of about 10). Flow-through and wash was collected after TEV digestion and concentrated using Vivaspin 20 centrifugal concentrator. TEV-protease and urea was removed from the concentrated peptide solution using a Highload 16/60 Superdex 75 prep grade column, equilibrated in 50 mM Tris-HCl

```

1 S L T L N L I T E M G R L P T F M T Q K
NS4A(1-48) DENV2 TCTCTGACCCTGAACCTAATCACAGAAATGGGTAGGCTCCCAACCTTCATGACTCAGAAG 60
NS4A(1-48) E.coli AGCCTGACCCTGAATCTGATTACCGAAATGGGTCGTCTGCCGACCTTTATGACCCAGAAA 60
***** ** ** * ***** * ** * ***** ***** *****

21 A R D A L D N L A V L H T A E A G G R A
NS4A(1-48) DENV2 GCAAGAGACGCACTGGACAACCTTAGCAGTGCTGCACACGGCTGAGGCAGGTGGAAGGGCG 120
NS4A(1-48) E.coli GCACGTGATGCACTGGATAATCTGGCAGTTCTGCATACCGCTGAAGCCGGTGGTTCGTGCA 120
*** * ** ***** ** * ***** ***** ** ***** ** ***** * **

41 Y N H A L S E L *
NS4A(1-48) DENV2 TACAACCATGCTCTCAGTGAAGTGTGA 147
NS4A(1-48) E.coli TATAATCATGCACTGAGCGAAGTGTAA 147

```

Figure 1. NS4A(1–48) coding sequence. ClustalW alignment [40] of the NS4A(1–48) coding sequence as found in the viral genome of DENV type 2 and following optimization for *E. coli* expression [21].
doi:10.1371/journal.pone.0086482.g001

pH 8, 150 mM NaCl at a flow rate of 1 ml/min. NS4A containing fractions were pooled and concentrated. Cleavage, separation efficiency and final purity of the NS4A peptides were evaluated using SDS-PAGE analysis, and concentrations were calculated by measuring the absorption at 280 nm. NS4A(1–48) and the mutant peptide were kept at 4°C for short-term storage or rapidly frozen in liquid nitrogen prior to long-term storage at –80°C.

TEV protease expression

TEV protease was produced using the plasmid pRK793 (Addgene). This plasmid codes for TEV fused to highly soluble maltose-binding protein that cleaves itself *in vivo* to generate a His-tagged TEV protease catalytic domain. Because of its S219V mutation this enzyme does not show the wild type typical auto-inactivation and allows the production of a stable and highly active enzyme. Expression and purification of the protease was performed as described [24].

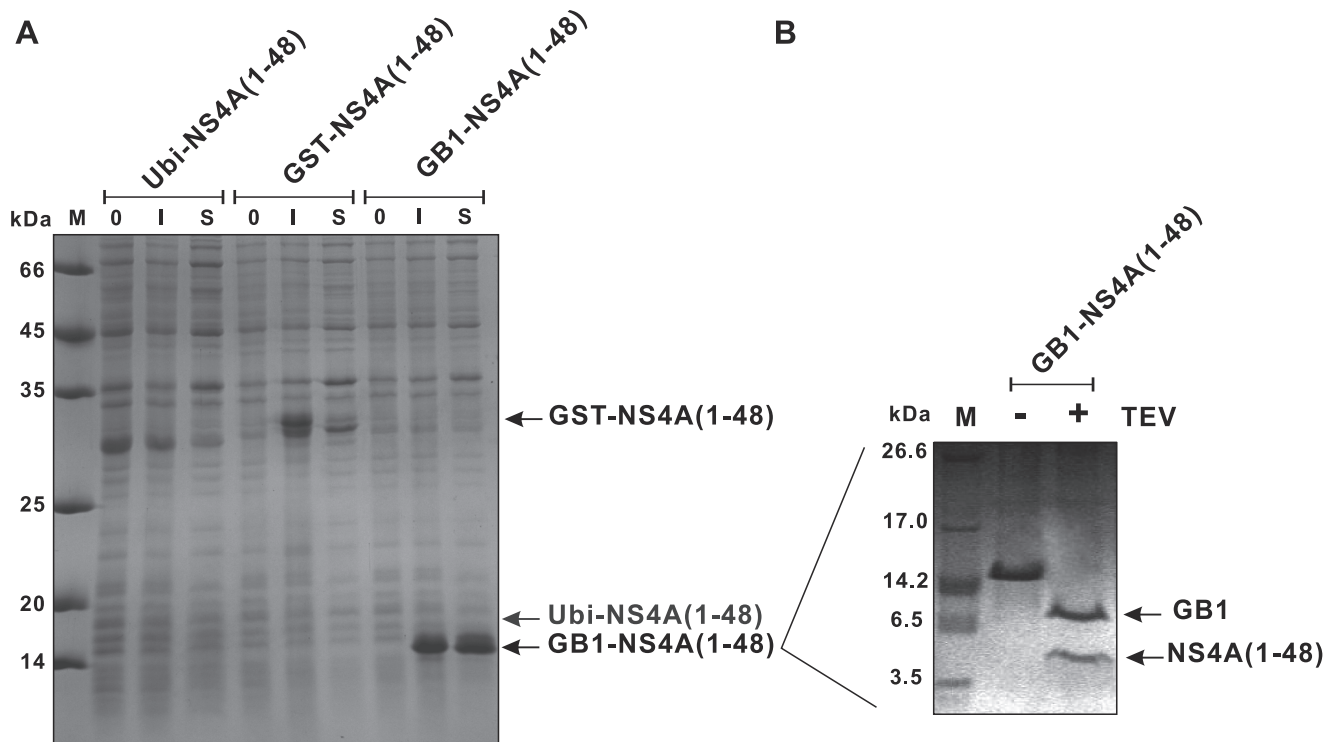


Figure 2. Comparative expression of NS4A(1–48) constructs containing single fusion tags. (A) SDS-PAGE analysis of the relative expression levels of NS4A fusions with ubiquitin (Ubi-NS4A(1–48)), glutathion-S-transferase (GST-NS4A(1–48)) and immunoglobulin-binding domain of streptococcal protein G (GB1-NS4A(1–48)). Aliquots of the expression cultures taken before (0) or 3 hours after IPTG induction (I) were applied. Aliquots of the supernatants after cell lysis (S) are shown as well. (B) TEV cleavage of the purified GB1-NS4A(1–48) fusion protein. Purified GB1-NS4A(1–48) fusion protein after size exclusion chromatography before (–) and after (+) TEV digestion together with a molecular weight marker (M; M3546, Sigma) were applied.
doi:10.1371/journal.pone.0086482.g002

Table 2. Average yields and purities of the studied NS4A(1–48) fusion proteins and of the resulting NS4A(1–48) target peptides obtained from 1 L of culture.

Fusion Tag	Yield		NS4A(1–48) Peptide					
	NS4A(1–48) Fusion Protein		after proteolytic cleavage and tag separation					
	after first purification step		Wild Type			Mutant		
	amount (mg)	purity (%)	amount (mg)	content (mg)	purity (%)	amount (mg)	recovery (%)	purity (%)
GB1	15	90	20	6.1	90	3	50	<80
GST-GB1	25	60	30	3.3	75	3	91	~98
GST-GB1*	35	60	40	4.7	75	4	85	~98

Due to the different sizes of the fusion tags (Ubi: 11.3 kDa, GST: 26.4 kDa, GB1: 7.6 kDa, GST-GB1: 34 kDa) the mass fractions of the target peptide differ significantly between the constructs (Ubi: 31.5%, GST: 16%, GB1: 40.6%, GST-GB1: 13.3%). Since Ubi and GST fusion constructs resulted in very low yields (>1 mg/l), data for these constructs have not been included. The values for GB1 and GST-GB1 have been used to calculate the theoretical NS4A(1–48) content after the first purification step for each of the constructs shown. Despite an unfavorable target peptide to fusion tag ratio highest recovery and purity values were obtained with the dual GST-GB1-NS4A(1–48) construct after proteolytic cleavage and tag removal. LB medium was used if not stated otherwise. An asterisk (*) indicates isotope (^{13}C , ^{15}N) or [^{15}N] labeled minimal growth medium. Note that the overall peptide yields were higher in minimal medium compared to those in rich LB medium. Amount and purity of the fusion protein tagged peptides as well as the purity of the free peptides has been estimated from SDS PAGE analysis. Final free peptide yields were additionally calculated by measuring the concentration of the peptides at 280 nm using an extinction coefficient of $1490 \text{ M}^{-1} \text{ cm}^{-1}$ in water.

doi:10.1371/journal.pone.0086482.t002

Mass spectrometric analysis

Identity of the NS4A peptides was confirmed using mass spectrometry. NS4A(1–48) peptide bands were excised from SDS polyacrylamide gels and subjected to tryptic digestion. Peptide fragment analysis was performed using an LC-MS/MS instrument (nanoUPLC-QTOF Premier, Waters Corp., Milford, MA, USA). These experiments were performed at the technology platform Integrated Functional Genomics of the Interdisciplinary Center for Clinical Research of the University of Münster, Germany.

NMR spectroscopy

2D (^1H - ^{15}N)-BEST-TROSY spectra [25] were recorded at 303.15 K on a Varian ^1H INNOVA NMR spectrometer equipped with a cryogenic Z-axis PFG triple resonance probe operating at a proton frequency of 600 MHz. Data were processed with NMRPipe [26] and analyzed with CcpNmr analysis [27]. NMR samples contained 1 mM [^{15}N] labeled NS4A(1–48) or NS4A(1–48; L6E, M10E), respectively, in 50 mM sodium phosphate buffer (pH 6.8) with 10% (v/v) deuterium oxide and 0.03% (w/v) NaN_3 .

Results and Discussion

Codon adaption of the NS4A(1–48) coding sequence

Only negligible amounts of NS4A peptide could be obtained when the original DENV type 2 cDNA sequence encoding the first 48 residues of NS4A, NS4A(1–48), was used in a pGEX expression vector. This may be explained by the fact that the viral DNA sequence for NS4A(1–48) is not optimal for expression in *E. coli* cells, due to different codon usage. Specifically several codons for leucine, isoleucine and arginine occurring in the viral gene sequence are “rare codons” in *E. coli* (Fig. 1). Rare codons are known to cause translational problems such as low protein expression and frame shifts [28]. Thus the codons were optimized for expression in *E. coli* cells and chemically synthesized oligonucleotides were used to create a synthetic NS4A(1–48) DNA cassette, which was then used to generate several NS4A(1–48) expression constructs.

Expression yields of NS4A(1–48) strongly vary between different fusion tags

To identify the ideal conditions for NS4A(1–48) expression, the expression levels of codon-optimized NS4A(1–48) linked to three different kinds of fusion tags in *E. coli* cells were tested (Fig. 2A). *E. coli* BL21 harboring pGEX-TEV-NS4A(1–48) and BL21(DE3) cells harboring pUbi-NS4A(1–48) or pGEV-NS4A(1–48) were induced with IPTG for the indicated time, a band corresponding to the full-length NS4A(1–48) fusion protein was detected in the Coomassie-stained gel for the GST and the GB1 fusions. A full-length NS4A(1–48) fusion protein could not be detected for Ubi-NS4A(1–48) using Coomassie staining. However, western blot analysis confirmed its expression (data not shown). Highest expression levels of NS4A(1–48) were detected with the GB1 fusion tag. As all the plasmids contained the same optimized NS4A sequence the GB1 domain seems to account for these high expression levels presumably by stabilizing the NS4A(1–48) peptide. In addition, only the GB1-NS4A(1–48) fusion protein could be efficiently extracted to the soluble fraction after cell lysis without adding detergents. These findings are in line with previous observations [18,29]. The average yields for the three expression constructs are summarized in the upper part of table 2. The highest amount of target peptide was produced with pGEV-NS4A(1–48). Subsequently, the GB1-NS4A(1–48) fusion was purified as described [18], however, TEV protease was used

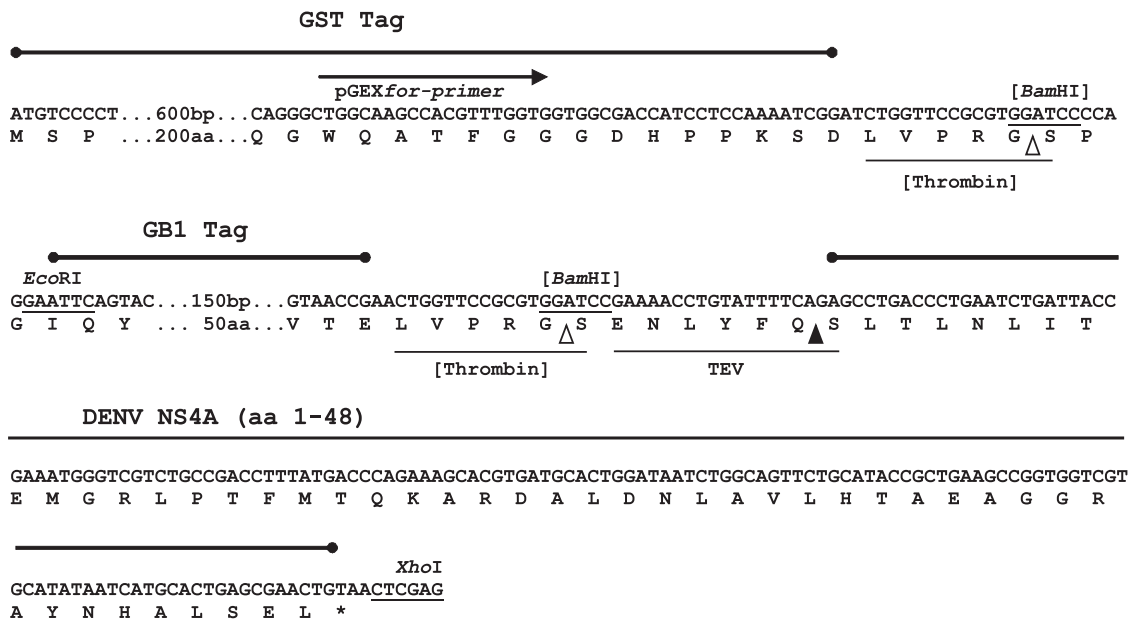


Figure 3. Expression/cloning region of pGEX-GB1-NS4A(1-48). The GB1-NS4A(1-48) sequence was inserted into pGEX-4T-2 between the *EcoRI* and *XhoI* sites. Protease recognition motifs are underlined while the cleavage sites are marked by triangles. The two thrombin sites, which originate from the vector backbone of pGEX and pGEV, respectively, are shown in brackets and were not used in our protocol. Note that TEV digestion produces a native NS4A peptide. doi:10.1371/journal.pone.0086482.g003

instead of Factor Xa. The optimum recognition site for TEV is Glu-Asn-Leu-Tyr-Phe-Gln-(Gly/Ser) (ENLYFQ(G/S)) and cleavage occurs between the Gln and Gly/Ser residues [30]. DENV NS4A starts with serine and thus TEV cleavage allows a very

specific and efficient removal of the fusion tag without any artificial overhang. Briefly, the GB1 fusion protein was extracted from the cell lysate by a simple heating step followed by size exclusion chromatography yielding approximately 90% pure

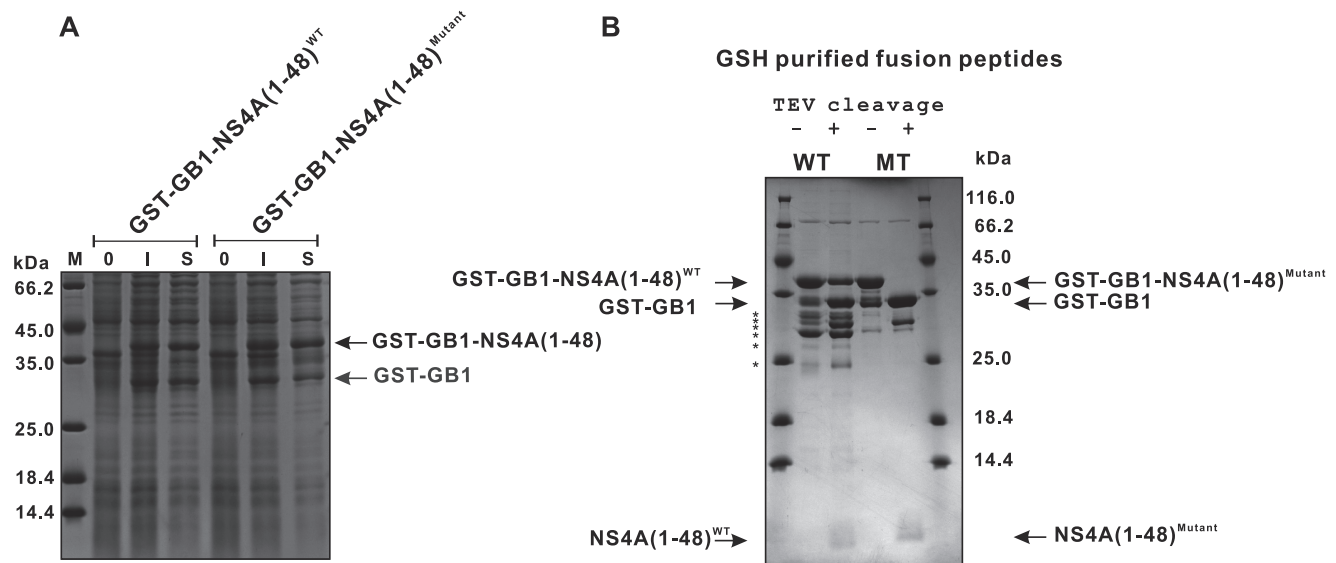


Figure 4. Expression of NS4A(1-48) wild type and mutant peptides using a dual GST-GB1 tag. (A) Relative expression levels of GST-GB1-NS4A(1-48) and the GST-GB1-NS4A(1-48; L6E, M10E) mutant were analyzed by SDS-PAGE using aliquots of the expression cultures. Shown are samples obtained from culture at 0 (0) or 3 hours (I) following IPTG induction or the supernatant after cell lysis (S). (B) TEV digest of GST-GB1-NS4A(1-48) wild type and mutant protein fusions. Aliquots of GSH-purified supernatants of wild type and mutant fusion proteins before and after TEV cleavage are shown. Note that besides the GST-GB1-NS4A(1-48) full-length product also shorter fragments, likely GST-GB1 and other truncation fragments, marked by asterisks were produced, which are present in the GSH-purified samples already prior to TEV cleavage. Because staining of free NS4A(1-48) peptides is very faint under the conditions used, the progress of the TEV digest is monitored by observing the decrease of the band for the dual tagged GST-GB1-NS4A(1-48) fusion protein in parallel with an increase of the band for the free GST-GB1 dual tag. A densitometric analysis of the respective bands revealed a cleavage efficiency of approximately 50% for the wild type peptide. doi:10.1371/journal.pone.0086482.g004

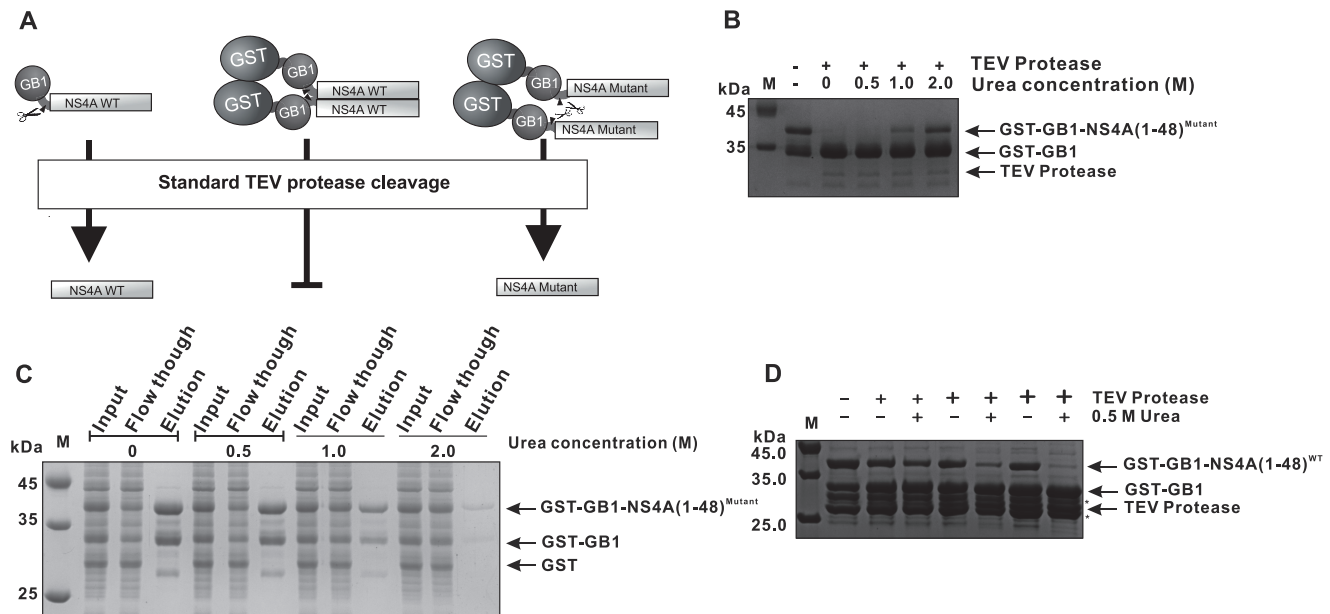


Figure 5. Optimization of TEV protease cleavage conditions. (A) A schematic model explaining the resistance of the GST-GB1 dual tagged wild type NS4A(1–48) peptide to TEV cleavage. Scissors illustrate the protease while the triangles represent the position of the cleavage sites. GST induced oligomerization of wild type NS4A(1–48) may block the protease cleavage site. (B) Analysis of the urea tolerance of TEV protease activity. GST-GB1 tag removal from NS4A(1–48; L6E, M10E) in the presence of different concentrations of urea (M). Fusion peptides were incubated with TEV protease at 20°C for 16 h at a fusion peptide to protease molar ratio of approximately 100. (C) Binding properties of GST-GB1-NS4A(1–48) to GSH sepharose in the presence of urea. Equal amounts of the fusion peptide were subjected to a mini-scale GSH-affinity chromatography in the presence of different concentrations of urea (M). Input, flow-through and elution fractions were analyzed by 15% SDS-PAGE. (D) TEV cleavage efficiency of wild type NS4A(1–48) peptide in the presence of urea. GST-GB1 tag removal from NS4A(1–48) in the presence of different concentrations of urea given in Molar. Fusion peptides were incubated in the absence (–) or presence (+) of TEV protease at 20°C for 16 h. The different “+” font sizes indicate the increasing amounts of TEV protease with fusion peptide to protease molar ratios of approximately 100, 50 and 10. The progress of the TEV digest is monitored by observing the decrease of the band of the dual tagged GST-GB1-NS4A(1–48) fusion protein and a parallel increase of the free GST-GB1 dual tag band (B, D).

doi:10.1371/journal.pone.0086482.g005

fusion protein. TEV cleavage of the GB1 fusion protein was complete after about 16 h when using a fusion protein to protease ratio of about 100 (Fig. 2B). However, we were not able to efficiently separate the cleaved NS4A(1–48) peptide from the GB1 domain. Separation by size exclusion chromatography was hampered by similar elution behavior of both molecules, which have similar molecular weights (5223.7 Da for NS4A(1–48) and 7585.3 Da for GB1). Thus IgG sepharose affinity chromatography was used following an established protocol [22]. However, the GB1 domain could not be completely removed even when IgG sepharose was applied in large excess. This suggests that the heating step might have caused misfolding of a substantial fraction (up to 20%) of GB1 causing the observed leakage during affinity chromatography. Subjecting the digest reaction to diverse reverse phase chromatography resins did not yield satisfying results either. The target NS4A(1–48) peptide showed a strong tendency to remain on the column even at high acetonitrile concentrations, presumably due to its amphipathic nature (data not shown). Consequently, the highest purity that could be achieved for untagged NS4A(1–48) was about 80% with an average recovery of 60% (see Table 2).

Additional tagging of GB1-NS4A with GST allows a simplified separation of NS4A(1–48) from the fusion tag

Due to the difficulties in separating NS4A(1–48) from GB1 after TEV protease cleavage as described above, we decided to add an additional amino terminal GST tag to the protein (Fig. 3). The relative expression levels achieved with this construct and the

respective mutant construct were evaluated using SDS-PAGE (Fig. 4A). The data demonstrate proper and stable expression of NS4A(1–48) fusion proteins. The GST-GB1 fusions could be easily purified using GSH sepharose. The average yields of the GST-GB1-NS4A peptide fusions are given in Table 2. TEV cleavage under standard conditions could efficiently remove the dual tag from the NS4A(1–48; L6E, M10E) mutant peptide. However, the GST-GB1-NS4A(1–48) wild type construct showed unexpectedly low cleavage efficiency (Fig. 4B).

Addition of urea improves the TEV cleavage of the wild type NS4A(1–48) peptide

GST is known to form dimers in solution [31–33]. Examples of GST-induced oligomerization of GST fusion proteins can be found in the literature [34–36]. Such a GST-induced oligomerization might also explain the observed resistance of a substantial fraction of wild type GST-GB1-NS4A(1–48) to TEV cleavage under standard conditions (Fig. 4B). Previous results from our laboratory indicate that the amino terminal AH of NS4A plays a role in the homo-oligomerization of NS4A [6]. We speculated that the purified GST-GB1-NS4A(1–48) peptides might self-associate and thus block the TEV recognition site (see Fig. 5A for explanation). The NS4A mutant peptide, which is expected to show a reduced self-association, was easily cleaved supporting the above notion. We optimized the TEV digestion reaction conditions with the aim to decrease the NS4A peptide self-association without reducing the proteolytic activity of TEV. Denaturing or chaotropic reagents like urea are typically used to

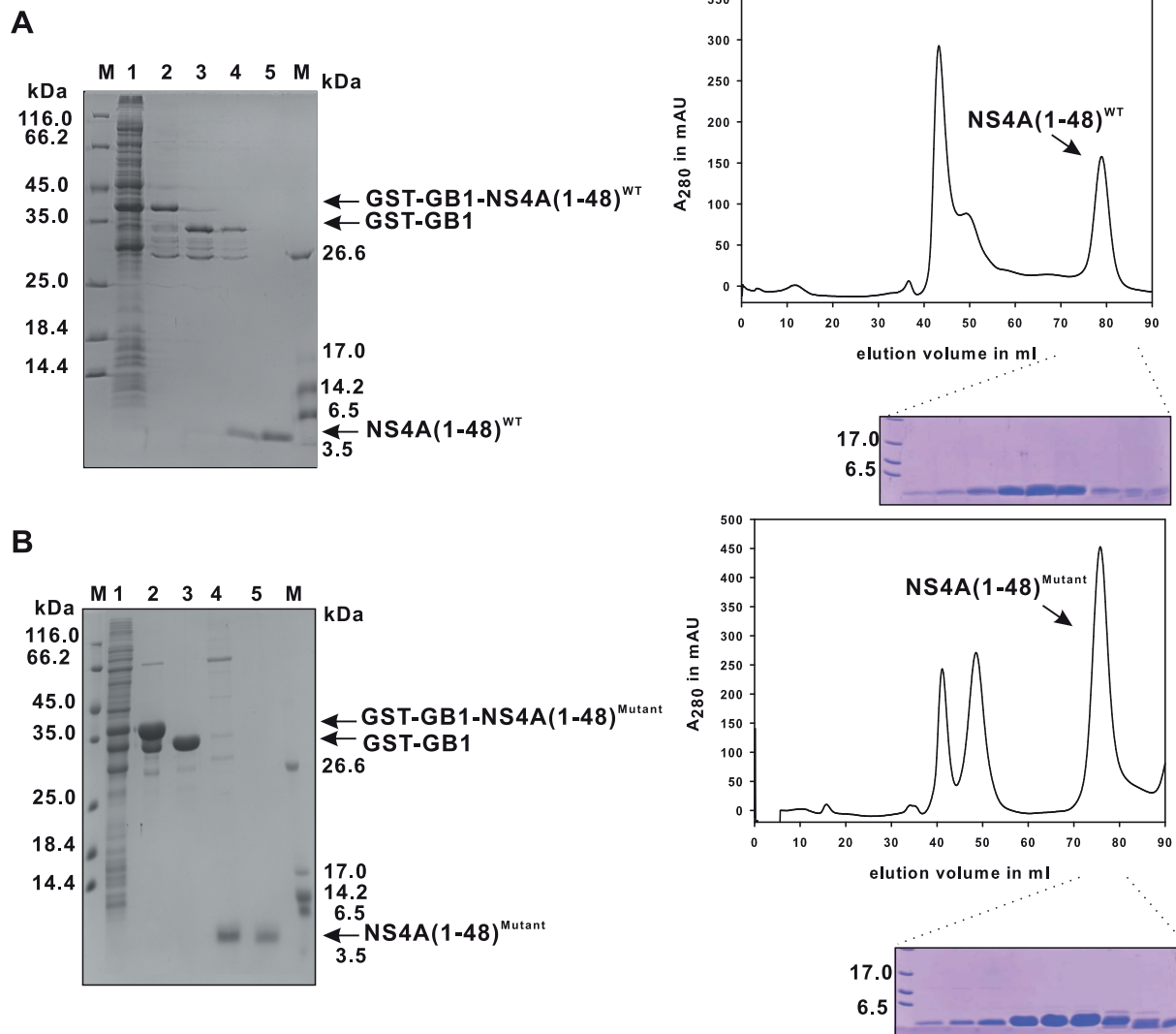


Figure 6. Purification of recombinant NS4A(1–48) wild type and mutant peptides. The 15% SDS-PAGE gel containing samples from various steps in the purification procedure is shown on the left. The wild type peptide is shown in (A) while the mutant is shown in (B). The supernatant after cell lysis is shown in lane 1. The lysate containing the peptide was loaded on a GSH sepharose column (lane 2), and cleaved by TEV protease on the column, the cleaved protein is shown in lane 3. The GSTfusion tag remained bound to the column, while the NS4A(1–48) peptide was collected from the flow-through (lane 4). The peptide was further purified by size exclusion chromatography (lane 5). The mutant peptide was purified using the same strategy (B). The respective size exclusion chromatography profiles (HiLoad 16/60 Superdex 75 prep grade) of the flow-through fraction from the TEV protease on column cleavage step - mainly containing TEV protease and NS4A(1–48; L6E, M10E) or NS4A(1–48) peptides - are shown on the right with the matching SDS-PAGE analysis of the NS4A containing fractions.

doi:10.1371/journal.pone.0086482.g006

break up such aggregates. TEV activity studies by Sun *et al.* suggested that a recombinant TEV protease can retain most of its activity at relatively high concentrations of denaturants such as 2 M urea [37]. In contrast Waugh *et al.* reported a lower urea tolerance of 0.5 M for TEV [38]. Therefore, we first tested the GST-GB1-NS4A(1–48; L6E, M10E) mutant construct, which easily can be digested without additives, to assay the urea tolerance of TEV protease under our experimental conditions. At low urea concentrations (up to 0.5 M), no loss of TEV activity was observed (Fig. 5B). Higher urea concentrations (1–2 M) resulted in a significant activity loss of more than 50%, as described by Waugh [38]. Our results indicate that the NS4A peptide aggregation is perhaps a cooperative process. Therefore, addition of chaotropic molecules early on in the purification process might further improve the final yield of target protein. In order to add urea

already to the lysis buffer further optimization was required. It was important to ensure that GST binding to GSH sepharose will not be affected by the added urea. An earlier study indicated that GST binds to GSH sepharose in presence of chaotropic reagents like 2–3 M guanidine hydrochloride or urea [39]. We independently assessed the binding properties of GST-GB1-NS4A(1–48) to GSH sepharose in the presence of increasing urea concentrations (Fig. 5C). Addition of 0.5 M of urea did not alter the binding behavior of GST to GSH sepharose. However, higher urea concentrations resulted in a drastic shift of the GST-GB1-NS4A(1–48) peak from the elution to the flow-through fractions. Next we assayed the TEV cleavage efficiency for the double tagged wild type NS4A(1–48) fusion construct in the presence of increasing urea concentrations. Conveniently, 0.5 M urea was sufficient to initiate the removal of GST-GB1 tag (figure 5D). Yet,

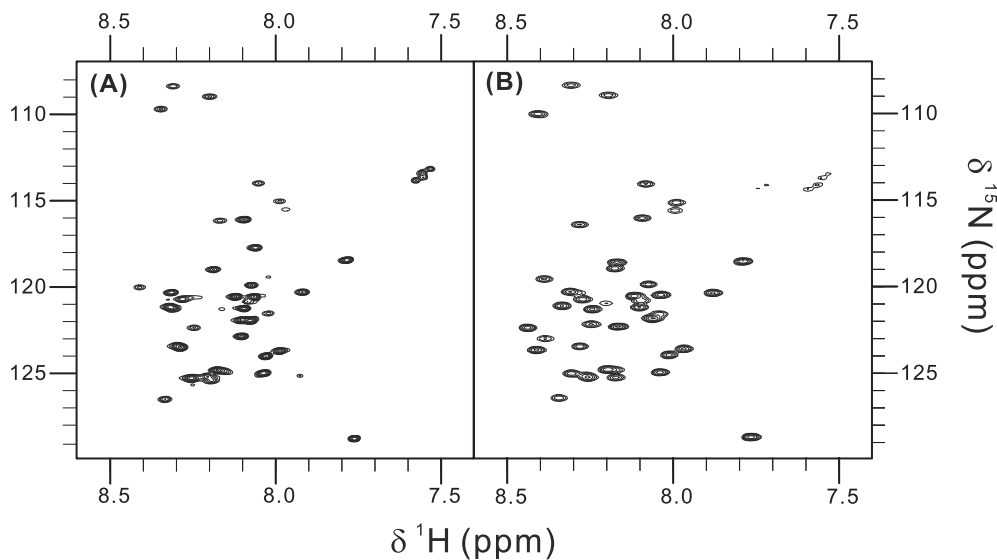


Figure 7. Recorded 2D (^1H , ^{15}N)-BEST-TROSY spectra of the purified NS4A peptides. Spectrum of 0.5 mM [^{15}N]-NS4A(1–48) wild type (A) and of 1 mM mutant (L6E, M10E) peptide (B) in 50 mM sodium phosphate buffer, pH 6.8. Data were recorded at 30°C. doi:10.1371/journal.pone.0086482.g007

TEV protease amounts had to be increased at least 5-fold compared to the cleavage reaction of the mutant peptide. Nevertheless, under these conditions, nearly complete removal of GST-GB1 from the wild type NS4A(1–48) peptide was achieved.

The GST-GB1 fusion allows a nearly identical purification protocol for both wild type and mutant NS4A peptides

Production of diverse mutant forms of NS4A(1–48) besides the wild type is necessary for an in-depth structure-function-analysis. Our aim was, to establish a general purification procedure applicable to various NS4A(1–48) mutant peptides. Therefore, purification steps that are sensitive to changes in peptide charge or hydrophobicity, as it would be the case when applying ion exchange or reverse phase chromatography, were avoided. The feasibility of our simple purification procedure, which is based exclusively on GSH-affinity and size exclusion chromatography, is demonstrated for the wild type peptide and for the NS4A(1–48; L6E, M10E) mutant as an example. This NS4A(1–48) mutant carries glutamate substitutions at positions 6 and 10 instead of leucine and methionine, respectively, resulting in a shift of the isoelectric point from 6 to 5 and a considerably decreased hydrophobicity of the peptide. The purification progress for the wild type and the mutant NS4A(1–48) peptides is summarized in figure 6. In both cases highly purified peptides could be obtained after size exclusion chromatography. The identity of the peptides was confirmed by in-gel tryptic digestion of the electrophoretically separated protein band and mass spectrometric peptide mapping. As summarized in table 2 we could obtain up to 3 mg untagged wild type and up to 4 mg mutant peptide of very high purity (approx. 98%) from 1 liter culture in rich medium. These values indicate an almost complete TEV cleavage as well as an efficient separation of the peptides from the dual tag, which was not possible with the GB1 single tag system. Thus, our dual tag strategy provides an efficient way for producing NS4A(1–48) in *E.coli*.

Peptide labeling with stable isotope and initial nuclear magnetic resonance spectra

Peptides labeled with the stable isotopes ^{15}N and ^{13}C can be studied in great detail by nuclear magnetic resonance (NMR) spectroscopy. Solution NMR is the method of choice for the structural investigation of conformationally flexible peptides. Using the double tagged GST-GB1-NS4A(1–48) fusion protein we could easily produce even higher amounts of labeled NS4A(1–48) by growing the *E. coli* cells in minimal medium supplemented with [^{15}N] ammonium chloride with either [$^{12}\text{C}_6$] or [$^{13}\text{C}_6$] glucose as sole nitrogen and carbon sources (Table 2). Production of uniformly ^{15}N -labeled NS4A(1–48) peptides in minimal medium resulted in very similar peptide yields and purity as in case of doubly labeled peptide. 2D (^1H - ^{15}N)-BEST-TROSY spectra of NS4A wild type and mutant peptides in aqueous buffer are shown in figure 7. The position and low spectral dispersion of the observed amide ^1H - ^{15}N cross signals indicate unstructured peptides. This is in good agreement with our earlier circular dichroism (CD) data on these two peptides in aqueous buffer [6]. These results indicate that the amount of highly pure isotope-labeled NS4A peptides produced using the described double tag strategy is sufficient for future multidimensional NMR experiments. These experiments are required for peptide resonance assignment and for gathering information regarding the structure of the peptides and their dynamics in presence of membranes or membrane mimetic model systems.

Conclusion

Our GST-GB1 fusion approach represents a valuable tool for preparing milligram amounts of unlabeled or isotope labeled NS4A(1–48) peptides. This is an important prerequisite for a detailed analysis of the structure-function relationship of the amino terminal region of NS4A with the aim to elucidate the mechanism how this region interacts with membranes. The results may lead to new antiviral strategies to fight DENV. In general the presented production procedure may also aid the characterization of other aggregation prone proteins that are frequently coded in viral genomes.

Acknowledgments

We thank David Waugh (Macromolecular Crystallography Laboratory, Center for Cancer Research, National Cancer Institute at Frederick, Frederick, Maryland, USA) for the TEV expression vector and Toshiyuki Kohno (Mitsubishi Kagaku Institute of Life Sciences (MITILS), Machida, Tokyo 194-8511, Japan) for pTKK19ubi. We are grateful to Simone König (Integrated Functional Genomics, Interdisciplinary Clinical Research Center, Medical Faculty, University of Münster, D-48149,

Germany) for mass spectrometric analysis and to Ella Sklan (Department Clinical Microbiology and Immunology, Sackler School of Medicine, Tel Aviv University) for improving this manuscript.

Author Contributions

Conceived and designed the experiments: SH BWK DW. Performed the experiments: YFH OV SS OS. Analyzed the data: YFH SH SS. Wrote the paper: SH YFH DW BWK.

References

- Bhatt S, Gething PW, Brady OJ, Messina JP, Farlow AW, et al. (2013) The global distribution and burden of dengue. *Nature*.
- Clyde K, Kyle JL, Harris E (2006) Recent advances in deciphering viral and host determinants of dengue virus replication and pathogenesis. *J Virol* 80: 11418–11431.
- Miller S, Kastner S, Krijnse-Locker J, Buhler S, Bartenschlager R (2007) The non-structural protein 4A of dengue virus is an integral membrane protein inducing membrane alterations in a 2K-regulated manner. *J Biol Chem* 282: 8873–8882.
- Mackenzie JM, Khromykh AA, Jones MK, Westaway EG (1998) Subcellular localization and some biochemical properties of the flavivirus Kunjin nonstructural proteins NS2A and NS4A. *Virology* 245: 203–215.
- Roosendaal J, Westaway EG, Khromykh A, Mackenzie JM (2006) Regulated cleavages at the West Nile virus NS4A-2K-NS4B junctions play a major role in rearranging cytoplasmic membranes and Golgi trafficking of the NS4A protein. *J Virol* 80: 4623–4632.
- Stern O, Hung YF, Valda O, Yaffe Y, Harris E, et al. (2013) An N-terminal amphipathic helix in the Dengue virus nonstructural protein 4A mediates oligomerization and is essential for replication. *J Virol*.
- Sapay N, Guernier Y, Delage G (2006) Prediction of amphipathic in-plane membrane anchors in monotopic proteins using a SVM classifier. *BMC Bioinformatics* 7: 255.
- Jao CC, Hegde BG, Gallop JL, Hegde PB, McMahon HT, et al. (2010) Roles of amphipathic helices and the bin/amphiphysin/rvs (BAR) domain of endophilin in membrane curvature generation. *J Biol Chem* 285: 20164–20170.
- Lee MC, Orci L, Hamamoto S, Futai E, Ravazzola M, et al. (2005) Sar1p N-terminal helix initiates membrane curvature and completes the fission of a COPII vesicle. *Cell* 122: 605–617.
- McMahon HT, Gallop JL (2005) Membrane curvature and mechanisms of dynamic cell membrane remodeling. *Nature* 438: 590–596.
- Elazar M, Cheong KH, Liu P, Greenberg HB, Rice CM, et al. (2003) Amphipathic helix-dependent localization of NS5A mediates hepatitis C virus RNA replication. *J Virol* 77: 6055–6061.
- Elazar M, Liu P, Rice CM, Glenn JS (2004) An N-terminal amphipathic helix in hepatitis C virus (HCV) NS4B mediates membrane association, correct localization of replication complex proteins, and HCV RNA replication. *J Virol* 78: 11393–11400.
- Gouttenoire J, Castet V, Montserret R, Arora N, Raussens V, et al. (2009) Identification of a novel determinant for membrane association in hepatitis C virus nonstructural protein 4B. *J Virol* 83: 6257–6268.
- Penin F, Brass V, Appel N, Ramboarina S, Montserret R, et al. (2004) Structure and function of the membrane anchor domain of hepatitis C virus nonstructural protein 5A. *J Biol Chem* 279: 40835–40843.
- Spuul P, Salonen A, Merits A, Jokitalo E, Kaariainen L, et al. (2007) Role of the amphipathic peptide of Semliki forest virus replicase protein nsP1 in membrane association and virus replication. *J Virol* 81: 872–883.
- Teterina NL, Gorbalenya AE, Egger D, Bienz K, Rinaudo MS, et al. (2006) Testing the modularity of the N-terminal amphipathic helix conserved in picornavirus 2C proteins and hepatitis C NS5A protein. *Virology* 344: 453–467.
- Cho NJ, Dvory-Sobol H, Lee C, Cho SJ, Bryson P, et al. (2010) Identification of a class of HCV inhibitors directed against the nonstructural protein NS4B. *Sci Transl Med* 2: 15ra16.
- Koenig BW, Rogowski M, Louis JM (2003) A rapid method to attain isotope labeled small soluble peptides for NMR studies. *J Biomol NMR* 26: 193–202.
- Kohno T, Xiang L, Inaoka Y, Hayashi K, Suzuki C, et al. (2008) High-Efficiency and Robust Expression System for Stable Isotope-Labeled Peptides. *Int J Pept Res Ther* 14: 157–165.
- Kohno T, Kusunoki H, Sato K, Wakamatsu K (1998) A new general method for the biosynthesis of stable isotope-enriched peptides using a decahistidine-tagged ubiquitin fusion system: an application to the production of mastoparan-X uniformly enriched with ¹⁵N and ¹⁵N/¹³C. *J Biomol NMR* 12: 109–121.
- Fath S, Bauer AP, Liss M, Spriestersbach A, Maertens B, et al. (2011) Multiparameter RNA and codon optimization: a standardized tool to assess and enhance autologous mammalian gene expression. *PLoS One* 6: e17596.
- Huth JR, Bewley CA, Jackson BM, Hinnebusch AG, Clore GM, et al. (1997) Design of an expression system for detecting folded protein domains and mapping macromolecular interactions by NMR. *Protein Sci* 6: 2359–2364.
- Hemsley A, Arnheim N, Toney MD, Cortopassi G, Galas DJ (1989) A simple method for site-directed mutagenesis using the polymerase chain reaction. *Nucleic Acids Res* 17: 6545–6551.
- Kapust RB, Tozser J, Fox JD, Anderson DE, Cherry S, et al. (2001) Tobacco etch virus protease: mechanism of autolysis and rational design of stable mutants with wild-type catalytic proficiency. *Protein Eng* 14: 993–1000.
- Favier A, Brutscher B (2011) Recovering lost magnetization: polarization enhancement in biomolecular NMR. *J Biomol NMR* 49: 9–15.
- Delaglio F, Grzesiek S, Vuister GW, Zhu G, Pfeifer J, et al. (1995) NMRPipe: a multidimensional spectral processing system based on UNIX pipes. *J Biomol NMR* 6: 277–293.
- Vranken WF, Boucher W, Stevens TJ, Fogh RH, Pajon A, et al. (2005) The CCPN data model for NMR spectroscopy: development of a software pipeline. *Proteins* 59: 687–696.
- Kane JF (1995) Effects of rare codon clusters on high-level expression of heterologous proteins in *Escherichia coli*. *Curr Opin Biotechnol* 6: 494–500.
- Bao WJ, Gao YG, Chang YG, Zhang TY, Lin XJ, et al. (2006) Highly efficient expression and purification system of small-size protein domains in *Escherichia coli* for biochemical characterization. *Protein Expr Purif* 47: 599–606.
- Kapust RB, Tozser J, Copeland TD, Waugh DS (2002) The P1' specificity of tobacco etch virus protease. *Biochem Biophys Res Commun* 294: 949–955.
- Kaplan W, Husler P, Klump H, Erhardt J, Sluis-Cremer N, et al. (1997) Conformational stability of pGEX-expressed *Schistosoma japonicum* glutathione S-transferase: a detoxification enzyme and fusion-protein affinity tag. *Protein Sci* 6: 399–406.
- Lim K, Ho JX, Keeling K, Gilliland GL, Ji X, et al. (1994) Three-dimensional structure of *Schistosoma japonicum* glutathione S-transferase fused with a six-amino acid conserved neutralizing epitope of gp41 from HIV. *Protein Sci* 3: 2233–2244.
- McTigue MA, Williams DR, Tainer JA (1995) Crystal structures of a schistosomal drug and vaccine target: glutathione S-transferase from *Schistosoma japonica* and its complex with the leading antischistosomal drug praziquantel. *J Mol Biol* 246: 21–27.
- Niedziela-Majka A, Rymarczyk G, Kochman M, Ozyhar A (1998) GST-Induced dimerization of DNA-binding domains alters characteristics of their interaction with DNA. *Protein Expr Purif* 14: 208–220.
- Qiu W, Derr ND, Goodman BS, Villa E, Wu D, et al. (2012) Dynein achieves processive motion using both stochastic and coordinated stepping. *Nat Struct Mol Biol* 19: 193–200.
- Tudyka T, Skerra A (1997) Glutathione S-transferase can be used as a C-terminal, enzymatically active dimerization module for a recombinant protease inhibitor, and functionally secreted into the periplasm of *Escherichia coli*. *Protein Sci* 6: 2180–2187.
- Sun C, Liang J, Shi R, Gao X, Zhang R, et al. (2012) Tobacco etch virus protease retains its activity in various buffers and in the presence of diverse additives. *Protein Expr Purif* 82: 226–231.
- Waugh DS (2011) An overview of enzymatic reagents for the removal of affinity tags. *Protein Expr Purif* 80: 283–293.
- Smith DB, Corcoran LM (2001) Expression and purification of glutathione-S-transferase fusion proteins. *Curr Protoc Mol Biol* Chapter 16: Unit16 17.
- Larkin MA, Blackshields G, Brown NP, Chenna R, McGettigan PA, et al. (2007) Clustal W and Clustal X version 2.0. *Bioinformatics* 23: 2947–2948.

3.3 Dengue virus NS4A cytoplasmic domain binding to liposomes stabilizes membrane curvature

Dengue virus NS4A cytoplasmic domain binding to liposomes stabilizes membrane curvature

Yu-Fu Hung^{a,b}, Melanie Schwarten^a, Sven Schünke^{a,1}, Pallavi Thiagarajan-Rosenkranz^{a,2}, Silke Hoffmann^a, Ella H. Sklan^c, Dieter Willbold^{a,b}, Bernd W. Koenig^{a,b,*}

^a Institute of Complex Systems, Structural Biochemistry (ICS-6), Forschungszentrum Jülich, 52425 Jülich, Germany

^b Institut für Physikalische Biologie, Heinrich-Heine-Universität Düsseldorf, Universitätsstraße 1, 40225 Düsseldorf, Germany

^c Department Clinical Microbiology and Immunology, Sackler School of Medicine, Tel Aviv University, Tel Aviv 69978, Israel

*Corresponding author:

E-mail address: b.koenig@fz-juelich.de

Phone: (+49) 2461 – 615 385

Fax: (+49) 2461 - 612 023

¹ Present address: Nestlé France, Atrium RDC, 7 Boulevard Pierre Carle, 77186 Noisiel, France

² Present address: Department of Chemistry, University of Illinois at Chicago, 845 West Taylor Street, Chicago, IL 60607, United States

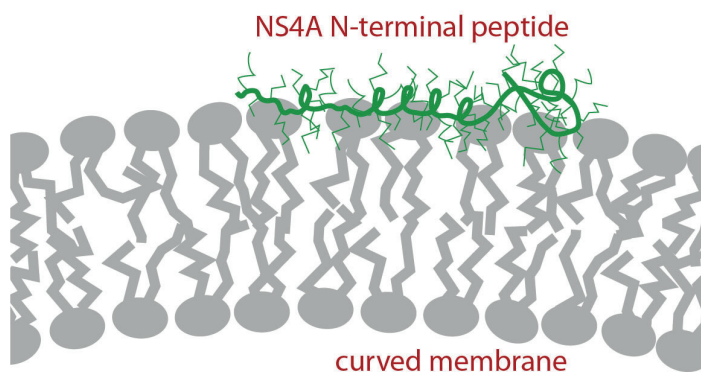
Abbreviations:

AH, amphipathic α -helix; CD, circular dichroism; DENV, dengue virus; DLS, dynamic light scattering; ER, endoplasmic reticulum; HCV, hepatitis C virus; NMR, nuclear magnetic resonance; NOE, nuclear Overhauser effect; NS4A, non-structural protein 4A; NS4A(1-48), amino acids 1 to 48 of NS4A; pTMS, predicted transmembrane segment; RCI, random coil index; RU, response units; SPR, surface plasmon resonance; SUV, small unilamellar vesicle; TLC, thin layer chromatography

Highlights

- NS4A(1-48) and peptide from replication deficient mutant are characterized
- NMR backbone assignments and peptide secondary structures in micelles are reported
- Both wild type and mutant peptides contain two amphipathic helices
- Wild type NS4A(1-48) shows stronger binding to liposomes compared to the mutant
- NS4A(1-48) binds preferentially to highly curved lipid membranes

Graphical Abstract:



Abstract

Dengue virus (DENV) infection is a growing public health threat with more than one-third of the world population at risk. Non-structural protein 4A (NS4A), one of the least characterized viral proteins, is a highly hydrophobic transmembrane protein thought to induce the membrane alterations that harbor the viral replication complex. The NS4A N-terminal (amino acids 1-48), has been proposed to contain an amphipathic α -helix (AH). Mutations (L6E;M10E) designed to reduce the amphipathic character of the predicted AH, abolished viral replication and reduced NS4A oligomerization. Nuclear magnetic resonance (NMR) spectroscopy was used to characterize the N-terminal cytoplasmic region (amino acids 1-48) of both wild type and mutant NS4A in presence of SDS micelles. Binding of the two N-terminal NS4A peptides to liposomes was studied as a function of membrane curvature and lipid composition. The NS4A N-terminal was found to contain two AHs separated by a non-helical linker. The above mentioned mutations did not significantly affect the helical secondary structure of this domain. However, they reduced the affinity of the N-terminal NS4A domain for lipid membranes. Binding of wild type NS4A(1-48) to liposomes is highly dependent on membrane curvature.

Keywords

Dengue Virus; non-structural protein NS4A; amphipathic helix; curvature sensing; NMR spectroscopy; peptide membrane interaction

1. Introduction

Dengue virus (DENV) is an enveloped, positive sense single-stranded RNA virus that belongs to the *Flaviviridae*, a family that includes other major pathogens. The mosquito-borne DENV is the causative agent of dengue fever, the most rapidly spreading arboviral disease in humans [1].

After entering the host cell via endocytic pathways [2], the viral RNA is translated into a single polyprotein which is then processed by cellular and viral proteases to produce the structural capsid (C), premembrane (prM) and envelope (E) proteins and the non-structural (NS) proteins NS1, NS2A, NS2B, NS3, NS4A, NS4B, and NS5 [3]. In contrast to the structural proteins, NS proteins, are not a part of the mature DENV particle, however most of them were shown to be involved in viral replication.

DENV RNA synthesis occurs within replication complexes containing essential NS proteins, such as NS5 the viral RNA-dependent RNA polymerase, the viral RNA and host cell factors [4]. The replication complexes are located within a virus-induced and endoplasmic reticulum (ER)-derived complex membrane network [5, 6] consisting of interconnected lipid vesicles and convoluted membranes [7]. NS4A localizes to the DENV replication complex and was found to be sufficient to induce host membrane alterations resembling the virus-induced membrane rearrangements [3].

NS4A is a hydrophobic 16 kDa transmembrane protein containing four predicted transmembrane segments (pTMSs) [3]. The C-terminal pTMS, also known as the 2K fragment, is a signal peptide for the ER localization of NS4B and is not part of the mature NS4A [8]. Experimental evidence shows that the predicted TMS1 and 3 indeed span the membrane. In contrast, pTMS2 does not span the membrane and is thought to be imbedded in the luminal side of the ER membrane [3]. It is still unknown, how NS4A contributes to the substantial membrane deformations that are required to form the membrane scaffold for replication complex assembly.

Different mechanisms have been described by which proteins can remodel cellular membranes [9, 10]. Insertion of amphipathic α -helices (AHs) into membranes is one of them. Embedding the hydrophobic face of the AH into one leaflet of a bilayer causes asymmetry that can induce local membrane curvature. Membrane curvature could also arise from asymmetrically shaped integral membrane proteins or complexes, and from oligomerization of membrane bound proteins in or above the polar lipid water interface [10]. A single membrane altering protein may use more than one of these mechanisms to exert its activities [10].

Some AHs act as membrane curvature sensors. They bind membranes in a curvature sensitive manner, which is important for membrane curvature-dependent assembly or disassembly of protein complexes and for vesicular transport [11].

AHs identified in various viral proteins were found to be essential for viral replication, including hepatitis C virus (HCV) NS5A [12, 13] and NS4B [14-16] and Semliki Forrest virus nsP1 [17]. AHs in viral proteins have been implicated in anchoring some of these non-

structural proteins to the membrane. It was speculated, that these AHs could also be involved in the remodeling of intracellular membranes to form the complex membrane structures that harbor the viral replication complexes [4].

Secondary structure prediction indicates that the conformation of the N-terminal amino acids 1-48 of NS4A should be dominated by α -helices [18]. Furthermore, if the peptide would indeed form a regular α -helix, 18 amino acid residue stretches in the N-terminal half of this helix would have a significant amphipathic character with hydrophobic moments ranging from 0.3 to 0.4 (analyzed by Heliquest [19] based on the hydrophobicity scale of Fauchere and Pliska [20]). Helices with hydrophobic moments above 0.6 are considered highly amphipathic [19].

To examine the functional relevance of AH formation, mutations were introduced into the N-terminal region of NS4A with the aim to preserve the tendency to form an α -helix, but reduce the hydrophobic moment of the putative helix in amino acids 3-20 [18]. When inserted in the context of a DENV reporter replicon these NS4A mutations (L6E;M10E) abolished viral replication. These mutations also reduced homo-oligomerization of NS4A, but did not affect its localization [18]. Apparently, the N-terminal cytoplasmic domain of NS4A is crucial for DENV replication. However, its exact role is still unclear. In contrast to other viral proteins such as NS5A from the related hepatitis C virus where the AH presents the sole membrane anchor [12], DENV NS4A is a transmembrane protein [3]. Thus it is unlikely that the AH of NS4A serves as a primary membrane anchor. The fact that the mentioned AH mutations affect the oligomerization of NS4A supports a possible role of this domain in the induction of membrane curvature.

Experimental data on the three-dimensional structure of the NS4A cytoplasmic N-terminal domain and on its interaction with membranes are required in order to better understand the role of this domain in viral replication. Structural analysis could assist in answering the fundamental question if part of the N-terminal domain of wild type NS4A indeed forms an amphipathic helix and in assessing the structural consequences of the two introduced mutations.

Previous circular dichroism (CD) data had indicated that about 40% of the amino acids of both wild type and mutant NS4A (amino acids 1-48) peptides are located in α -helices in presence of membrane mimicking micelles [18]. However, the CD data did not provide the sequence location and extension of these helices. In order to address these questions peptides corresponding to the N-terminal domain (amino acids 1-48) of wild type and mutant NS4A were recombinantly produced. These two peptides were analyzed in membrane mimicking micelles using liquid state NMR spectroscopy. CD and surface plasmon resonance (SPR) experiments were used to study the interaction of wild type and mutant NS4A (amino acids 1-48) peptides with liposomes resembling the lipid composition of human ER membranes and to test the influence of membrane curvature on the peptide membrane interaction.

2. Materials and methods

2.1. Recombinant protein production

A peptide (SLTLNLITEM GRLPTFMTQK ARDALDNLAV LHTAEAGGRA YNHALSEL) corresponding to the N-terminal 48 amino acid residues of the non-structural protein NS4A of dengue virus serotype 2 (NCBI Protein database accession number: NP739588) and a mutant version of this peptide were recombinantly produced in *E.coli* BL21 cells. The peptides were expressed as fusion proteins with a double tag (GST and GB1 domains) preceding the amino acid sequence of the peptide as described [21]. The double tag was removed by enzymatic cleavage using TEV protease, resulting in an N-terminal serine in the produced peptides. This serine matches the N-terminal amino acid of DENV NS4A, i.e., the studied peptides do not contain any additional residues. Uniform isotope labeling with ^{15}N or ^{13}C , ^{15}N was achieved by expression in M9 medium containing ^{15}N ammonium chloride and ^{13}C glucose (Eurisotop, Saarbrücken, Germany) as the sole source of nitrogen and carbon, respectively. Unlabeled peptides were expressed in LB medium. The mutant peptide NS4A(1-48, L6E;M10E) carries two point mutations: L6E and M10E.

2.2. Lipids

Lipids were all purchased in chloroform solution from Avanti Polar Lipids (Alabaster, AL, USA) including: 1-palmitoyl-2-oleoyl-*sn*-glycero-3-phosphocholine (POPC); 1-palmitoyl-2-oleoyl-*sn*-glycero-3-phosphoethanolamine (POPE); 1,2-dioleoyl-*sn*-glycero-3-phospho-L-serine (sodium salt) (DOPS); L- α -phosphatidylinositol of bovine liver (sodium salt) (PI); sphingomyelin from chicken egg (SM); L- α -phosphatidic acid from chicken egg (sodium salt) (PA); and cardiolipin of bovine heart (sodium salt) (CL). Cholesterol (>99%) powder (Sigma-Aldrich, Taufkirchen, Germany) was dissolved in chloroform at 10 mg mL⁻¹.

Besides single component POPC membranes we studied two lipid mixtures: a POPC/DOPS mixture at a molar ratio of 4:1 and a multicomponent mixture resembling the composition of membranes in the ER [22]. A synthetic ER lipid mix with the following components was used: POPC/bovine heart CL/bovine liver PI/POPE/ DOPS/chicken egg PA/chicken egg SM/cholesterol with molar ratios of 59 : 0.37 : 7.7 : 18 : 3.1 : 1.2 : 3.4 : 7.8.

2.3. Nuclear magnetic resonance

NMR samples contained 1 mM [U - ^{15}N]- or [U - ^{15}N , ^{13}C]-labeled NS4A(1-48) or NS4A(1-48, L6E;M10E) in 50 mM sodium phosphate buffer (pH 6.8), 10% (v/v) deuterium oxide, 0.03% (w/v) NaN_3 , with or without 100 mM perdeuterated sodium dodecyl sulfate (SDS- d_{25}). SDS- d_{25} and $^2\text{H}_2\text{O}$ were obtained from Eurisotop.

NMR experiments were performed at 30 °C on Varian ^{Unity}INOVA, VNMRS and Bruker Avance III HD NMR instruments, equipped with cryogenic Z-axis pulse-field-gradient (PFG) triple resonance probes operating at proton frequencies of 600, 800, and 900 MHz.

Resonance assignment of protein backbone was accomplished using a combined set of heteronuclear multidimensional NMR experiments: 2D (^1H - ^{15}N)-HSQC [23, 24], 2D (^1H - ^{15}N)-BEST-TROSY (BT) correlation [25], 2D (^1H - ^{13}C)-HSQC [26], 3D HNCACB [27], 3D BT-HNCACB [28], 3D HNCO [29], 3D BT-HNCO [28], and 3D HNHA [30]. ^1H and ^{13}C chemical shifts were referenced directly to internal DSS at 0 ppm and ^{15}N chemical shifts were referenced indirectly to DSS using the absolute ratio of the ^{15}N and ^1H zero point frequencies [31]. NMR data were processed using NMRPipe, v.8.1 [32] and evaluated with CcpNmr v.2.3 [33] and TALOS-N software [34].

Heteronuclear $\{^1\text{H}\}$ - ^{15}N NOEs (nuclear Overhauser effects) were derived from 2D spectra recorded at 18.8 T with or without 6 s of proton saturation [35]. The heteronuclear NOE is the ratio of the integral peak intensities of a given ^1H - ^{15}N correlation measured with and without saturation, respectively.

2.4. Chemical shift-based analysis

The software program TALOS-N [34] predicts protein secondary structure from experimental protein backbone $^{13}\text{C}\alpha$, $^{13}\text{C}\beta$, $^{13}\text{C}'$, $^1\text{H}\alpha$, ^{15}N , and $^1\text{H}_\text{N}$ NMR chemical shift data and database knowledge. TALOS-N classifies secondary structure either as helix (H), extended strand (E) or coil (L) [34]. In addition, TALOS-N provides insight into protein backbone dynamics based on the random coil index (RCI) method. An empirical correlation between the model-free backbone order parameter S^2 [36] and protein backbone secondary chemical shifts is exploited for deriving the order parameter RCI- S^2 [37, 38].

2.5. Small unilamellar lipid vesicles (SUVs)

SUVs were prepared by extrusion or sonication using either a single lipid component or a synthetic mixture of different lipids. Appropriate volumes of the lipid chloroform stocks were transferred to a glass test tube at the desired molar ratios with a total amount of 5 mg of lipid per sample. Chloroform was removed by passing a gentle stream of nitrogen gas over the solution while slowly rotating the test tube, resulting in a thin film of lipid on the inner wall of the tube. High vacuum was applied for at least 3 h to remove chloroform traces. Lipid films were suspended under vortexing in 500 μL of sodium phosphate buffer (50 mM sodium phosphate, pH 6.8, 150 mM NaCl). Samples were subjected to three cycles of freezing and thawing in liquid nitrogen and a 60 $^\circ\text{C}$ water bath. Liposome solutions were passed 15 times or more through a Nuclepore polycarbonate membrane with nominal pore diameter of either 30 or 50 nm (GE Healthcare, Freiburg, Germany) using a handheld LiposoFast Extruder (Avestin Europe, Mannheim, Germany) equipped with two 0.5 mL syringes. Sonicated lipid vesicles were produced starting from SUV solution obtained by extrusion through a 30 nm Nuclepore membrane. Volumes of 500 μL per sample were transferred to 1.5 mL Eppendorf tubes, kept on ice and treated with a 3 mm microtip of a Branson 250 sonifier. Ten cycles of sonication (20 s) and intermediate cooling (2 min) were applied. Finally, the hydrodynamic radius of the liposomes was determined by dynamic light scattering. Liposomes were checked for lipid degradation products by thin layer chromatography (TLC) using Alugram SIL G

sheets (Macherey-Nagel, Düren, Germany) and a mobile phase of chloroform, methanol, and aqueous ammonia (25%) in a volume ratio of 13:7:1.

2.6. Circular dichroism (CD)

CD data were measured with a Jasco J-1100 instrument (Jasco, Groß-Ulmstadt, Germany) at 30 °C using a QS quartz cell with optical path length of 1 mm (Hellma, Müllheim, Germany). All samples were prepared in 50 mM sodium phosphate buffer, pH 6.8, 150 mM NaCl. Appropriate amounts of extruded or sonicated liposome stock and buffer were supplemented with peptide stock to give a final lipid concentration of 10 mg mL⁻¹, i.e., about 13 mM, in all liposome samples. Additional samples contained peptide in buffer or micelles (100 mM SDS). Concentration of NS4A(1-48) or NS4A(1-48, L6E;M10E) peptides was 40 µM in all samples. Light scattering due to the large size of liposomes and light extinction due to high concentration of chloride ions limited acquisition of CD data to the wavelength range above 205 nm. CD data were recorded in continuous scan mode (scan speed 50 nm min⁻¹, bandwidth 1 nm, integration time constant 0.5 s, accumulation of 5 scans). Appropriate background spectra reflecting contributions from the buffer, liposome or detergent solution were subtracted from each curve.

2.7. Surface plasmon resonance (SPR)

SPR data were collected with a Biacore X instrument using L1 sensor chips (GE Healthcare, Freiburg, Germany). L1 chips were equilibrated with 50 mM sodium phosphate buffer pH 6.8 for 30 min and then stripped with short pulses (1 min at a flow rate of 20 µL min⁻¹) of 20 mM CHAPS (3-((3-cholamidopropyl)-dimethylammonio)-1-propane sulfonate). The entire flow path was washed with phosphate buffer. For liposome immobilization, the SUV solution (80 µL, with a nominal lipid concentration of 2 mg mL⁻¹, extruded through a 50 nm Nuclepore membrane) was injected at a flow rate of 2 µL min⁻¹. Three short pulses of 50 mM NaOH were applied at 10 µL min⁻¹ in order to remove loosely bound liposomes and to achieve a stable baseline. A solution of 0.1 mg mL⁻¹ bovine serum albumin (BSA, Sigma-Aldrich) was injected for 1 min at a flow rate of 10 µL min⁻¹ in order to block potential non-specific ligand binding sites on the surface. Initial blank injections with running buffer only and binding experiments with 30 µM of the NS4A peptide were performed at a flow rate of 20 µL min⁻¹. In the binding experiments the analyte solution was injected for 30 s (association phase) followed by buffer injection for 100 s or longer (dissociation phase). A corrected sensorgram was obtained by subtracting the sensorgram of the blank injection from that of the immediately following binding experiment. Complete return of the response (RU) signal to pre-injection level could not be achieved, neither by extending the running buffer injection times to several hours nor by established regeneration procedures such as high salt concentration or extreme pH buffers. Therefore, the L1 sensor chip was completely stripped of lipids and protein with repeated short pulses of 20 mM CHAPS until the RU value became similar to the original values. Stripping was repeated after every single binding experiment.

2.8. Dynamic light scattering (DLS)

Data were measured using the Dyna Pro instrument (Protein Solutions, Lakewood, NJ, USA) equipped with a 3 mm path length 45 μ L quartz cell. Liposome solutions (10 mg of lipid per mL) were diluted 100-fold with buffer (50 mM sodium phosphate pH 6.8, 150 mM NaCl) directly after extrusion or sonication and measured immediately. Data were analyzed with Dynamics V6 software distributed with the instrument. Experimental data were fitted to the model of Rayleigh spheres.

3. Results

3.1. NMR backbone signal assignment

Both wild type and mutant NS4A(1-48) peptides were analysed using liquid state NMR spectroscopy in presence of 100 mM SDS-d₂₅. An almost complete backbone resonance assignment of the two peptides was accomplished. In total, 98% of the expected resonances of both NS4A(1-48) and NS4A(1-48, L6E;M10E) were identified. Resonance assignments for the two NS4A N-terminal peptides have been deposited at the Biological Magnetic Resonance Data Bank (BMRB) under accession numbers 25179 (wild type) and 25180 (mutant).

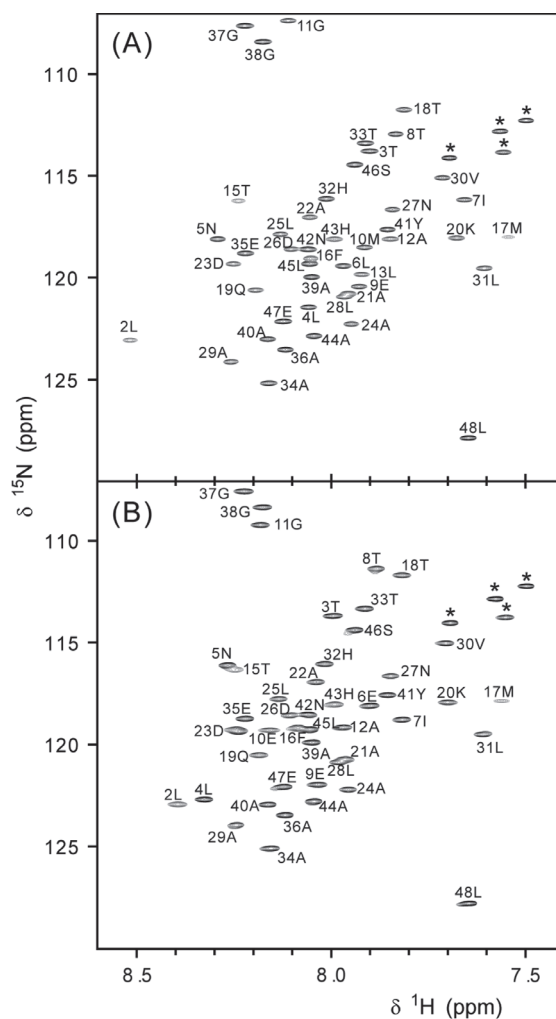


Figure 1:

(¹H-¹⁵N)-HSQC spectra of [*U*-¹⁵N]-labeled NS4A(1-48) (A) or NS4A(1-48, L6E;M10E) (B) in presence of 100 mM SDS-d₂₅. All assigned backbone amide ¹H_N-¹⁵N correlations are labeled with the corresponding amino acid sequence position and type (in one letter code). Side chain ¹H-¹⁵N correlations are denoted by asterisks.

3.2. NMR-based secondary structure analysis

Highly resolved two-dimensional (^1H - ^{15}N) correlation spectra were obtained for both wild type and mutant NS4A peptides in membrane mimicking SDS micelles (Fig. 1) and in detergent-free buffer at 30 °C. The low spectral dispersion and the occupied range of $^1\text{H}_\text{N}$ chemical shifts in the NMR spectra of both peptides in buffer (see Fig. 7 in [21]) are in agreement with a random coil conformational ensemble, which was also suggested by earlier CD data [18]. Addition of SDS increases the spectral dispersion and causes a clear upfield shift, in particular in the proton dimension, for many of the observed cross-peaks, very likely indicating the formation of secondary structure elements.

The experimental data was used for secondary structure prediction employing the TALOS-N software package [34]. Figure 2A displays the resulting chemical shift-based secondary structure prediction for the two NS4A peptides. Solid and open bars indicate amino acids with helical secondary structure in the wild type (residues 5-to-9 and 15-to-31) and mutant (residues 4-to-7 and 15-to-31) NS4A peptides in presence of SDS micelles. The height of the bars reflects the probability of helical structure for the given residue. No indications for amino acid residues in extended strand conformations were found. Prediction was inconclusive for Pro14 (wild type) and for the N- and C-terminal residues. All remaining residues were assigned as “coil” by the program. Clearly, addition of SDS causes formation of two helical segments, designated helix 1 and 2, connected by an unstructured linker. This conformation occurred both in the wild type and mutant NS4A(1-48) peptides.

3.3. Backbone dynamics

RCI- S^2 values reported by TALOS-N and heteronuclear $\{^1\text{H}\}$ - ^{15}N -NOEs of the two NS4A peptides are presented in figure 2B and C, respectively. The model-free backbone order parameter S^2 [36] as well as $\{^1\text{H}\}$ - ^{15}N -NOE-ratios reflect protein dynamics on the pico- to nanosecond timescale [39]. The magnitude of the parameter values is sensitive to small scale conformational fluctuations. Rigid secondary structure elements are characterized by large RCI- S^2 above 0.85 [38] and large positive $\{^1\text{H}\}$ - ^{15}N -NOEs ratios around 0.8 [40], while flexible residues show significantly lower values. The data in figure 2 indicate a rather rigid α -helix 2 with slightly increased dynamics at the C-terminus of helix 2 in both peptides. Rapid internal motions become increasingly prominent in the following sequence: helix 1, interhelical linker, N- and C-terminus of the peptide.

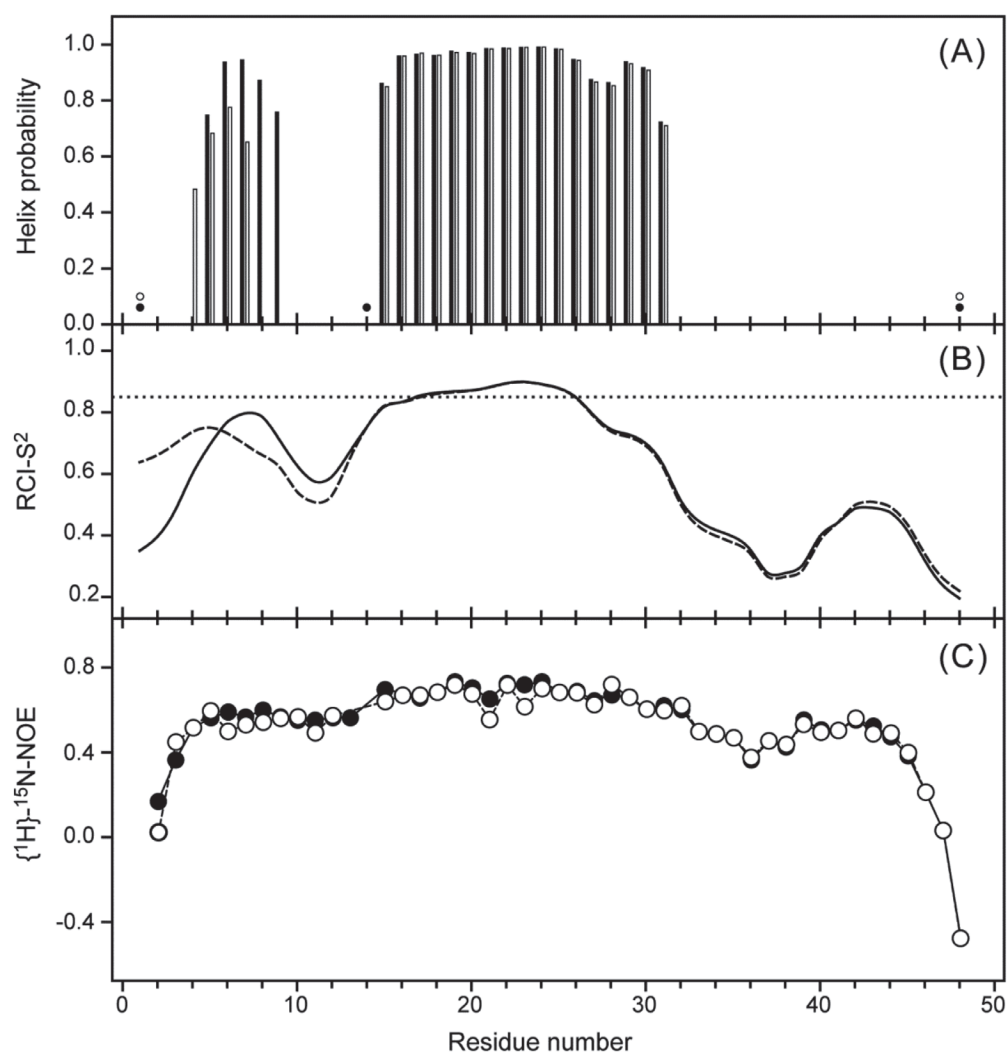


Figure 2:

Secondary structure prediction (A), RCI-based order parameter RCI-S^2 (B), and $\{^1\text{H}\}\text{-}^{15}\text{N}$ heteronuclear NOE intensity ratios (C) for NS4A(1-48) (filled bars and circles in (A, C), solid line in (B)) and NS4A(1-48, L6E;M10E) (open bars and circles in (A, C), broken line in (B)) in buffer containing 100 mM SDS- d_{25} . Data shown in A and B are based on secondary chemical shifts and were provided by TALOS-N. Bars in panel A report residues with helical secondary structure. None of the residues was predicted to adopt an extended strand conformation. Circles indicate lack of prediction at the termini of the peptides or an inconclusive prediction in case of P14 of the wild type sequence. All remaining amino acid residues were predicted as “coil”. Predicted RCI-S^2 values (B) are connected by a cubic spline function. The dotted line indicates $\text{RCI-S}^2 = 0.85$.

3.4. Interaction of NS4A peptides with immobilized liposomes

In an attempt to further assess the role of the N-terminal of NS4A we previously determined its ability to bind membranes using SPR experiments [18]. Here SPR was used to further test the binding of NS4A(1-48) and NS4A(1-48, L6E;M10E) peptides to lipid bilayers modelling the lipid composition at the ER membrane [22].

Both the wild type and mutant peptides bound to the studied liposomes. Association and dissociation of the main fraction of peptides occurred on a rapid timescale, reflected by the fast rise and steep decline of the response signal that immediately followed the beginning and the end of analyte injection. Such fast dissociation is a characteristic of low stability complexes. The maximum response of wild type peptide was about sevenfold higher than that of the mutant (Fig. 3) indicating a higher affinity of the wild type peptide towards the membranes. Dissociation of the wild type peptide from the membranes was slower than that of the mutant peptide. Furthermore, the wild type peptide showed lipid-specific differences in the association and dissociation kinetics (Fig. 3A). Both processes were more rapid for NS4A(1-48) binding to POPC and slower for peptide binding to ER mix and POPC/DOPS membranes. It is conceivable, that peptide association to the liposomes involves different mechanisms or binding sites with different affinity and kinetics. The initial fast association and dissociation phases are apparently followed by slower rising and declining responses, respectively (Fig. 3). This behavior might be explained, for example, by peptide oligomerization that follows the initial rapid peptide binding to the liposome. During the dissociation phase a large fraction of the liposome-associated peptide is rapidly released, while some of the peptide molecules seem to be irreversibly bound. These empirical observations are more pronounced for the wild type peptide. In order to show that the SRP results are not due to non-specific direct binding of the peptide to the chip, 0.1 mg mL⁻¹ BSA immobilization was used instead of liposomes. In these experiments, both NS4A peptides yielded responses lower than 20 RU. This observation confirms that the sensorgrams shown in figure 3 are not a result of non-specific interactions of the NS4A peptides with the L1 chip. Taken together these results suggest that the two point mutations reduce the strength of liposome binding and/or the homo-oligomerization tendency of the NS4A(1-48) peptide.

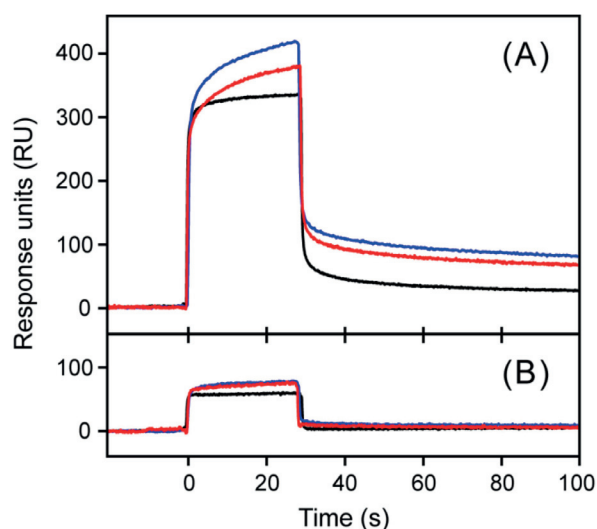


Figure 3:

Surface plasmon resonance sensorgrams reflecting the interaction of NS4A wild type (A) and mutant peptide (B) with immobilized liposomes composed of POPC (black); POPC/DOPS (4 : 1) (blue), and a mix of lipids resembling human ER membranes (red). Peptide injection started at time 0 s and lasted for 30 s.

3.5. Interaction of NS4A peptides with liposomes

CD spectroscopy was used to monitor formation of helical secondary structure upon NS4A peptide interaction with liposomes of different lipid composition and surface curvature. CD spectra of α -helices show two characteristic minima at 208 and 222 nm. The depth of the minima increases with the helix content in the sample [41]. CD spectra of NS4A wild type (left) and mutant peptide (right) in various environments are presented in figure 4. CD data of NS4A peptides recorded in the presence of liposomes or micelles are population-weighted averages of the CD curves of free and bound peptide conformations in the corresponding sample. Both peptides display less than 10% helical structure in buffer (Fig. 4, dashed black line) but the α -helix content increases to about 36% (wild type) and 30% (mutant) upon addition of 100 mM SDS (Fig. 4, solid black line) [18].

Addition of extruded liposomes (hydrodynamic radius $r_h = 33$ nm) consisting of either POPC, POPC/DOPS (4:1), or a synthetic ER lipid mix, respectively, to a final concentration of about 13 mM lipid (10 mg mL^{-1}) resulted in an increase in the helicity of the wild type peptide, but did not significantly affect the mutant CD data (Fig. 4, blue). Almost identical but more noisy CD curves were obtained when using extruded liposomes at the same lipid concentration but with $r_h = 48$ nm instead of 33 nm (data not shown). When sonicated liposomes ($r_h = 26$ nm) instead of extruded ones were added at the same lipid concentration (Fig. 4, red), higher helix content is found in the wild type peptide samples. Only marginal changes occur with the mutant peptide.

CD curves of wild type NS4A peptide in presence of SDS micelles or either one of three differently composed, sonicated liposomes display high similarity (Fig. 4A, C and E). The most likely interpretation of the matching CD curves is a similar conformation and a similar fraction of bound NS4A peptide in all four samples. If we further assume that NS4A(1-48) binds all types of liposomes in an identical conformation, then it becomes clear from figure 4 that a significantly smaller fraction of NS4A(1-48) binds to the larger (extruded) liposomes in comparison to smaller (sonicated) ones. Apparently, NS4A(1-48) binding to liposomes is sensitive to membrane curvature and shows a steep dependence on liposome size when r_h is close to 30 nm. The difference in the lipid composition of the membranes used for the CD measurements shown in figure 4 does not have a strong influence on NS4A peptide binding. The mutant NS4A peptide shows no increase in helical secondary structure upon addition of either extruded or sonicated liposomes at the lipid and peptide concentrations used in these experiments.

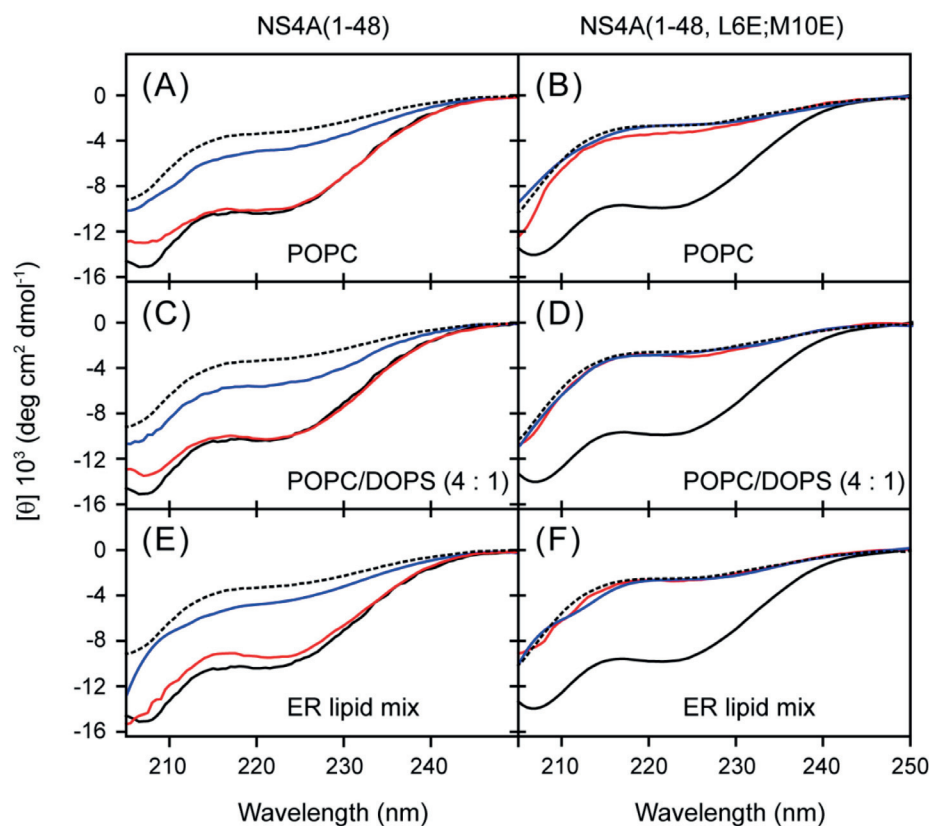


Figure 4:

Mean residue ellipticity of NS4A wild type (left) and mutant peptide (right) in presence of liposomes (10 mg lipid per mL) prepared from POPC (A, B); POPC/DOPS (4 : 1) (C, D); and a mix of lipids resembling the lipid composition of human ER membranes (E, F). Liposomes were produced by extrusion (blue) or by sonication (red). CD spectra of the peptides in phosphate buffer (black, dashed line) and in micelle solution (100 mM SDS, black) have been added for comparison. Peptide concentration was 40 μ M in all samples.

4. Discussion

4.1. Implications of the NS4A peptide structure

We conducted the first characterization of the three-dimensional structure and dynamics of the N-terminal 48 amino acid peptide of DENV NS4A protein in membrane mimicking micelles. The amino acid sequence of NS4A(1-48) shows an intrinsic bias for α -helix formation. Application of multiple secondary structure prediction algorithms results in a consensus structure with three helices, encompassing residues 4-10, 15-35, and 40-47 of NS4A(1-48) [18]. In case of the NS4A mutant peptide, different algorithms strongly disagree on length and position of the most N-terminal helix. Very little, if any secondary structure was experimentally detected for the NS4A peptides in aqueous buffer devoid of membranes and detergent micelles. Addition of membrane mimicking SDS micelles induced formation of two helices in each of the peptides. The predicted N-terminal helix 1 in the wild type peptide almost matches the NMR data. The experimentally determined helix 2 (amino acid residues 15-31) is slightly shorter than the prediction (residues 15-35). The third predicted helix could not be experimentally confirmed under the conditions used.

Helices 1 and 2 were found to be connected via an unstructured linker. Reduced RCI-S² values of the amino acid residues in the linker (Fig. 2B) indicate higher dynamics in comparison to the helices. According to our results the starting point of helix 2 is Tyr15. Interestingly, the preceding residue is a proline (Pro14). Proline has the lowest helix propensity among all 20 naturally occurring amino acids due to both its unique geometry and the lack of an amide hydrogen required for helix stabilizing hydrogen bonding [42]. The relatively few prolin residues found in the interior of α -helices cause a disruption or a kink of the helix because steric restrictions prevent prolin from forming canonical α -helical geometry [43]. Mutation of Pro14 to alanine in the context of a DENV reporter replicon abolished viral replication [18]. This mutation may cause an N-terminal extension of α -helix 2, since alanine is the amino acid with highest helix propensity [42]. It is conceivable that the separation of helices 1 and 2 by a flexible linker or at least a kink is a crucial requirement for functional interaction of NS4A with membranes and/or proteins. Interestingly, a recent study showed that a specific interaction between the N-terminal of NS4A (amino acids 1-50) and cytoskeleton protein vimentin is crucial for correct regulation of DENV replication complex construction [44], indicating that this idea is feasible.

The observed helices display an amphipathic character. A regular α -helix formed by NS4A amino acid residues 15-31 (helix 2) has a moderate hydrophobic moment $\langle\mu_h\rangle$ of 0.287 (<http://heliquist.ipmc.cnrs.fr>) [19]. However, the central 13 amino acid residues of this α -helix display a very strongly amphipathic character ($\langle\mu_h\rangle = 0.512$). Helical wheel plots of the very short helix 1 of wild type and mutant NS4A, respectively, reveal distinct polar and hydrophobic faces, too. However, the two mutations of hydrophobic amino acids Leu6 and Met10 to anionic glutamate cause a counterclockwise rotation of the hydrophobic face of this short helix by $\sim 45^\circ$, perhaps explaining the observed shift of helix 1 by one residue along the sequence. Acknowledging the amphipathic character of the experimentally identified helices 1 and 2, we will refer to them as AH1 and AH2 of Dengue virus protein NS4A.

Dengue virus carrying the two mutations L6E and M10E in the NS4A protein is replication deficient. However, the structural consequences of the two mutations are rather small in the micelle bound peptide and appear to be limited to the N-terminal AH1, which includes one and is very close to the second mutation site. Most likely, AH1 extends from Asn5 to Glu9 in wild type NS4A(1-48) and from Leu4 to Ile7 in the mutant. In addition to its apparent shift by one residue towards the N-terminus, helix 1 of the mutant shows a lower helix probability for the individual amino acid residues and has lower order parameters indicating increased conformational fluctuations in comparison to the wild type sequence (Fig. 2A, B). Taken together these small changes may reflect a reduced free energy gain upon micelle binding of the mutant as compared to the wild type peptide. Nevertheless, at the high concentration of potential peptide binding sites present at 100 mM SDS, a large fraction of both wild type and mutant peptide binds and shows α -helix formation. The dramatically different amount of helical conformation observed in the wild type vs. mutant peptide upon addition of liposomes, in particular at a lipid concentration of 10 mg mL⁻¹ (cf. figure 4) is perhaps caused by a reduced membrane affinity of the mutant in comparison with the wild type peptide.

Putative AH forming peptides are often unstructured in aqueous buffer while addition of liposomes or detergent micelles induces helix formation. SDS micelles and lipid bilayers both have a polar head group water interface and a hydrophobic interior. Differences between the two membrane mimics include the nature of the head groups and hydrocarbon chains as well as the surface curvature. Micelles are highly dynamic with continuous exchange of detergent molecules between the monomeric and micellar state. NMR provides a detailed characterization of the structure and dynamics of micelle bound peptide. However, membrane and micelle bound peptide conformations are not necessarily identical. Similar CD data of the wild type NS4A peptide in SDS micelles and sonicated liposomes (Fig. 4) are an argument for similar structures of the bound peptide in both systems. The situation with the mutant peptide is less clear. The peptide might bind to the liposome without a CD-detectable change of its conformation. Alternatively, the affinity of the mutant peptide for the membrane may be too low for induction of a significant fraction of membrane-bound peptide under the conditions of the CD experiments reported here. If the second option applies, then the liposome- and the SDS micelle-bound conformations of the mutant peptide may be very similar, too. However, different experimental conditions, e.g., higher lipid concentration, would be required for induction of mutant peptide binding and assessment of its membrane-bound conformation. The SPR data shown in figure 3 indicate a reduced membrane affinity of the mutant peptide in comparison to the wild type NS4A(1-48), and thus support the second of the above discussed options.

4.2. NS4A(1-48) binds preferentially to highly curved liposomes

A protein might bind to a membrane without undergoing a conformational change. On the other hand, the increase of helical secondary structure of the wild type NS4A(1-48) observed upon addition of liposomes clearly indicates binding. Assuming a partially helical membrane-bound and an almost random coil unbound NS4A(1-48) conformation, we can use the degree of helicity reflected in the CD curves of wild type NS4A(1-48) as an indicator of peptide

binding to liposomes. The CD data in figure 4 suggest preferential binding of NS4A(1-48) to the convex face of highly curved lipid membranes.

The L6E;M10E mutations reduced the affinity of the N-terminal NS4A peptide for immobilized liposomes (Fig. 3) and virtually abandoned helix formation upon addition of all liposome types tested in the CD experiments (Fig. 4). Extending the CD-based interaction assay to liposome concentrations above 10 mg mL⁻¹ was not possible due to strong light scattering and absorption.

Binding of AH peptides to membranes often involves three stages: i) electrostatically driven accumulation of the peptide next to the (normally) negatively charged membrane surface, ii) insertion of hydrophobic side chains into the membrane and release of water (hydrophobic effect), and iii) coil-to- α -helix transition in the membrane interface region, which may easily contribute more than 50% of the free energy of lipid peptide binding [11, 45]. Electrostatics likely plays only a minor role for the wild type NS4A peptide (net charge $z=-1$), but may reduce the concentration of the mutant peptide ($z=-3$) in the vicinity of ER membranes. Residues 2 to 17 present the most hydrophobic region of wild type NS4A, but the L6E and M10E mutations reduce this hydrophobicity by ~30%. This reduced hydrophobicity might be a major factor in the reduced binding of the mutant peptide to membranes.

Insertion of hydrophobic amino acid side chains into tightly packed membranes is energetically less favorable than intercalation into existing lipid bilayer packing defects. Such defects are abundant in the strained outer leaflet of small liposomes and have been implicated in curvature-dependent binding of a number of AH motifs to membranes [11, 46, 47].

Variation of the lipid composition had only small effects on the interaction of NS4A(1-48) with liposomes in comparison to the introduction of mutations (L6E;M10E) or the influence of membrane curvature (Figs. 3 and 4). Exploration of the more subtle effects of membrane composition will require additional systematic and quantitative studies.

4.3. Potential role of curvature sensing motif in NS4A(1-48) in curvature stabilization

NS4A localizes to the ER and to virus-induced ER-derived membranes. Individual expression of DENV NS4A lacking the 2K fragment was previously shown to be sufficient to induce comparable membrane alterations [3]. Our results may suggest a role for NS4A in the formation of highly curved membrane entities. Such entities occurring during DENV replication were previously described as vesicular structures that are ~80 to 90 nm in diameter. These vesicles show tubular connections to the cytoplasm with a radius of ~10 nm [7, 48]. The N-terminus of NS4A maps to the cytoplasmic, i.e., the inner side of these structures. Both spherical vesicles and tubules are concave on the inner side. However, a more complex, saddle-shaped geometry with both negative and positive curvature occurs in neck regions connecting vesicles and tubules [9]. The vesicular structures are thought to develop from invaginations of the ER membrane. Recent molecular dynamics simulations on a NS4A model encompassing the membrane spanning domains pTMS1 and pTMS3 as well as the membrane associated domain pTMS2 indicate, that this NS4A model induces membrane undulation and local bending with a radius comparable to the reported vesicular structures

[48]. The N-terminal region of NS4A inclusive of AH1 and AH2 was not part of the NS4A model studied by Lin et al. [48]. These AHs may drive the protein into convex regions of the undulated ER membrane where the protein could accumulate, oligomerize, or participate in complex formation and perhaps induce or support formation of the vesicle neck. Energetically favorable insertion of hydrophobic amino acid side chains into existing defects in the cytoplasmic leaflet of locally bend ER membranes would stabilize existing curvature of the membrane while subsequent NS4A oligomerization or complex formation in or on the membrane may increase, modify or induce local curvature. This, of course, is a highly speculative model that should be further confirmed by additional experimental evidence.

Hepatitis C virus NS4B is a key player in the induction of the membrane rearrangements leading to the formation of the HCV replication complex [15, 49]. Recent studies performed with hepatitis C virus NS4B indicated a crucial role of NS4B oligomerization in membranous web formation and identified multiple determinants, including an amphipathic helix in the N-terminal region of NS4B, that are responsible for its oligomerization [50]. HCV NS4B can perform both homotypic and heterotypic interactions [50]. Additional complementary information regarding the mechanism of DENV NS4A oligomerization will be essential in order to determine if the two N-terminal AHs identified in the current study have a direct role in this process. It is crucial to understand if these AHs interact with themselves, with a different part of the protein or with a different protein.

In summary, we provide the first characterization of the three dimensional structure of the N-terminal of NS4A, a central protein in the life cycle of DENV. The NS4A N-terminal was found to contain two AHs separated by an unstructured linker. The NS4A(1-48) peptide binds to liposomes in a membrane curvature-dependent manner. The double mutation L6E and M10E in the NS4A sequence abandons DENV replication in a replicon system [18]. The same two mutations strongly reduce lipid membrane binding. The two AHs in the N-terminus of NS4A may be crucial for membrane binding, curvature sensing and stabilization. The NS4A N-terminal may play a role in NS4A oligomerization and accumulation in highly curved membrane regions. These events in turn might be crucial for the formation of the viral replication complex, a critical step in the viral life cycle. Better understanding of the molecular details of the discussed mechanisms might lead to the development of novel anti-DENV strategies.

Acknowledgements

We thank Omer Stern and Julian Glück for fruitful discussions. Y.-F. H. was a scholarship holder of the Graduate School Molecules of Infection (MOI), funded by the Jürgen Manchot Foundation.

References

- [1] S. Bhatt, P.W. Gething, O.J. Brady, J.P. Messina, A.W. Farlow, C.L. Moyes, J.M. Drake, J.S. Brownstein, A.G. Hoen, O. Sankoh, M.F. Myers, D.B. George, T. Jaenisch, G.R. Wint, C.P. Simmons, T.W. Scott, J.J. Farrar, S.I. Hay, The global distribution and burden of dengue, *Nature*, 496 (2013) 504-507.
- [2] E.G. Acosta, V. Castilla, E.B. Damonte, Alternative infectious entry pathways for dengue virus serotypes into mammalian cells, *Cell Microbiol*, 11 (2009) 1533-1549.
- [3] S. Miller, S. Kastner, J. Krijnse-Locker, S. Buhler, R. Bartenschlager, The non-structural protein 4A of dengue virus is an integral membrane protein inducing membrane alterations in a 2K-regulated manner, *Journal of Biological Chemistry*, 282 (2007) 8873-8882.
- [4] S. Miller, J. Krijnse-Locker, Modification of intracellular membrane structures for virus replication, *Nat Rev Microbiol*, 6 (2008) 363-374.
- [5] A. Salonen, T. Ahola, L. Kaariainen, Viral RNA replication in association with cellular membranes, *Curr Top Microbiol*, 285 (2005) 139-173.
- [6] J. Mackenzie, Wrapping things up about virus RNA replication, *Traffic*, 6 (2005) 967-977.
- [7] S. Welsch, S. Miller, I. Romero-Brey, A. Merz, C.K.E. Bleck, P. Walther, S.D. Fuller, C. Antony, J. Krijnse-Locker, R. Bartenschlager, Composition and Three-Dimensional Architecture of the Dengue Virus Replication and Assembly Sites, *Cell Host & Microbe*, 5 (2009) 365-375.
- [8] C. Lin, S.M. Amberg, T.J. Chambers, C.M. Rice, Cleavage at a novel site in the NS4A region by the yellow fever virus NS2B-3 proteinase is a prerequisite for processing at the downstream 4A/4B signalase site, *J Virol*, 67 (1993) 2327-2335.
- [9] J. Zimmerberg, M.M. Kozlov, How proteins produce cellular membrane curvature, *Nat Rev Mol Cell Biol*, 7 (2006) 9-19.
- [10] H.T. McMahon, J.L. Gallop, Membrane curvature and mechanisms of dynamic cell membrane remodelling, *Nature*, 438 (2005) 590-596.
- [11] G. Drin, B. Antonny, Amphipathic helices and membrane curvature, *FEBS letters*, 584 (2010) 1840-1847.
- [12] V. Brass, E. Bieck, R. Montserret, B. Wolk, J.A. Hellings, H.E. Blum, F. Penin, D. Moradpour, An amino-terminal amphipathic alpha-helix mediates membrane association of the hepatitis C virus nonstructural protein 5A, *Journal of Biological Chemistry*, 277 (2002) 8130-8139.
- [13] M. Elazar, K.H. Cheong, P. Liu, H.B. Greenberg, C.M. Rice, J.S. Glenn, Amphipathic helix-dependent localization of NS5A mediates hepatitis C virus RNA replication, *Journal of Virology*, 77 (2003) 6055-6061.
- [14] M. Elazar, P. Liu, C.M. Rice, J.S. Glenn, An n-terminal amphipathic helix in hepatitis C virus (HCV) NS4B mediates membrane association, correct localization of replication complex proteins, and HCV RNA replication, *Journal of Virology*, 78 (2004) 11393-11400.
- [15] J. Gouttenoire, V. Castet, R. Montserret, N. Arora, V. Raussens, J.M. Ruysschaert, E. Diesis, H.E. Blum, F. Penin, D. Moradpour, Identification of a Novel Determinant for Membrane Association in Hepatitis C Virus Nonstructural Protein 4B, *Journal of Virology*, 83 (2009) 6257-6268.
- [16] N.J. Cho, H. Dvory-Sobol, C. Lee, S.J. Cho, P. Bryson, M. Masek, M. Elazar, C.W. Frank, J.S. Glenn, Identification of a Class of HCV Inhibitors Directed Against the Nonstructural Protein NS4B, *Sci Transl Med*, 2 (2010).
- [17] P. Spuul, A. Salonen, A. Merits, E. Jokitalo, L. Kaariainen, T. Ahola, Role of the amphipathic peptide of semliki forest virus replicase protein nsP1 in membrane association and virus replication, *Journal of Virology*, 81 (2007) 872-883.
- [18] O. Stern, Y.F. Hung, O. Valda, Y. Yaffe, E. Harris, S. Hoffmann, D. Willbold, E.H. Sklan, An N-Terminal Amphipathic Helix in Dengue Virus Nonstructural Protein 4A Mediates Oligomerization and Is Essential for Replication, *Journal of Virology*, 87 (2013) 4080-4085.
- [19] R. Gautier, D. Douguet, B. Antonny, G. Drin, HELIQUEST: a web server to screen sequences with specific alpha-helical properties, *Bioinformatics*, 24 (2008) 2101-2102.

- [20] J.L. Fauchere, V. Pliska, Hydrophobic Parameters- Π of Amino-Acid Side-Chains from the Partitioning of N-Acetyl-Amino-Acid Amides, *Eur J Med Chem*, 18 (1983) 369-375.
- [21] Y.F. Hung, O. Valda, S. Schunke, O. Stern, B.W. Koenig, D. Willbold, S. Hoffmann, Recombinant production of the amino terminal cytoplasmic region of dengue virus non-structural protein 4A for structural studies, *PloS one*, 9 (2014) e86482.
- [22] H. Nemesio, F. Palomares-Jerez, J. Villalain, NS4A and NS4B proteins from dengue virus: Membranotropic regions, *Bba-Biomembranes*, 1818 (2012) 2818-2830.
- [23] G. Bodenhausen, D.J. Ruben, Natural abundance nitrogen-15 NMR by enhanced heteronuclear spectroscopy, *Chem.Phys.Lett.*, 69 (1980) 185-189.
- [24] S. Grzesiek, A. Bax, Amino acid type determination in the sequential assignment procedure of uniformly $^{13}\text{C}/^{15}\text{N}$ -enriched proteins, *J.Biomol.NMR.*, 3 (1993) 185-204.
- [25] A. Favier, B. Brutscher, Recovering lost magnetization: polarization enhancement in biomolecular NMR, *J Biomol Nmr*, 49 (2011) 9-15.
- [26] L.E. Kay, P. Keifer, T. Saarinen, Pure absorption gradient enhanced heteronuclear single quantum correlation spectroscopy with improved sensitivity, *J.Am.Chem.Soc.*, 114 (1992) 10663-10665.
- [27] M. Wittekind, L. Mueller, HNCACB, a high-sensitivity 3D NMR experiment to correlate amide-proton and nitrogen resonances with the α - and β -carbon resonances in proteins, *J.Magn.Reson.B*, 101 (1993) 201-205.
- [28] Z. Solyom, M. Schwarten, L. Geist, R. Konrat, D. Willbold, B. Brutscher, BEST-TROSY experiments for time-efficient sequential resonance assignment of large disordered proteins, *J Biomol Nmr*, 55 (2013) 311-321.
- [29] M. Ikura, L.E. Kay, A. Bax, A novel approach for sequential assignment of ^1H , ^{13}C , and ^{15}N spectra of proteins: heteronuclear triple-resonance three-dimensional NMR spectroscopy. Application to calmodulin, *Biochemistry*, 29 (1990) 4659-4667.
- [30] G.W. Vuister, A. Bax, Quantitative J correlation: A new approach for measuring homonuclear three-bond $J(\text{H}_\text{N}-\text{H}_\alpha)$ coupling constants in ^{15}N -enriched proteins, *J.Am.Chem.Soc.*, 115 (1993) 7772-7777.
- [31] D.S. Wishart, C.G. Bigam, A. Holm, R.S. Hodges, B.D. Sykes, ^1H , ^{13}C and ^{15}N random coil NMR chemical shifts of the common amino acids. I. Investigations of nearest-neighbor effects, *J.Biomol.NMR.*, 5 (1995) 67-81.
- [32] F. Delaglio, S. Grzesiek, G.W. Vuister, G. Zhu, J. Pfeifer, A. Bax, NMRPipe: a multidimensional spectral processing system based on UNIX pipes, *J. Biomol. NMR*, 6 (1995) 277-293.
- [33] W.F. Vranken, W. Boucher, T.J. Stevens, R.H. Fogh, A. Pajon, M. Llinas, E.L. Ulrich, J.L. Markley, J. Ionides, E.D. Laue, The CCPN data model for NMR spectroscopy: development of a software pipeline, *Proteins*, 59 (2005) 687-696.
- [34] Y. Shen, A. Bax, Protein backbone and sidechain torsion angles predicted from NMR chemical shifts using artificial neural networks, *J Biomol Nmr*, 56 (2013) 227-241.
- [35] N.A. Farrow, R. Muhandiram, A.U. Singer, S.M. Pascal, C.M. Kay, G. Gish, S.E. Shoelson, T. Pawson, J.D. Forman-Kay, L.E. Kay, Backbone dynamics of a free and phosphopeptide-complexed Src homology 2 domain studied by ^{15}N NMR relaxation, *Biochemistry*, 33 (1994) 5984-6003.
- [36] G. Lipari, A. Szabo, Model-free approach to the interpretation of nuclear magnetic resonance relaxation in macromolecules. 1. Theory and range of validity, *J.Am.Chem.Soc.*, 104 (1982) 4546-4559.
- [37] M.V. Berjanskii, D.S. Wishart, A simple method to predict protein flexibility using secondary chemical shifts, *Journal of the American Chemical Society*, 127 (2005) 14970-14971.
- [38] M.V. Berjanskii, D.S. Wishart, Application of the random coil index to studying protein flexibility, *J Biomol Nmr*, 40 (2008) 31-48.
- [39] L. Salmon, G. Bouvignies, P. Markwick, M. Blackledge, Nuclear Magnetic Resonance Provides a Quantitative Description of Protein Conformational Flexibility on Physiologically Important Time Scales, *Biochemistry*, 50 (2011) 2735-2747.

- [40] L.E. Kay, D.A. Torchia, A. Bax, Backbone dynamics of proteins as studied by ¹⁵N inverse detected heteronuclear NMR spectroscopy: application to staphylococcal nuclease, *Biochemistry*, 28 (1989) 8972-8979.
- [41] N. Greenfield, G.D. Fasman, Computed circular dichroism spectra for the evaluation of protein conformation, *Biochemistry*, 8 (1969) 4108-4116.
- [42] C.N. Pace, J.M. Scholtz, A helix propensity scale based on experimental studies of peptides and proteins, *Biophysical Journal*, 75 (1998) 422-427.
- [43] H.R. Wilman, J. Shi, C.M. Deane, Helix kinks are equally prevalent in soluble and membrane proteins, *Proteins*, 82 (2014) 1960-1970.
- [44] C.S. Teo, J.J. Chu, Cellular vimentin regulates construction of dengue virus replication complexes through interaction with NS4A protein, *J Virol*, 88 (2014) 1897-1913.
- [45] J. Seelig, Thermodynamics of lipid-peptide interactions, *Biochim Biophys Acta*, 1666 (2004) 40-50.
- [46] G. Drin, J.F. Casella, R. Gautier, T. Boehmer, T.U. Schwartz, B. Antonny, A general amphipathic alpha-helical motif for sensing membrane curvature, *Nat Struct Mol Biol*, 14 (2007) 138-146.
- [47] N.S. Hatzakis, V.K. Bhatia, J. Larsen, K.L. Madsen, P.Y. Bolinger, A.H. Kunding, J. Castillo, U. Gether, P. Hedegard, D. Stamou, How curved membranes recruit amphipathic helices and protein anchoring motifs, *Nature chemical biology*, 5 (2009) 835-841.
- [48] M.H. Lin, H.J. Hsu, R. Bartenschlager, W.B. Fischer, Membrane undulation induced by NS4A of Dengue virus: a molecular dynamics simulation study, *Journal of biomolecular structure & dynamics*, (2013).
- [49] D. Egger, B. Wolk, R. Gosert, L. Bianchi, H.E. Blum, D. Moradpour, K. Bienz, Expression of hepatitis C virus proteins induces distinct membrane alterations including a candidate viral replication complex, *Journal of Virology*, 76 (2002) 5974-5984.
- [50] J. Gouttenoire, P. Roingeard, F. Penin, D. Moradpour, Amphipathic alpha-helix AH2 is a major determinant for the oligomerization of hepatitis C virus nonstructural protein 4B, *J Virol*, 84 (2010) 12529-12537.

Summary

Dengue virus (DENV) is a mosquito-transmitted positive single strand RNA virus of the Flaviviridae family. DENV is the causative agent of dengue fever, currently the world's fastest-spreading tropical disease. There is an urgent need for the development of a specific treatment and anti-DENV vaccines, because severe forms of the disease are life threatening. One crucial step in the viral life cycle is the amplification of the viral RNA genome in specialized replication complexes (RCs) that are localized inside invaginated membrane vesicles at the endoplasmatic reticulum (ER). However, up to now the details of RC formation are incompletely understood.

The DENV non-structural protein 4A (NS4A) is an integral ER-resident protein that consists of a conserved, cytoplasm-exposed amino terminal region, two transmembrane (TM) domains and one membrane-associated, ER-lumen facing domain that links the two TM segments. NS4A was proposed to be a key player in the formation of the DENV replication factories. NS4A was suggested to mediate membrane alterations and hence may promote membrane vesicle formation. Recently, conserved putative amphipathic helix (AH) forming amino acid sequences had been identified inside the cytoplasmic amino terminal region of NS4A by secondary structure prediction. Mutations designed to disrupt the amphipathic nature of this region showed that this part of NS4A is critical for viral replication.

This thesis is based on the hypothesis that the amino terminal region of NS4A, i.e., amino acid residues 1-48, contains structural elements that are essential for DENV replication. The structure of NS4A(1-48) was studied by nuclear magnetic resonance (NMR) spectroscopy both in presence and absence of model membranes. Biophysical techniques were used to probe the interaction between NS4A(1-48) and lipid bilayer membranes. In addition, the mutated peptide NS4A(1-48, L6E;M10E) was studied. These two point mutations of NS4A are sufficient to render DENV replication deficient. NMR-based structure determination requires milligram amounts of (^{15}N , ^{13}C) isotope-labeled peptide. A new procedure for recombinant expression and purification of the two NS4A peptides was established. The peptides were expressed as a fusion with a dual tag. Tobacco etch virus protease mediated cleavage generated the NS4A peptides without any artificial overhang. A final yield of about 4 to 5 milligrams peptide per liter of culture medium was obtained. Circular dichroism (CD) data revealed that both NS4A(1-48) and NS4A(1-48, L6E;M10E) are unstructured in aqueous buffer. However, addition of membrane mimicking DPC, SDS, or CTAB detergent micelles induced various degrees of α -helical conformation in wild type and mutant NS4A(1-48).

A detailed analysis of the secondary structure of both peptides was conducted on the basis of NMR backbone chemical shift data. Chemical shifts of both wild type and mutant peptide changed significantly upon addition of detergent micelles and indicated α -helix formation in SDS micelles. Position and length of the α -helices are very similar in both peptides, with a short helix of 6 amino acids in front of a longer helix containing 15 amino acids. The mutations reduce the helix propensity of the short, N-terminal helix by $\sim 10\%$. In SPR measurements NS4A(1-48) and NS4A(1-48, L6E;M10E) show different membrane binding characteristics. NS4A(1-48) showed more pronounced binding to lipid bilayers of various compositions, while the mutant peptide displayed only weak, presumably unspecific binding.

Zusammenfassung

Das Denguevirus (DENV) besitzt ein einzelsträngiges RNA-Genom in Plusstrangorientierung und gehört zur Familie der Flaviviridae. Dengueviren werden durch den Stich einer infizierten Mücke auf den Menschen übertragen und sind Auslöser von Denguefieber, aktuell der Tropenkrankheit mit der rasantesten Ausbreitung weltweit. Obwohl gefährliche Verläufe der Krankheit lebensbedrohend sind, stehen bislang weder eine Schutzimpfung noch antivirale Medikamente gegen Dengueviren zur Verfügung. Ein wichtiger Schritt im viralen Lebenszyklus ist die Vervielfältigung des viralen RNA Genoms. Dies erfolgt bei DENV in spezialisierten Replikationskomplexen (RCs) innerhalb umgestülpter Membranvesikel des endoplasmatischen Retikulums (ERs), wobei dieser Vorgang bislang nur teilweise verstanden ist.

Das DENV Nichtstrukturprotein 4A (NS4A) ist ein im ER lokalisiertes, integrales Membranprotein. Es besitzt eine konservierte, im Zytoplasma lokalisierte, aminoterminal Region sowie zwei Transmembrandomänen, welche durch eine membranassoziierte und im ER-Lumen lokalisierte Domäne miteinander verbunden sind. Es weist vieles darauf hin, dass NS4A eine wichtige Rolle bei der Entstehung der viralen Replikationsfabriken spielt. NS4A scheint Membranänderungen hervorrufen zu können und könnte somit an der Ausbildung der Membranvesikel beteiligt sein. Kürzlich wurde mittels Sekundärstrukturvorhersage gezeigt, dass die konservierte, aminoterminal Region von NS4A eine amphipathische Helix (AH) ausbilden könnte. Mutationsstudien mit dem Ziel, den vorhergesagten amphipathischen Charakter dieser Region zu zerstören, zeigten, dass diese NS4A Region kritisch für die Replikation ist.

Diese Doktorarbeit basiert auf der Hypothese, dass sich in der aminoterminalen Region von NS4A, also innerhalb der Aminosäurepositionen 1 bis 48, Strukturelemente ausbilden, die essentiell für die Replikationsfähigkeit von DENV sind. Es wurde die Struktur von NS4A(1-48) mit Hilfe der kernmagnetischen Resonanzspektroskopie (NMR) sowohl in Ab- als auch in Anwesenheit von Modellmembranen analysiert. Zur Untersuchung der Wechselwirkung von NS4A(1-48) mit Lipiddoppelschichtmembranen wurden biophysikalische Techniken eingesetzt, wobei ebenfalls eine replikationsdefiziente Mutante NS4A(1-48, L6E;M10E) analysiert wurde. Die NMR-basierte Strukturaufklärung setzt das Vorhandensein (¹⁵N, ¹³C)-isotopenmarkierter Peptide im Milligramm-Maßstab voraus. Es wurde ein einheitliches Expressions- und Reinigungsprotokoll für beide Peptide etabliert, welches die Verwendung eines dualen Fusionsanhangs sowie dessen proteolytische Abtrennung mittels Tobacco Etch Virus Protease beinhaltet. So konnten 4 bis 5 mg der Peptide, welche keinerlei artifiziellen Überhang aufweisen, pro Liter Kulturmedium gewonnen werden. Dass sowohl NS4A(1-48) als auch NS4A(1-48, L6E;M10E) in wässriger Lösung unstrukturiert vorliegen, konnte mittels Circular dichroismus (CD)-Spektroskopie gezeigt werden. Die Zugabe von Modellmembranen wie DPC-, SDS- oder CTAB-Mizellen induziert die Ausbildung einer α -helikalen Konformation in unterschiedlicher Ausprägung in beiden Peptiden.

NMR-Daten, wie die chemischen Verschiebungen des Peptidrückgrates, wurden für eine detaillierte Analyse der Sekundärstruktur beider Peptide herangezogen. Nach Zugabe von Detergenz-Mizellen änderten sich die chemischen Verschiebungen sowohl bei NS4A(1-48) als auch bei der Mutante, was auf die Ausbildung α -helikaler Strukturen in SDS-Mizellen hindeutet. Die Position und die Länge der α -Helices sind in beiden Peptiden sehr ähnlich, mit einer kurzen, 6 Reste umfassenden Helix und einer darauf folgenden längeren Helix, die 15 Reste umfasst. Die eingeführten Mutationen verringern dabei die Auftrittswahrscheinlichkeit der ersten, kürzeren Helix um etwa 10%. Oberflächenplasmonenresonanz (SPR) Messungen zeigten, dass NS4A(1-48) und NS4A(1-48, L6E;M10E) unterschiedliche Membranbindungseigenschaften aufweisen. Während NS4A(1-48) eine deutlich ausgeprägte Bindung an Lipiddoppelschichten verschiedener Zusammensetzungen zeigt, bindet die Mutante möglicherweise nur unspezifisch und deutlich schwächer.

A. Appendix

A.1 Material

The regular chemicals used in this study were of purity grade *pro analysis* (p.a.) and were purchased from AppliChem (Darmstadt, Germany), Carl Roth GmbH (Karlsruhe, Germany), Merck KGaA (Darmstadt, Germany) and Sigma-Aldrich Chemie GmbH (Steinheim, Germany). Selected chemicals, enzymes, detergents and lipids utilized in this study are listed in table 1. The water used for bacterial growth media and buffer preparations was deionized water supplied by a Milli-Q-Biocell-System and then filtered through a 0.22 µm Millipack-20-filter device (Millipore GmbH, Schwalbach, Germany). The bacterial growth media were autoclaved for 20 min at 1.5 bar and 120 °C. All buffers were filtered with 0.22 µm Polytetrafluorethylene (PTFE) membrane filter.

A.1.1 Chemicals, enzymes, detergents and lipids

Table 1. Chemicals and enzymes

Chemical	Supplier
6x DNA Loading Dye	Fermentas, St. Lean-Rot, Germany
[¹³ C ₆ , 99 %]-Glucose	Cambridge Isotope Labs, Andover, MA, USA
[¹⁵ N, 99 %]-Ammonium chloride	Cambridge Isotope Labs, Andover, MA, USA
Acrylamide 4K solution (30 %)-Mix 29:1	AppliChem, Darmstadt, Germany
Agarose MP	AppliChem, Darmstadt, Germany
Ampicillin	AppliChem, Darmstadt, Germany
Bovine serum albumin (BSA)	Sigma-Aldrich Chemie, Steinheim, Germany
Complete protease inhibitor cocktail tablet	Roche, Freiburg, Germany
Coomassie Brilliant Blue	Merck, Darmstadt, Germany
Deoxynucleotide triphosphate (dNTP)	Fermentas, St. Lean-Rot, Germany
Deuterium oxide (² H ₂ O) 99.99 %	Sigma-Aldrich Chemie, Steinheim, Germany
Dithiothreitol (DTT)	AppliChem, Darmstadt, Germany
Ethylenediaminetetraacetic acid (EDTA)	AppliChem, Darmstadt, Germany
Ethidium bromide solution 1 %	AppliChem, Darmstadt, Germany
Glutathione (reduced)	AppliChem, Darmstadt, Germany
Glutathione Sepharose 4B (GSH Sepharose)	GE Healthcare, Freiburg, Germany
His-tagged TEV protease S219V	Recominantly produced at ICS-6
Kanamycin	AppliChem, Darmstadt, Germany
Isopropyl-beta-D-thiogalactoside (IPTG)	Carl Roth, Karlsruhe, Germany
Nickel nitrilotriacetic acid (Ni-NTA)	Qiagen, Hilden, Germany

Table 2. Detergents

Detergents	Supplier
3-((3-cholamidopropyl)-dimethylammonio)-1-propane sulfonate (CHAPS)	AppliChem, Darmstadt, Germany
Cetyltrimethylammonium bromide (CTAB)	Sigma-Aldrich Chemie, Steinheim, Germany
n-Dodecyl- β -D-Maltopyranoside (DDM)	Anatrace, Maumee, OH, USA
n-Dodecylphosphocholine (DPC)	Anatrace, Maumee, OH, USA
Sodium dodecyl sulfate (SDS)	AppliChem, Darmstadt, Germany
Sodium dodecyl sulfate, perdeuterated (SDS-d25)	Cambridge Isotope Labs, Andover, MA, USA

Table 3. Lipids

Lipids	Supplier
Cardiolipin (Heart, Bovine) (CA)	Avanti Polar Lipids, Alabaster, AL, USA
Cholesterol	Sigma-Aldrich Chemie, Steinheim, Germany
1-palmitoyl-2-oleoyl-sn-glycero-3-phosphocholine (POPC)	Avanti Polar Lipids, Alabaster, AL, USA
1-palmitoyl-2-oleoyl-sn-glycero-3-phosphoethanolamine (POPE)	Avanti Polar Lipids, Alabaster, AL, USA
1,2-dioleoyl-sn-glycero-3-phospho-L-serine (DOPS)	Avanti Polar Lipids, Alabaster, AL, USA
L- α -phosphatidic acid (Egg) (PA)	Avanti Polar Lipids, Alabaster, AL, USA
L- α -phosphatidylinositol (Liver, Bovine) (PI)	Avanti Polar Lipids, Alabaster, AL, USA
Liver Total Lipid Extract (Bovine) (LTE)	Avanti Polar Lipids, Alabaster, AL, USA
Sphingomyelin (Egg) (SM)	Avanti Polar Lipids, Alabaster, AL, USA

A.1.2 Bacterial strains

The bacterial strain *E. coli* Mach 1-T1, was used for gene cloning of NS4A(1-48). *E. coli* BL21 or *E. coli* BL21-(DE3) cells were used for NS4A(1-48) expression. *E. coli* BL21 Codon Plus (DE3) RIL cells were employed for TEV protease production. Information on the genotype of the bacteria is shown in table 4.

Table 4. Bacterial strains and genotype

<i>E. coli</i> strain	Genotype	Supplier
<i>E. coli</i> Mach 1-T1	F- ϕ 80(lacZ) Δ M15 Δ lacX74 <i>hsdR</i> (r_K^- , m_K^+) Δ recA1398 <i>endA1 tonA</i>	Invitrogen, Darmstadt, Germany
<i>E. coli</i> BL21	<i>E. coli</i> B F ⁻ <i>dcm ompT hsdS</i> (r_B^- m_B^-) <i>gal</i>	GE Healthcare, Freiburg, Germany
<i>E. coli</i> BL21-(DE3)	<i>E. coli</i> B F ⁻ <i>dcm ompT hsdS</i> (r_B^- m_B^-) <i>gal</i> λ (DE3)	Agilent Technologies, Santa Clara, CA, USA
<i>E. coli</i> BL21 Codon Plus (DE3) RIL	<i>E. coli</i> B, F ⁻ , <i>dcm</i> , <i>ompT</i> , <i>hsdS</i> (r_B^- m_B^-), <i>gal</i> , λ (DE3), <i>endA</i> , <i>Hte</i> , [<i>argU ileY leuW Camr</i>]	Agilent Technologies, Santa Clara, CA, USA

A.1.3 Vectors

The pTKK19ubi was a kind gift from Toshiyuki Kohno (Mitsubishi Kagaku Institute of Life Sciences (MITILS), Machida, Tokyo, Japan) [110] and pRK793 (plasmid #8827) was obtained from the Addgene plasmid depository (<http://addgene.org>). The vectors used for production of NS4A(1-48) peptides and tobacco etch virus (TEV) protease are listed in table 5.

Table 5. Vectors

Vector name	Resistance	Characteristics
pTKK19ubi	Kanamycin	Template for protein expression with amino terminal yeast ubiquitin fusion
pRK793	Ampicillin	Expression of TEV protease with point mutation S219V
pGEX-4T-2	Ampicillin	Template for protein expression with amino terminal GST
pGEV-2	Ampicillin	Template for protein expression with amino terminal GB1
pGEV-TEV-NS4A(1-48)	Ampicillin	Expression of NS4A(1-48) with amino terminal GB1 followed by TEV protease recognition site
pGEV-TEV-NS4A(1-48, L6E;M10E)	Ampicillin	Expression of NS4A(1-48, L6E;M10E) with amino terminal GB1 followed by TEV protease recognition site
pGEX- GB1-NS4A(1-48)	Ampicillin	Expression of NS4A(1-48) with sequential amino terminal GST and GB1 followed by TEV protease recognition site
pGEX-GB1-NS4A(1-48, L6E;M10E)	Ampicillin	Expression of NS4A(1-48, L6E;M10E) with sequential amino terminal GST and GB1 followed by TEV protease recognition site
pUbi-NS4A(1-48)	Kanamycin	Expression of NS4A(1-48) with amino terminal ubiquitin followed by a yeast ubiquitin hydrolase recognition motif

A.1.4 Primers

Synthetic oligonucleotides were purchased from BioTez (Berlin, Germany). Strategies for primer usage are described in the methods section of the already published manuscript in chapter 3.2.

Table 6. Primers used for cloning of NS4A(1-48) vectors

Primer	Sequence(5' - 3')
1	agcctgaccctgaatctgattaccgaaatgggtcgtctgccgacctttatgaccagaaagca cgtgatgcactggataatctgg
2	cagttctgcataccgctgaagccggtgggtcgtgcatataatcatgcactgagcgaaactgtaag
3	tgctttctgggtcataaaggctcggcagacgacccatttcggtaatcagattcagggtcaggct
4	gacccctacagttcgctcagtgcatgattatatgcacgaccaccggcttcagcggtatgcaga actgccagattatccagtgcacac
5	ggaggaggatccgaaaacctgtattttcagagcctgaccctgaatctgattacc <i>Bam</i> HI
6	ggaggagtcgac <u>ctcgag</u> ttacagttcgctcagtg <i>Xho</i> I
7	gcgcgaattcagttacaagcttgctctgaacgg

	<i>EcoRI</i>
8	gctagttattgctcagcgg (T7-Terminator-Primer; Novagen #69337-3)
9	ggaggaccgcggcggtagcctgaccctgaatctga
	<i>SacII</i>
10	ggaggagtcgacctcgagttacagttcgctcagtgc
	<i>SalI</i>
11	gaaattaccgaagagggtcgtctgccgac
12	attcagggtcaggctctgaaaatacaggtt

A.1.5 Kits

Commercial kits used for DNA purification are listed in table 7.


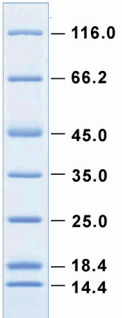
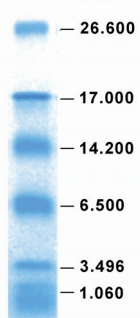
Table 7. Commercial kits

Name of the kit	Supplier
NucleoBond AX 100	Macherey-Nagel, Düren, Germany
NucleoSpin Gel and PCR Clean-up	Macherey-Nagel, Düren, Germany

A.1.6 Gel electrophoresis markers

Table 8 displays the molecular weight markers used for DNA and protein analysis on 1 % agarose and 15 % SDS PAGE gels, respectively.

Table 8. Molecular weight markers used for this work

GeneRuler 1 kb DNA Ladder (Fermentas)	Unstained protein molecular weight marker (Fermentas)	Ultra-low range molecular weight marker (Sigma-Aldrich)
 <p>bp</p> <p>10000 8000 6000 5000 4000 3500 3000 2500 2000 1500 1000 750 500 250</p>	 <p>kDa</p> <p>116.0 66.2 45.0 35.0 25.0 18.4 14.4</p>	 <p>kDa</p> <p>26.600 17.000 14.200 6.500 3.496 1.060</p>

A.1.7 Laboratory equipment

Table 9. Instruments, equipment and consumables

Equipment	Supplier
ÄKTA purifier chromatography system	GE Healthcare, Freiburg, Germany
Aquatron incubation shaker	Infors-HT, Einsbach, Germany
Centrifuge 5415D	Eppendorf, Hamburg, Germany
Centrifuge 5804R	Eppendorf, Hamburg, Germany
Centrifuge Avanti J-20 XP	Beckman Coulter, Krefeld, Germany
ChemiDoc MP	Bio-Rad, Munich, Germany
Eppendorf UVette cuvettes	Sigma-Aldrich, Munich, Germany
GelDoc 2000	Bio-Rad, Munich, Germany
HEΛIOS Q spectrophotometer	Thermo Scientific, Waltham, MA, USA
HiLoad 16/60 Superdex 75 pg	GE Healthcare, Freiburg, Germany
HiLoad 26/60 Superdex 75 pg	GE Healthcare, Freiburg, Germany
Nuclepore polycarbonate membrane	GE Healthcare, Freiburg, Germany
Mighty small II deluxe mini vertical electrophoresis unit	Hoefer, Holliston, MA, USA
Horizontal DNA electrophoresis apparatus	GE Healthcare, Freiburg, Germany
iCycler PCR machine	Bio-Rad, Munich, Germany
JASCO J-810 CD spectrometer	Gross-Umstadt, Germany
JASCO J-1100 CD spectrometer	Gross-Umstadt, Germany
Lambda 25 UV/VIS spectrometer	Perkin Elmer, Waltham, MA, USA
LiposoFast-Basic extruder	Avestin, Mannheim, Germany
Lyophilizer Alpha 1-4	Martin Christ, Osterode, Germany
Milli-Q-Biocell system	Millipore, Schwalbach, Germany
Microfluidizer M-100P	Microfluidics, Worcestershire, UK
pH-Meter	Mettler-Toledo, Gießen, Germany
Protein Solutions DynaPro DLS	Wyatt Technology, Santa Barbara, USA
Quartz cuvette (Hellma 100-QS)	Hellma, Müllheim, Germany
0.22 µm Polytetrafluorethylene (PTFE)	Sartorius, Göttingen, Germany
Semi-micro balance CP225D	Sartorius, Göttingen, Germany
Series S Sensor Chip L1	GE Healthcare, Freiburg, Germany
Spectra/Por dialysis membranes (1 kDa MWCO)	Carl Roth, Karlsruhe, Germany
Unitron incubation shaker	Infors-HT, Einsbach, Germany
Vivaspin 20 concentrator (3 kDa MWCO)	Sartorius, Göttingen, Germany

A.1.8 Software and databases

The amino acid sequence 1 to 48 of NS4A from dengue virus type 2 was obtained from the Protein data bank at NCBI (<http://www.ncbi.nlm.nih.gov/protein>) under accession code NP_739588.2. A gene coding for DENV NS4A(1-48) and optimized for codon-usage in *E.coli* was designed using the GeneOptimizer software provided online by Life Technologies Corporation (<https://www.lifetechnologies.com/de/de/home/lifescience/cloning/genesynthesis/geneart-gene-synthesis/geneoptimizer.html>). The ProtParam tool was used for extinction coefficient calculation of

proteins (<http://web.expasy.org/protparam/>). The helical wheel analysis was performed on the web server HELIQUEST (<http://heliquest.ipmc.cnrs.fr>) [111].

Table 10. Software used for NMR data analysis

Software	Version	Reference or commercial source
CcpNmr	v.2.3	Vranken, Boucher, Stevens, Fogh, Pajon, Llinas, Ulrich, Markley, Ionides and Laue [112]
NMRpipe	v.7.9	Delaglio, Grzesiek, Vuister, Zhu, Pfeifer and Bax [113]
TALOS-N	4.01	Shen and Bax [90]
VnmrJ	2.3c	Agilent Technologies (previously: Varian) (proprietary)

A.2 Methods

A2.1 Bacterial cultures

For plasmid amplification or protein expression, the *E. coli* cells were transformed with vectors listed in table 5. For transformation, the chemically competent *E. coli* cells were thawed for 10 minutes from -80 °C. Transformation was performed by mixing 100 ng of plasmid DNA with 100 µl competent *E. coli* stock. The mixture was incubated at 42 °C for 1 min and then placed on ice immediately for 2 min. The transformed *E. coli* cells were cultured on LB plates for 16h at 37 °C. A single colony was picked from the plate and cultured in LB medium for 16h at 37 °C. For protein expression the *E. coli* were continually cultured in LB or M9 medium, and the details are described in A.2.3.1. The culture media used are listed below. Lysogeny broth, M9 medium and TS2 trace-element solution are prepared in pure H₂O. Vitamin-cocktail solution, thiamine hydrochloride stock (5 g/L), and Fe(III)-citrate stock (10 mM) are prepared in 20 mM phosphate buffer at pH 7.0.

Lysogeny broth (LB)

Chemicals	Concentration
Tryptone	10 g/L
Yeast extract	5 g/L
NaCl	5 g/L
MgSO ₄	2 mM

LB agar

Chemicals	Concentration
Tryptone	10 g/L
Yeast extract	5 g/L
NaCl	5 g/L
Agar	15 g/L

Minimal medium 9 (M9)

Chemicals	Concentration
[¹⁵ N]-NH ₄ Cl	1 g/L
[¹³ C ₆]-Glucose	2 g/L
Na ₂ HPO ₄	51 mM
KH ₂ PO ₄	22 mM
NaCl	8.5 mM
CaCl ₂	0.1 mM
MgSO ₄	2 mM
Fe(III)-citrate	10 µM
trace-element solution	0.2 % (v/v)
vitamin-cocktail solution	0.1 % (v/v)
Thiamine hydrochloride	5 mg/L
pH 7.4	

TS2 trace-element solution

Chemicals	Concentration
MnCl ₂ ·4H ₂ O	30 mg/L
ZnSO ₄ ·7H ₂ O	100 mg/L
H ₃ BO ₃	300 mg/L
CoCl ₂ ·6H ₂ O	200 mg/L
NiCl ₂ ·6H ₂ O	20 mg/L
CuCl ₂ ·2H ₂ O	10 mg/L
Na ₂ MoO ₄ ·2H ₂ O	900 mg/L
Na ₂ SeO ₃	20 mg/L

Vitamin-cocktail solution

Chemicals	Concentration
d-Biotin	1 g/L
Choline chloride	1 g/L
Folic acid	1 g/L
Nicotinamide	1 g/L
Sodium-D-pantothenate	1 g/L
Pyridoxal hydrochloride	1 g/L
Riboflavin	0.1 g/L

A.2.2 DNA preparation methods

A.2.2.1 Plasmid DNA isolation

The DNA vector was first transformed into *E. coli* Mach 1-T1 cells and cultured in 2 mL LB medium for 16 h at 37 °C. The plasmid DNA was then isolated from *E. coli* Mach 1-T1 cells with a commercial kit, NucleoBond AX 100.

A.2.2.2 Concentration determination of DNA samples

The concentration of DNA was determined based on the measurement of light absorption in the ultraviolet range using a Lambda 25 UV/VIS spectrometer and a quartz cuvette with an optical path length of 1 cm. The concentration of DNA is estimated on the basis of the Beer-Lambert law. It is assumed that a measured absorption value of 1.0 at the wavelength of 260 nm corresponds to 50 µg/ml of double-stranded DNA [114].

A.2.2.3 DNA agarose gel electrophoresis

The DNA fragments in this study were separated in 1 % (w/v) agarose gels in a horizontal gel electrophoresis apparatus. The agarose gels were prepared by dissolving 1 g agarose and 1 mg/L ethidium bromide in 100 mL TAE buffer (40 mM Tris acetate pH 8.0, 1 mM EDTA). The DNA samples were loaded into the agarose gel with 6x DNA Loading Dye and the electrophoresis was performed with a constant voltage of 90 V. The negatively charged DNA molecules experience a force in the electric field. Movement of the DNA molecules in this field is slowed down by frictional forces due to the agarose matrix resulting in a DNA-size-dependent migration velocity. This effect facilitates effective separation of DNA molecules in the agarose gel. The agarose gels were documented using the GelDoc2000 system.

A.2.2.4 Polymerase chain reaction (PCR)

The DNA for creating the vectors, pGEX-GB1-NS4A(1-48)/(1-48, L6E;M10E), were produced by PCR using the iCycler PCR machine. The primers are primer number 7 and 8 in table 6. The template DNA were pGEV-TEV-NS4A(1-48) and pGEV-TEV-NS4A(1-48, L6E;M10E). The PCR reaction components and condition are listed in table 11 and table 12.

Table 11. PCR reaction components in a 0.2 ml PCR tube

Component	Volume (μl)	Final concentration
Reaction buffer (10×)	5	1×
dNTP solution mix (10 mM)	1.5	250 μM
Primer no.7	0.5	0.3 μM
Primer no.8	0.5	0.3 μM
Template DNA	2	0.5 μM
Vent DNA polymerase	1	2 units
MgSO ₄	0.75	1.5 mM
H ₂ O	Bring reaction to the final volume of 50 μl	

Table 12. PCR reaction condition

Step	Temperature	Time
Initial denaturation	95 °C	1 minute
25 cycles	95 °C	30 seconds
	55 °C	50 seconds
	72 °C	50 seconds
	72 °C	2 minutes
Final extension	72 °C	2 minutes
Hold	4 °C	

A.2.2.5 Construction of pGEX-GB1-NS4A(1-48)/(1-48, L6E;M10E)

The amplified GB1-TEV-NS4A(1-48)/(1-48, L6E;M10E) DNA fragments, for insertion, and the pGEX-4T-2 vector DNA were digested with restriction enzymes, EcoRI and XhoI. After restriction digestion, the 5'-phosphate groups of cleaved DNA are removed by shrimp alkaline phosphatase (SAP). T4 DNA ligase was applied to catalyze the ligation of the insert DNA fragment and the vector. All procedures were carried out according to manufacturer's recommendations. After ligation, the plasmids were transformed into *E. coli* Mach 1-T1 cells and cultured on LB agar plates containing 100 μg/mL ampicillin for 16 h at 37 °C. Isolated single colonies from the plates were utilized for plasmid amplification (cf. A.2.1). The plasmids were sequenced with 5'-primer (no. 7 in table 6) or 3'-primer (no. 8), each 0.25 pmol, at SeqLab (Sequence Laboratories Göttingen, Germany).

A.2.3 NS4A(1-48) fusion protein preparations

In order to overcome the problem of low protein expression levels encountered with the ubiquitin fusion strategy and the difficulties in separating NS4A peptides from GB1 after TEV protease cleavage when using the GB1 fusion strategy, an N-terminal glutathione S-transferase (GST) affinity tag was added to the GB1-TEV-NS4A(1-48) and GB1-TEV-NS4A(1-48, L6E;M10E) fusions, respectively, by cloning the initial plasmids into pGEX4T-2. Protein expression and purification of the GST-GB1-NS4A(1-48) and GST-GB1-NS4A(1-48, L6E;M10E) will be described in more detail in the following section.

A.2.3.1 Expression and purification of GST-GB1-NS4A(1-48) fusion proteins

Fusion proteins intended for NMR studies on the NS4A peptides were produced with M9 medium containing [^{15}N]- NH_4Cl and [$^{13}\text{C}_6$]-glucose as sole nitrogen and carbon sources, respectively. All other fusion proteins were produced in LB medium. For protein expression, the *E. coli* BL21 cells were transformed with vector pGEX-GB1-TEV-NS4A(1-48) or pGEX-GB1-TEV-NS4A(1-48, L6E;M10E). After growing a preculture of 50 ml in LB medium for 16 h, the cells were collected by centrifugation (5000 \times g, 5 minutes, room temperature) and used to inoculate LB or M9 medium to give an optical density at 600 nm (OD_{600}) of 0.1. Ampicillin was added to the medium to give a concentration of 100 $\mu\text{g}/\text{ml}$ and the *E. coli* cells were cultured at 37 $^\circ\text{C}$ in the Unitron incubation shaker at 150 rpm. When the OD_{600} reached 0.8, the gene expression was induced by adding Isopropyl-beta-D-thiogalactoside (IPTG) to a final concentration of 1 mM. Cells were incubated for another 5 h. Finally, *E. coli* cells were harvested by centrifugation (5000 \times g, 30 min, 4 $^\circ\text{C}$) and stored at -20 $^\circ\text{C}$.

Cell pellets from pGEX-GB1-NS4A(1-48) or pGEX-GB1-NS4A(1-48, L6E;M10E) transformed cells, harvested from 1 L expression culture, were thawed and resuspended on ice in 25 mL lysis buffer (50 mM Tris-HCl pH 8.0, 150 mM NaCl) supplemented with a complete protease inhibitor cocktail tablet. Cells were lysed using 4-5 cycles in the Microfluidizer M-100P. The crude lysate was clarified by centrifugation (50000 \times g, 30 min, 4 $^\circ\text{C}$). Subsequent purification steps were performed at 22 $^\circ\text{C}$. The supernatant was applied onto a gravity flow column (column volume (CV) of 5 mL) packed with GSH sepharose 4B and pre-equilibrated with lysis buffer. Unbound material was removed by washing with 10 CV of lysis buffer. The pure NS4A(1-48) or NS4A(1-48, L6E;M10E) was liberated from the fusion protein by TEV protease digestion.

TEV protease digestion of NS4A(1-48, L6E;M10E) can be performed on column under standard conditions (peptide-to-TEV ratio of about 100) overnight at 22 $^\circ\text{C}$. The standard buffer for TEV protease digestion is the lysis buffer supplemented with 0.5 mM EDTA and 1 mM DTT. After 16 h digestion, unbound material was eluted and the column was washed. The NS4A(1-48, L6E;M10E) peptide and TEV protease containing flow-through and wash fractions were pooled and

concentrated to 5 mL using a Vivaspin 20 centrifugal concentrator (MWCO: 3 kDa). Separation of TEV protease (~29 kDa) from NS4A mutant peptide (5.2 kDa) was accomplished with a HiLoad 16/60 Superdex 75 prep grade column on an ÄKTA purifier system at 22 °C with a flow rate of 1 mL/min.

Digestion of the double tagged GST-GB1-NS4A(1-48) fusion protein containing the wild type NS4A(1-48) peptide sequence was not successful under these standard conditions. Here, cell lysis had to be done in lysis buffer supplemented with 0.5 mM EDTA, 1 mM DTT and additionally 0.5 M urea. GSH-binding and on column cleavage had to be done in the presence of 0.5 M urea and enzymatic cleavage required a higher TEV concentration (50 µM, peptide-to-TEV ratio of about 10). The flow-through was collected after TEV digestion and concentrated using a Vivaspin 20 centrifugal concentrator. The concentrated peptide solution was further purified using a Highload 16/60 Superdex 75 prep grade column, equilibrated with 50 mM Tris-HCl pH 8, 150 mM NaCl but without urea at a flow rate of 1 mL/min. NS4A(1-48) containing fractions were pooled and concentrated. Cleavage, separation efficiency and final purity of the NS4A peptides were evaluated using SDS-PAGE analysis. NS4A(1-48) and the mutant peptide were kept at 4 °C for short-term storage or rapidly frozen in liquid nitrogen prior to long-term storage at -80 °C.

A.2.3.2 Protein gel electrophoresis

Protein analysis was performed with sodium dodecyl sulphate polyacrylamide gel electrophoresis (SDS-PAGE [115]) using discontinuous gels. The gels are composed of a 5 % (polyacrylamide containing) stacking gel and a 15 % separating gel. The protein samples are prepared by adding 4× sample buffer at a volume ratio of 1:3 and loaded onto the gel in parallel with protein markers (cf. A.1.7). The SDS-PAGE was carried out in a vertical electrophoresis unit (Mighty small II) at 40 mA per gel for 1 h in SDS running buffer. The protein gels were soaked in fixing solution for at least 1 h. Then the gels were stained with Coomassie blue stain solution for at least 30 minutes and destained in water. The destained gels were documented using the ChemiDoc MP system.

5 % Stacking gel		15 % Separating gel	
Chemicals	Concentration	Chemicals	Concentration
Acrylamide	4.85 % (w/v)	Acrylamide	14.55 % (w/v)
N,N'-methylene-bis-acrylamide	0.15 % (w/v)	N,N'-methylene-bis -acrylamide	0.45 % (w/v)
Tris/HCl, pH 6.8	125 mM	Tris/HCl, pH 8.8	375 mM
SDS	0.1 % (w/v)	SDS	0.1 % (w/v)
APS	0.1 % (w/v)	APS	0.1 % (w/v)
TEMED	0.1 % (w/v)	TEMED	0.1 % (w/v)

SDS Running buffer		4× Sample buffer	
Chemicals	Concentration	Chemicals	Concentration
Tris/HCl, pH 8.3	50 mM	Tris/HCl, pH 8.0	200 mM
Glycine	385mM	SDS	8 %
SDS	0.1 %	β-mercaptoethanol	8 %
		Glycerol	40 %
		Bromphenol blue	0.05 %

Fixing solution		Coomassie blue stain solution	
Chemicals	Concentration	Chemicals	Concentration
Acetic acid	10 % (v/v)	Acetic acid	10 % (v/v)
Methanol	50 % (v/v)	Isopropanol	25 % (v/v)
H ₂ O	40 % (v/v)	Coomassie brilliant blue R-250	0.5 g/L

A.2.3.3 Protein concentration determination

The ultraviolet light absorption of the protein sample was measured at 280 nm using the Lambda 25 UV/VIS spectrometer and a cuvette with an optical path length of 1 cm. The respective absorbance value and extinction coefficient of the protein at 280 nm were used for concentration calculation on the basis of the Beer-Lambert law.

A.2.4 Liposome preparation

The lipids for liposome preparation are listed in table 3. Lipids in chloroform solution were purchased from Avanti Polar Lipids. The cholesterol (>99 %) powder was purchased from Sigma-Aldrich and was dissolved in chloroform at 10 mg mL⁻¹. Besides the single component lipid POPC and the total lipid extract from bovine liver we studied two lipid mixtures: a POPC/DOPS mixture at a molar ratio of 4 : 1 and a multicomponent mixture resembling the composition of membranes in the endoplasmic reticulum (ER). Following previous work [116] a synthetic ER lipid mix with the following components was used: POPC/bovine heart CL/bovine liver PI/POPE/ DOPS/chicken egg PA/chicken egg SM/cholesterol with molar ratios of 59 : 0.37 : 7.7 : 18 : 3.1 : 1.2 : 3.4 : 7.8. The final liposome samples were checked for lipid degradation products by thin layer chromatography (TLC) using Alugram SIL G sheets (Macherey-Nagel, Düren, Germany) and a mobile phase of chloroform, methanol, and aqueous ammonia (25%) in a volume ratio of 13:7:1.

A.2.4.1 Preparation of extruded liposomes

Small unilamellar lipid vesicles for CD and SPR experiments were prepared by extrusion using either a single lipid component or a synthetic mixture of different lipids. Appropriate volumes of the lipid chloroform stocks were transferred to a glass test tube at the desired molar ratios with a total amount of 5 mg of lipid per sample. Chloroform was removed by passing a gentle stream of nitrogen gas over the solution while slowly rotating the test tube, resulting in a thin film of lipid on the inner wall of the tube. High vacuum was applied for at least 3 h to remove chloroform traces. Lipid films were suspended under vortexing in 500 μ L of sodium phosphate buffer (50 mM sodium phosphate, pH 6.8, 150 mM NaCl). Samples were subjected to three cycles of freezing and thawing in liquid nitrogen and a 60 °C water bath. Liposome solutions were passed 15 times or more through a Nuclepore polycarbonate membrane with nominal pore diameter of either 30 or 50 nm (GE Healthcare, Freiburg, Germany) using a handheld LiposoFast Extruder (Avestin Europe GmbH, Mannheim, Germany) equipped with two 0.5 mL syringes. Finally, the hydrodynamic radius of the liposomes was determined by dynamic light scattering (DLS).

A.2.4.2 Preparation of sonicated liposomes

Sonicated lipid vesicles were produced starting from SUV solution obtained by extrusion through a 30 nm Nuclepore membrane. Volumes of 500 μ L per sample were transferred to 1.5 mL Eppendorf tubes, kept on ice and treated with a 3 mm microtip of a Branson 250 sonifier. Ten cycles of sonication (20 sec) and intermediate cooling (2 min) were applied. Finally, the hydrodynamic radius of the liposomes was determined by DLS.

A.2.5 SPR analysis of NS4A peptide binding to liposomes

The SPR experiments were performed on a Biacore X instrument using L1 sensor chips. The NS4A(1-48) and NS4A(1-48, L6E;M10E) peptides were produced in LB medium using the same fusion protein expression systems and purification protocols described above for the NMR samples. The purified peptides were dialyzed twice against 50 mM sodium phosphate buffer (pH 6.8) at 4 °C. The dialysis volume ratio was 1:1000 in each of the two dialysis steps lasting for 6 and 16 h, respectively. The final NS4A peptide concentration was 30 μ M. The liposomes were prepared in the same buffer.

A.2.5.1 Liposome immobilization on L1 chip

L1 chips were equilibrated with 50 mM sodium phosphate buffer pH 6.8 for 30 min and then stripped with short pulses (1 min at a flow rate of 20 μ L min⁻¹) of 20 mM CHAPS (3-((3-cholamidopropyl)-dimethylammonio)-1-propane sulfonate). The entire flow path was rinsed with phosphate buffer. For liposome immobilization, the SUV solution (80 μ L, with a nominal lipid concentration of 2 mg mL⁻¹, extruded through a 50 nm Nuclepore membrane) was injected at a flow rate of 2 μ L min⁻¹. Three short pulses of 50 mM NaOH were applied at 10 μ L min⁻¹ in order to remove

loosely bound liposomes and to achieve a stable baseline. A solution of 0.1 mg mL⁻¹ bovine serum albumin (BSA, Sigma-Aldrich) was injected for 1 min at a flow rate of 10 µL min⁻¹ in order to block potential non-specific ligand binding sites on the surface. Initial blank injections with running buffer only and binding experiments with 30 µM of the NS4A peptide were performed at a flow rate of 20 µL min⁻¹.

A.2.5.2 SPR experiments

Initial blank injections with buffer only and binding experiments with 30 µM NS4A peptide were performed at a flow rate of 20 µL min⁻¹. In binding experiments the analyte solution was injected for 30 sec (association phase) followed by buffer injection for 100 sec or longer (dissociation phase). A corrected sensorgram was obtained by subtracting the sensorgram of the blank injection from that of the immediately following binding experiment.

Complete return of the response (RU) signal to pre-injection level could be achieved neither after extended buffer injection times of several hours nor by established regeneration procedures with high salt concentration or extreme pH buffers. Therefore, the L1 sensor chip was completely stripped of lipids and protein with repeated short pulses of 20 mM CHAPS until the RU value became similar to the original value observed prior to the first liposome immobilization. Stripping had to be repeated after every single binding experiment.

A.2.6 Circular dichroism (CD) experiments

CD data were measured with a Jasco J-1100 instrument (Jasco, Groß-Ulmstadt, Germany) at 30 °C using a QS quartz cell with optical path length of 1 mm (Hellma, Müllheim, Germany). All samples were prepared in 50 mM sodium phosphate buffer, pH 6.8, 150 mM NaCl. Appropriate amounts of extruded or sonicated liposome stock and buffer were supplemented with peptide stock to give a final lipid concentration of 10 mg mL⁻¹, i.e., about 13 mM, in all liposome samples. Additional samples contained peptide in buffer or micelles (100 mM SDS). Concentration of NS4A(1-48) or NS4A(1-48, L6E;M10E) peptides was 40 µM in all samples. Light scattering due to the large size of liposomes and light extinction due to high concentration of chloride ions limited acquisition of CD data to the wavelength range above 205 nm. CD data were recorded in continuous scan mode (scan speed 50 nm min⁻¹, bandwidth 1 nm, integration time constant 0.5 s, accumulation of 5 scans). Appropriate background spectra reflecting contributions from the buffer, liposome or detergent solution were subtracted from each curve.

A.2.7 NMR spectroscopy experiments

A.2.7.1 Sample preparation of NS4A(1-48) proteins

The isotopically labeled peptides were produced with M9 medium (cf. A.2.1). The purification procedure is described in A.2.3.1. After purification, peptides were dialyzed with Spectra/Por dialysis membranes (1 kDa MWCO) in 50 mM sodium phosphate buffer (pH 6.8) for 3 h at the first time and 16 h for the second time at 4 °C. The buffer to sample volume ratio was 500 in each of the two dialysis steps. The final NMR samples contained 1 mM [U-¹⁵N]- or [U-¹⁵N, ¹³C]-labeled NS4A(1-48) or NS4A(1-48, L6E;M10E) in 50 mM sodium phosphate buffer (pH 6.8), 10% (v/v) deuterium oxide, 0.03% (w/v) NaN₃, with or without 100 mM perdeuterated sodium dodecyl sulfate (SDS-d25).

A.2.7.2 NMR experiments

NMR experiments were performed at 30 °C on Varian UnityINOVA, VNMRS and Bruker Avance III HD NMR instruments, equipped with cryogenic Z-axis pulse-field-gradient (PFG) triple resonance probes operating at proton frequencies of 600, 800, and 900 MHz. Resonance assignment of protein backbone nuclei was accomplished using a combined set of heteronuclear multidimensional NMR experiments: 2D (¹H-¹⁵N)-HSQC [117, 118], 2D (¹H-¹⁵N)-BEST-TROSY [119], 2D (¹H-¹³C)-HSQC [120], 3D HNCACB [121], 3D HNCO [122], and 3D HNHA [123]. Decoupling of ¹⁵N and ¹³C nuclei during ¹H acquisition was achieved by the GARP sequence [124]. ¹H and ¹³C chemical shifts were referenced directly to internal DSS at 0 ppm and ¹⁵N chemical shifts were referenced indirectly to DSS using the absolute ratio 0.101329118 of the ¹⁵N and ¹H zero point frequencies [125]. NMR data were processed using NMRPipe, v.8.1 [113] and evaluated with CcpNmr v.2.3 [112] and TALOS-N [90] software.

Heteronuclear {¹H}-¹⁵N NOEs (nuclear Overhauser effects) were derived from 2D spectra recorded at 18.8 T with or without 6 s of proton saturation [126]. The heteronuclear NOE is the ratio of the integral peak intensities of a given ¹H-¹⁵N correlation measured with and without saturation, respectively.

Table 13.
NMR experiments performed on NS4A(1-48) and selected acquisition parameters

Experiment	sw1 [ppm]	t1 [pts]	sw2 [ppm]	t2 [pts]	sw3 [ppm]	t3 [pts]	nt	d1 [s]
2D (¹⁵ N- ¹ H)-BEST-TROSY	23.1	100	14.9	1880	-	-	4	0.2
ct-2D (¹ H- ¹³ C) HSQC	110.4	674	15.6	1500	-	-	32	1
3D HNCACB	61.4	146	23.5	40	14.9	1882	32	0.3
3D HNCO	14.1	74	23.5	43	13.3	1684	8	0.28
3D HNHA	5.9	58	23.5	35	13.3	1024	24	1.7

Table 14.**NMR experiments performed on NS4A(1-48, L6E;M10E) and selected acquisition parameters**

Experiment	sw1 [ppm]	t1 [pts]	sw2 [ppm]	t2 [pts]	sw3 [ppm]	t3 [pts]	nt	d1 [s]
2D (^{15}N - ^1H)-HSQC	23.1	100	19.9	2040	-	-	4	1
ct-2D (^1H - ^{13}C) HSQC	93.3	120	19.9	1280	-	-	64	1
3D HNCACB	59.67	30	23.1	120	19.9	1678	16	1
3D HNCO	12.0	30	23.1	48	19.9	1798	8	1
3D HNHA	6.6	59	30.5	80	13.3	1280	8	1.5

A.2.7.3 NMR resonance assignment

Both wild type and mutant NS4A(1-48) peptides were analysed using liquid state NMR spectroscopy in presence of 100 mM SDS-d25. In total, 98% of the expected backbone resonances of both NS4A(1-48) and NS4A(1-48, L6E;M10E) were assigned. Resonance assignments for the two NS4A N-terminal peptides have been deposited at the Biological Magnetic Resonance Data Bank (BMRB) under accession numbers 25179 (wild type) and 25180 (mutant).

A.2.7.4 Secondary structure and backbone dynamics analysis

The software program TALOS-N [90] contains the artificial neural network (ANN) module SS-ANN for prediction of the three-state secondary structure (SS) from experimental protein backbone $^{13}\text{C}\alpha$, $^{13}\text{C}\beta$, $^{13}\text{C}'$, $^1\text{H}\alpha$, ^{15}N , and ^1HN NMR chemical shift data and database knowledge. A definition of the three SS classes, i.e., helix (H), extended strand (E) and coil (L), can be found in [90]. The SS-ANN algorithm correlates chemical shift and sequence data of pentapeptide fragments of the target protein with closely matching pentapeptide fragments from a dedicated database of 580 proteins containing their backbone chemical shifts and atomic coordinates. The module has been shown to correctly predict the SS class of the center residue of query pentapeptides with an average sensitivity (Q_3 score) of 88.6 % in a representative validation test [69]. The experimental backbone chemical shifts of the two NS4A peptides were analysed by the SS-ANN module for secondary structure prediction. The model-free backbone order parameter S^2 [127] provides a popular description of protein dynamics on the pico- to nanosecond timescale [128]. An empirical correlation has been described between protein backbone secondary chemical shifts and S^2 values derived from NMR relaxation data [129]. The random coil index (RCI) method allows estimation of S^2 values, referred to as RCI- S^2 , from measured backbone chemical shifts and tabulated random coil shifts alone [129, 130]. The magnitude of the RCI- S^2 manifests conformational flexibility. Rigid secondary structure elements are characterized by large RCI- S^2 values, while flexible residues show order parameters of less than 0.85 [130] and large positive $\{^1\text{H}\}$ - ^{15}N -NOEs ratios around 0.8 [131].

Bibliography

- [1] D.J. Gubler, Dengue and dengue hemorrhagic fever, *Clin Microbiol Rev*, 11 (1998) 480-496.
- [2] S. Bhatt, P.W. Gething, O.J. Brady, J.P. Messina, A.W. Farlow, C.L. Moyes, J.M. Drake, J.S. Brownstein, A.G. Hoen, O. Sankoh, M.F. Myers, D.B. George, T. Jaenisch, G.R. Wint, C.P. Simmons, T.W. Scott, J.J. Farrar, S.I. Hay, The global distribution and burden of dengue, *Nature*, 496 (2013) 504-507.
- [3] A. Wilder-Smith, K.-E. Renhorn, H. Tissera, S.A. Bakar, L. Alphey, P. Kittayapong, S. Lindsay, J. Logan, C. Hatz, P. Reiter, J. Rocklöv, P. Byass, V.R. Louis, Y. Tozan, E. Massad, A. Tenorio, C. Lagneau, , G. Ambert, D. Brooks, J. Wegerdt, D. Gubler, DengueTools: innovative tools and strategies for the surveillance and control of dengue, *Glob Health Action* (2012) 5: 17273 - DOI: 10.3402/gha.v5i0.17273.
- [4] Gjenero-Margan I, Aleraj B, Krajcar D, Lesnikar V, Klobučar A, Pem-Novosel I, Kurečić-Filipović S, Komparak S, Martić R, Đuričić S, Betica-Radić L, Okmađžić J, Vilibić-Čavlek T, Babić-Erceg A, Turković B, Av.ić-Županc T, Radić I, Ljubić M, .arac K, Benić N, Mlinarić-Galinović G. Autochthonous dengue fever in Croatia, August–September 2010. *Euro Surveill.* (2011) 16(9):pii=19805.
- [5] R. Allwinn, Significant increase in travel-associated dengue fever in Germany, *Med Microbiol Immunol*, 200 (2011) 155-159.
- [6] B.D. Lindenbach, H.-J.T.C.M. Rice, *Flaviviridae: Viruses and Their Replication*, in: *Fields Virology*, Lippincott Williams & Wilkins, New York, 2007, pp. 1101-1151.
- [7] B.E. Martina, P. Koraka, A.D. Osterhaus, Dengue virus pathogenesis: an integrated view, *Clin Microbiol Rev*, 22 (2009) 564-581.
- [8] K. Clyde, J.L. Kyle, E. Harris, Recent advances in deciphering viral and host determinants of dengue virus replication and pathogenesis, *Journal of virology*, 80 (2006) 11418-11431.
- [9] B.R. Murphy, S.S. Whitehead, Immune response to dengue virus and prospects for a vaccine, *Annu Rev Immunol*, 29 (2011) 587-619.
- [10] J.C. Nikos Vasilakis, Kathryn A. Hanley, Edward C. Holmes, a.S.C. Weaver, Fever from the forest: prospects for the continued emergence of sylvatic dengue virus and its impact on public health, *Nature*, 9 (2011) 532-541.
- [11] D. Wallace, V. Canouet, P. Garbes, T.A. Wartel, Challenges in the clinical development of a dengue vaccine, *Curr Opin Virol*, 3 (2013) 352-356.
- [12] B.S. Schneider, S. Higgs, The enhancement of arbovirus transmission and disease by mosquito saliva is associated with modulation of the host immune response, *Transactions of The Royal Society of Tropical Medicine and Hygiene*, 102 (2008) 400-408.
- [13] E.G. Acosta, V. Castilla, E.B. Damonte, Functional entry of dengue virus into *Aedes albopictus* mosquito cells is dependent on clathrin-mediated endocytosis, *The Journal of general virology*, 89 (2008) 474-484.

- [14] M.N. Krishnan, B. Sukumaran, U. Pal, H. Agaisse, J.L. Murray, T.W. Hodge, E. Fikrig, Rab 5 Is Required for the Cellular Entry of Dengue and West Nile Viruses, *Journal of virology*, 81 (2007) 4881-4885.
- [15] H.M. van der Schaar, M.J. Rust, C. Chen, H. van der Ende-Metselaar, J. Wilschut, X. Zhuang, J.M. Smit, Dissecting the Cell Entry Pathway of Dengue Virus by Single-Particle Tracking in Living Cells, *PLoS Pathog*, 4 (2008) e1000244.
- [16] M. Nawa, T. Takasaki, K. Yamada, I. Kurane, T. Akatsuka, Interference in Japanese encephalitis virus infection of Vero cells by a cationic amphiphilic drug, chlorpromazine, *The Journal of general virology*, 84 (2003) 1737-1741.
- [17] T. Mizutani, M. Kobayashi, Y. Eshita, K. Shirato, T. Kimura, Y. Ako, H. Miyoshi, T. Takasaki, I. Kurane, H. Kariwa, T. Umemura, I. Takashima, Involvement of the JNK-like protein of the *Aedes albopictus* mosquito cell line, C6/36, in phagocytosis, endocytosis and infection of West Nile virus, *Insect molecular biology*, 12 (2003) 491-499.
- [18] E.G. Acosta, V. Castilla, E.B. Damonte, Alternative infectious entry pathways for dengue virus serotypes into mammalian cells, *Cellular microbiology*, 11 (2009) 1533-1549.
- [19] R.J. Kuhn, W. Zhang, M.G. Rossmann, S.V. Pletnev, J. Corver, E. Lenches, C.T. Jones, S. Mukhopadhyay, P.R. Chipman, E.G. Strauss, T.S. Baker, J.H. Strauss, Structure of dengue virus: implications for flavivirus organization, maturation, and fusion, *Cell*, 108 (2002) 717-725.
- [20] S. Mukhopadhyay, R.J. Kuhn, M.G. Rossmann, A structural perspective of the flavivirus life cycle, *Nature reviews. Microbiology*, 3 (2005) 13-22.
- [21] S. Miller, S. Kastner, J. Krijnse-Locker, S. Buhler, R. Bartenschlager, The non-structural protein 4A of dengue virus is an integral membrane protein inducing membrane alterations in a 2K-regulated manner, *The Journal of biological chemistry*, 282 (2007) 8873-8882.
- [22] S. Welsch, S. Miller, I. Romero-Brey, A. Merz, C.K. Bleck, P. Walther, S.D. Fuller, C. Antony, J. Krijnse-Locker, R. Bartenschlager, Composition and three-dimensional architecture of the dengue virus replication and assembly sites, *Cell Host Microbe*, 5 (2009) 365-375.
- [23] I.M. Yu, W. Zhang, H.A. Holdaway, L. Li, V.A. Kostyuchenko, P.R. Chipman, R.J. Kuhn, M.G. Rossmann, J. Chen, Structure of the immature dengue virus at low pH primes proteolytic maturation, *Science*, 319 (2008) 1834-1837.
- [24] R. Bartenschlager, S. Miller, Molecular aspects of Dengue virus replication, *Future microbiology*, 3 (2008) 155-165.
- [25] Y. Modis, S. Ogata, D. Clements, S.C. Harrison, Structure of the dengue virus envelope protein after membrane fusion, *Nature*, 427 (2004) 313-319.
- [26] T.L. Yap, T. Xu, Y.L. Chen, H. Malet, M.P. Egloff, B. Canard, S.G. Vasudevan, J. Lescar, Crystal structure of the dengue virus RNA-dependent RNA polymerase catalytic domain at 1.85-angstrom resolution, *Journal of virology*, 81 (2007) 4753-4765.
- [27] B.D. Lindenbach, C.M. Rice, Genetic interaction of flavivirus nonstructural proteins NS1 and NS4A as a determinant of replicase function, *Journal of virology*, 73 (1999) 4611-4621.

- [28] A.E. Aleshin, S.A. Shiryayev, A.Y. Strongin, R.C. Liddington, Structural evidence for regulation and specificity of flaviviral proteases and evolution of the Flaviviridae fold, *Protein science : a publication of the Protein Society*, 16 (2007) 795-806.
- [29] C.C. Wang, Z.S. Huang, P.L. Chiang, C.T. Chen, H.N. Wu, Analysis of the nucleoside triphosphatase, RNA triphosphatase, and unwinding activities of the helicase domain of dengue virus NS3 protein, *FEBS letters*, 583 (2009) 691-696.
- [30] B.H. Tan, J. Fu, R.J. Sugrue, E.H. Yap, Y.C. Chan, Y.H. Tan, Recombinant dengue type 1 virus NS5 protein expressed in *Escherichia coli* exhibits RNA-dependent RNA polymerase activity, *Virology*, 216 (1996) 317-325.
- [31] M. Ackermann, R. Padmanabhan, De novo synthesis of RNA by the dengue virus RNA-dependent RNA polymerase exhibits temperature dependence at the initiation but not elongation phase, *The Journal of biological chemistry*, 276 (2001) 39926-39937.
- [32] I.A. Rodenhuis-Zybert, J. Wilschut, J.M. Smit, Dengue virus life cycle: viral and host factors modulating infectivity, *Cellular and molecular life sciences : CMLS*, 67 (2010) 2773-2786.
- [33] J.L. Munoz-Jordan, G.G. Sanchez-Burgos, M. Laurent-Rolle, A. Garcia-Sastre, Inhibition of interferon signaling by dengue virus, *Proceedings of the National Academy of Sciences of the United States of America*, 100 (2003) 14333-14338.
- [34] M. Jones, A. Davidson, L. Hibbert, P. Gruenwald, J. Schlaak, S. Ball, G.R. Foster, M. Jacobs, Dengue Virus Inhibits Alpha Interferon Signaling by Reducing STAT2 Expression, *Journal of virology*, 79 (2005) 5414-5420.
- [35] J.E. McLean, A. Wudzinska, E. Datan, D. Quaglino, Z. Zakeri, Flavivirus NS4A-induced autophagy protects cells against death and enhances virus replication, *The Journal of biological chemistry*, 286 (2011) 22147-22159.
- [36] M.H. Lin, H.J. Hsu, R. Bartenschlager, W.B. Fischer, Membrane undulation induced by NS4A of Dengue virus: a molecular dynamics simulation study, *Journal of biomolecular structure & dynamics*, 32 (2014) 1552-1562.
- [37] R. Anandarao, S. Swaminathan, N. Khanna, The identification of immunodominant linear epitopes of dengue type 2 virus capsid and NS4a proteins using pin-bound peptides, *Virus research*, 112 (2005) 60-68.
- [38] S.A. Shiryayev, A.V. Chernov, A.E. Aleshin, T.N. Shiryayeva, A.Y. Strongin, NS4A regulates the ATPase activity of the NS3 helicase: a novel cofactor role of the non-structural protein NS4A from West Nile virus, *The Journal of general virology*, 90 (2009) 2081-2085.
- [39] A. Salonen, T. Ahola, L. Kaariainen, Viral RNA replication in association with cellular membranes, *Current topics in microbiology and immunology*, 285 (2005) 139-173.
- [40] S. Miller, J. Krijnse-Locker, Modification of intracellular membrane structures for virus replication, *Nature reviews. Microbiology*, 6 (2008) 363-374.

- [41] R. Gosert, D. Egger, V. Lohmann, R. Bartenschlager, H.E. Blum, K. Bienz, D. Moradpour, Identification of the hepatitis C virus RNA replication complex in Huh-7 cells harboring subgenomic replicons, *Journal of virology*, 77 (2003) 5487-5492.
- [42] J. Roosendaal, E.G. Westaway, A. Khromykh, J.M. Mackenzie, Regulated Cleavages at the West Nile Virus NS4A-2K-NS4B Junctions Play a Major Role in Rearranging Cytoplasmic Membranes and Golgi Trafficking of the NS4A Protein, *Journal of virology*, 80 (2006) 4623-4632.
- [43] D.C. Rees, L. DeAntonio, D. Eisenberg, Hydrophobic organization of membrane proteins, *Science*, 245 (1989) 510-513.
- [44] W.S. Davidson, A. Jonas, D.F. Clayton, J.M. George, Stabilization of α -Synuclein Secondary Structure upon Binding to Synthetic Membranes, *Journal of Biological Chemistry*, 273 (1998) 9443-9449.
- [45] A. Echeverri, R. Banerjee, A. Dasgupta, Amino-terminal region of poliovirus 2C protein is sufficient for membrane binding, *Virus research*, 54 (1998) 217-223.
- [46] P. Spuul, A. Salonen, A. Merits, E. Jokitalo, L. Kaariainen, T. Ahola, Role of the amphipathic peptide of Semliki forest virus replicase protein nsP1 in membrane association and virus replication, *Journal of virology*, 81 (2007) 872-883.
- [47] M. Elazar, P. Liu, C.M. Rice, J.S. Glenn, An N-terminal amphipathic helix in hepatitis C virus (HCV) NS4B mediates membrane association, correct localization of replication complex proteins, and HCV RNA replication, *Journal of virology*, 78 (2004) 11393-11400.
- [48] V. Brass, E. Bieck, R. Montserret, B. Wolk, J.A. Hellings, H.E. Blum, F. Penin, D. Moradpour, An amino-terminal amphipathic alpha-helix mediates membrane association of the hepatitis C virus nonstructural protein 5A, *The Journal of biological chemistry*, 277 (2002) 8130-8139.
- [49] J.M. Mackenzie, A.A. Khromykh, M.K. Jones, E.G. Westaway, Subcellular localization and some biochemical properties of the flavivirus Kunjin nonstructural proteins NS2A and NS4A, *Virology*, 245 (1998) 203-215.
- [50] J. Zimmerberg, M.M. Kozlov, How proteins produce cellular membrane curvature, *Nature reviews. Molecular cell biology*, 7 (2006) 9-19.
- [51] J. Gouttenoire, V. Castet, R. Montserret, N. Arora, V. Raussens, J.M. Ruyschaert, E. Diesis, H.E. Blum, F. Penin, D. Moradpour, Identification of a novel determinant for membrane association in hepatitis C virus nonstructural protein 4B, *Journal of virology*, 83 (2009) 6257-6268.
- [52] M. Choi, S. Lee, T. Choi, C. Lee, A hepatitis C virus NS4B inhibitor suppresses viral genome replication by disrupting NS4B's dimerization/multimerization as well as its interaction with NS5A, *Virus genes*, 47 (2013) 395-407.
- [53] N.J. Cho, H. Dvory-Sobol, C. Lee, S.J. Cho, P. Bryson, M. Masek, M. Elazar, C.W. Frank, J.S. Glenn, Identification of a class of HCV inhibitors directed against the nonstructural protein NS4B, *Science translational medicine*, 2 (2010) 15ra16.

- [54] J. Deisenhofer, O. Epp, K. Miki, R. Huber, H. Michel, Structure of the protein subunits in the photosynthetic reaction centre of *Rhodospseudomonas viridis* at 3Å resolution, *Nature*, 318 (1985) 618-624.
- [55] J.A. Alberts Bruce, Lewis Julian, Martin Raff, Keith Roberts, Peter Walter Membrane structure, in: *Molecular Biology of the Cell*, Garland Science, 2008, pp. 583.
- [56] G. van Meer, D.R. Voelker, G.W. Feigenson, Membrane lipids: where they are and how they behave, *Nature reviews. Molecular cell biology*, 9 (2008) 112-124.
- [57] A. Krogh, B. Larsson, G. von Heijne, E.L.L. Sonnhammer, Predicting transmembrane protein topology with a hidden markov model: application to complete genomes, *Journal of Molecular Biology*, 305 (2001) 567-580.
- [58] J.P. Overington, B. Al-Lazikani, A.L. Hopkins, How many drug targets are there?, *Nature reviews. Drug discovery*, 5 (2006) 993-996.
- [59] P.L. Yeagle, *The membranes of cells*, 2nd ed., Academic press, San Diego, 1993.
- [60] V. Kiessling, C. Wan, L.K. Tamm, Domain coupling in asymmetric lipid bilayers, *Biochimica et biophysica acta*, 1788 (2009) 64-71.
- [61] C. Hunte, Specific protein-lipid interactions in membrane proteins, *Biochemical Society transactions*, 33 (2005) 938-942.
- [62] C.L. Young, Z.T. Britton, A.S. Robinson, Recombinant protein expression and purification: A comprehensive review of affinity tags and microbial applications, *Biotechnology Journal*, 7 (2012) 620-634.
- [63] T. Raschle, S. Hiller, M. Etzkorn, G. Wagner, Nonmicellar systems for solution NMR spectroscopy of membrane proteins, *Current opinion in structural biology*, 20 (2010) 471-479.
- [64] D. Nietlispach, A. Gautier, Solution NMR studies of polytopic alpha-helical membrane proteins, *Current opinion in structural biology*, 21 (2011) 497-508.
- [65] C. Kang, Q. Li, Solution NMR study of integral membrane proteins, *Current opinion in chemical biology*, 15 (2011) 560-569.
- [66] C.G. Tate, Practical considerations of membrane protein instability during purification and crystallisation, *Methods in molecular biology*, 601 (2010) 187-203.
- [67] J.-L. Popot, T. Althoff, D. Bagnard, J.-L. Banères, P. Bazzacco, E. Billon-Denis, L.J. Catoire, P. Champeil, D. Charvolin, M.J. Cocco, G. Crémel, T. Dahmane, L.M. de la Maza, C. Ebel, F. Gabel, F. Giusti, Y. Gohon, E. Goormaghtigh, E. Guittet, J.H. Kleinschmidt, W. Kühlbrandt, C. Le Bon, K.L. Martinez, M. Picard, B. Pucci, J.N. Sachs, C. Tribet, C. van Heijenoort, F. Wien, F. Zito, M. Zoonens, Amphipols From A to Z*, *Annual review of biophysics*, 40 (2011) 379-408.
- [68] E. Sezgin, P. Schwille, Model membrane platforms to study protein-membrane interactions, *Mol Membr Biol*, 29 (2012) 144-154.
- [69] H.-H. Shen, T. Lithgow, L. Martin, Reconstitution of Membrane Proteins into Model Membranes: Seeking Better Ways to Retain Protein Activities, *International journal of molecular sciences*, 14 (2013) 1589-1607.

- [70] S.J. Opella, Structure Determination of Membrane Proteins by Nuclear Magnetic Resonance Spectroscopy, *Annual Review of Analytical Chemistry*, 6 (2013) 305-328.
- [71] S. Agah, S. Faham, Crystallization of Membrane Proteins in Bicelles, in: N. Vaidehi, J. Klein-Seetharaman (Eds.) *Membrane Protein Structure and Dynamics*, vol. 914, Humana Press, 2012, pp. 3-16.
- [72] T.H. Bayburt, S.G. Sligar, Membrane protein assembly into Nanodiscs, *FEBS letters*, 584 (2010) 1721-1727.
- [73] F. Hagn, M. Etzkorn, T. Raschle, G. Wagner, Optimized Phospholipid Bilayer Nanodiscs Facilitate High-Resolution Structure Determination of Membrane Proteins, *Journal of the American Chemical Society*, 135 (2013) 1919-1925.
- [74] J.M. Glück, M. Wittlich, S. Feuerstein, S. Hoffmann, D. Willbold, B.W. Koenig, Integral Membrane Proteins in Nanodiscs Can Be Studied by Solution NMR Spectroscopy, *Journal of the American Chemical Society*, 131 (2009) 12060-12061.
- [75] J. Frauenfeld, J. Gumbart, E.O. Sluis, S. Funes, M. Gartmann, B. Beatrix, T. Mielke, O. Berninghausen, T. Becker, K. Schulten, R. Beckmann, Cryo-EM structure of the ribosome-SecYE complex in the membrane environment, *Nature structural & molecular biology*, 18 (2011) 614-621.
- [76] S. Inagaki, R. Ghirlando, R. Grishammer, Biophysical characterization of membrane proteins in nanodiscs, *Methods*, 59 (2013) 287-300.
- [77] D.S. Wishart, B.D. Sykes, F.M. Richards, Relationship between nuclear magnetic resonance chemical shift and protein secondary structure, *Journal of Molecular Biology*, 222 (1991) 311-333.
- [78] A.W. Overhauser, Polarization of Nuclei in Metals, *Physical Review*, 92 (1953) 411-415.
- [79] J.L. Battiste, G. Wagner, Utilization of site-directed spin labeling and high-resolution heteronuclear nuclear magnetic resonance for global fold determination of large proteins with limited nuclear overhauser effect data, *Biochemistry*, 39 (2000) 5355-5365.
- [80] G. Cornilescu, F. Delaglio, A. Bax, Protein backbone angle restraints from searching a database for chemical shift and sequence homology, *Journal of biomolecular NMR*, 13 (1999) 289-302.
- [81] A. Bax, Weak alignment offers new NMR opportunities to study protein structure and dynamics, *Protein Science*, 12 (2003) 1-16.
- [82] R.E. Bruccoleri, M. Karplus, Prediction of the folding of short polypeptide segments by uniform conformational sampling, *Biopolymers*, 26 (1987) 137-168.
- [83] D. Bassolino-Klimas, R. Tejero, S.R. Krystek, W.J. Metzler, G.T. Montelione, R.E. Bruccoleri, Simulated annealing with restrained molecular dynamics using a flexible restraint potential: Theory and evaluation with simulated NMR constraints, *Protein Science*, 5 (1996) 593-603.
- [84] D.S. Wishart, B.D. Sykes, Chemical shifts as a tool for structure determination, *Methods in enzymology*, 239 (1994) 363-392.

- [85] S. Schwarzing, G.J. Kroon, T.R. Foss, P.E. Wright, H.J. Dyson, Random coil chemical shifts in acidic 8 M urea: implementation of random coil shift data in NMRView, *Journal of biomolecular NMR*, 18 (2000) 43-48.
- [86] S. Schwarzing, G.J. Kroon, T.R. Foss, J. Chung, P.E. Wright, H.J. Dyson, Sequence-dependent correction of random coil NMR chemical shifts, *Journal of the American Chemical Society*, 123 (2001) 2970-2978.
- [87] D.S. Wishart, B.D. Sykes, F.M. Richards, The chemical shift index: a fast and simple method for the assignment of protein secondary structure through NMR spectroscopy, *Biochemistry*, 31 (1992) 1647-1651.
- [88] D. Wishart, B. Sykes, The ¹³C Chemical-Shift Index: A simple method for the identification of protein secondary structure using ¹³C chemical-shift data, *Journal of biomolecular NMR*, 4 (1994) 171-180.
- [89] Y. Shen, F. Delaglio, G. Cornilescu, A. Bax, TALOS+: a hybrid method for predicting protein backbone torsion angles from NMR chemical shifts, *Journal of biomolecular NMR*, 44 (2009) 213-223.
- [90] Y. Shen, A. Bax, Protein backbone and sidechain torsion angles predicted from NMR chemical shifts using artificial neural networks, *Journal of biomolecular NMR*, 56 (2013) 227-241.
- [91] C. Tian, M.D. Karra, C.D. Ellis, J. Jacob, K. Oxenoid, F. Sönnichsen, C.R. Sanders, Membrane Protein Preparation for TROSY NMR Screening, in: L.J. Thomas (Ed.) *Methods in enzymology*, vol. Volume 394, Academic Press, 2005, pp. 321-334.
- [92] R. Verardi, N.J. Traaseth, L.R. Masterson, V.V. Vostrikov, G. Veglia, Isotope labeling for solution and solid-state NMR spectroscopy of membrane proteins, *Advances in experimental medicine and biology*, 992 (2012) 35-62.
- [93] W.D. Van Horn, H.J. Kim, C.D. Ellis, A. Hadziselimovic, E.S. Sulistijo, M.D. Karra, C. Tian, F.D. Sönnichsen, C.R. Sanders, Solution nuclear magnetic resonance structure of membrane-integral diacylglycerol kinase, *Science*, 324 (2009) 1726-1729.
- [94] S. Hiller, R.G. Garces, T.J. Malia, V.Y. Orekhov, M. Colombini, G. Wagner, Solution structure of the integral human membrane protein VDAC-1 in detergent micelles, *Science*, 321 (2008) 1206-1210.
- [95] M.P. Bokoch, Y. Zou, S.G. Rasmussen, C.W. Liu, R. Nygaard, D.M. Rosenbaum, J.J. Fung, H.J. Choi, F.S. Thian, T.S. Kobilka, J.D. Puglisi, W.I. Weis, L. Pardo, R.S. Prosser, L. Mueller, B.K. Kobilka, Ligand-specific regulation of the extracellular surface of a G-protein-coupled receptor, *Nature*, 463 (2010) 108-112.
- [96] F. Penin, V. Brass, N. Appel, S. Ramboarina, R. Montserret, D. Ficheux, H.E. Blum, R. Bartenschlager, D. Moradpour, Structure and Function of the Membrane Anchor Domain of Hepatitis C Virus Nonstructural Protein 5A, *Journal of Biological Chemistry*, 279 (2004) 40835-40843.

- [97] N. Sapay, R. Montserret, C. Chipot, V. Brass, D. Moradpour, G. Deléage, F. Penin, NMR Structure and Molecular Dynamics of the In-Plane Membrane Anchor of Nonstructural Protein 5A from Bovine Viral Diarrhea Virus†,‡, *Biochemistry*, 45 (2006) 2221-2233.
- [98] C. Hilty, G. Wider, C. Fernandez, K. Wuthrich, Membrane protein-lipid interactions in mixed micelles studied by NMR spectroscopy with the use of paramagnetic reagents, *Chembiochem : a European journal of chemical biology*, 5 (2004) 467-473.
- [99] A.P. Subasinghage, D. O'Flynn, J.M. Conlon, C.M. Hewage, Conformational and membrane interaction studies of the antimicrobial peptide alyteserin-1c and its analogue [E4K]alyteserin-1c, *Biochimica et Biophysica Acta (BBA) - Biomembranes*, 1808 (2011) 1975-1984.
- [100] B. AB, *Biacore Sensor Surface Handbook*, BR-1005-71 Edition AB ed., 2005.
- [101] M.A. Cooper, A. Hansson, S. Löfås, D.H. Williams, A Vesicle Capture Sensor Chip for Kinetic Analysis of Interactions with Membrane-Bound Receptors, *Analytical Biochemistry*, 277 (2000) 196-205.
- [102] C.L. Baird, E.S. Courtenay, D.G. Myszka, Surface plasmon resonance characterization of drug/liposome interactions, *Anal Biochem*, 310 (2002) 93-99.
- [103] G. Anderluh, M. Besenicar, A. Kladnik, J.H. Lakey, P. Macek, Properties of nonfused liposomes immobilized on an L1 Biacore chip and their permeabilization by a eukaryotic pore-forming toxin, *Anal Biochem*, 344 (2005) 43-52.
- [104] M. Beseničar, P. Maček, J.H. Lakey, G. Anderluh, Surface plasmon resonance in protein–membrane interactions, *Chemistry and Physics of Lipids*, 141 (2006) 169-178.
- [105] G. Anderluh, P. Macek, J.H. Lakey, Peeking into a secret world of pore-forming toxins: membrane binding processes studied by surface plasmon resonance, *Toxicon : official journal of the International Society on Toxinology*, 42 (2003) 225-228.
- [106] H. Mozsolits, W.G. Thomas, M.I. Aguilar, Surface plasmon resonance spectroscopy in the study of membrane-mediated cell signalling, *Journal of peptide science : an official publication of the European Peptide Society*, 9 (2003) 77-89.
- [107] S.M. Kelly, T.J. Jess, N.C. Price, How to study proteins by circular dichroism, *Biochimica et Biophysica Acta (BBA) - Proteins and Proteomics*, 1751 (2005) 119-139.
- [108] A.S. Maltsev, J. Ying, A. Bax, Impact of N-Terminal Acetylation of α -Synuclein on Its Random Coil and Lipid Binding Properties, *Biochemistry*, 51 (2012) 5004-5013.
- [109] A.L. Lai, A.E. Moorthy, Y. Li, L.K. Tamm, Fusion Activity of HIV gp41 Fusion Domain Is Related to Its Secondary Structure and Depth of Membrane Insertion in a Cholesterol-Dependent Fashion, *Journal of Molecular Biology*, 418 (2012) 3-15.
- [110] T. Kohno, H. Kusunoki, K. Sato, K. Wakamatsu, A new general method for the biosynthesis of stable isotope-enriched peptides using a decahistidine-tagged ubiquitin fusion system: an application to the production of mastoparan-X uniformly enriched with ^{15}N and $^{15}\text{N}/^{13}\text{C}$, *Journal of biomolecular NMR*, 12 (1998) 109-121.

- [111] R. Gautier, D. Douguet, B. Antonny, G. Drin, HELIQUEST: a web server to screen sequences with specific α -helical properties, *Bioinformatics*, 24 (2008) 2101-2102.
- [112] W.F. Vranken, W. Boucher, T.J. Stevens, R.H. Fogh, A. Pajon, M. Llinas, E.L. Ulrich, J.L. Markley, J. Ionides, E.D. Laue, The CCPN data model for NMR spectroscopy: development of a software pipeline, *Proteins*, 59 (2005) 687-696.
- [113] F. Delaglio, S. Grzesiek, G.W. Vuister, G. Zhu, J. Pfeifer, A. Bax, NMRPipe: a multidimensional spectral processing system based on UNIX pipes, *Journal of biomolecular NMR*, 6 (1995) 277-293.
- [114] J. Sambrook, Fritsch, E.F. & Maniatis, T., *Molecular Cloning: a laboratory manual*, 2nd ed ed., New York, 1989.
- [115] U.K. Laemmli, Cleavage of structural proteins during the assembly of the head of bacteriophage T4, *Nature*, 227 (1970) 680-685.
- [116] H. Nemesio, F. Palomares-Jerez, J. Villalain, NS4A and NS4B proteins from dengue virus: membranotropic regions, *Biochimica et biophysica acta*, 1818 (2012) 2818-2830.
- [117] G. Bodenhausen, D.J. Ruben, Natural abundance nitrogen-15 NMR by enhanced heteronuclear spectroscopy, *Chemical Physics Letters*, 69 (1980) 185-189.
- [118] S. Grzesiek, A. Bax, Amino acid type determination in the sequential assignment procedure of uniformly $^{13}\text{C}/^{15}\text{N}$ -enriched proteins, *Journal of biomolecular NMR*, 3 (1993) 185-204.
- [119] A. Favier, B. Brutscher, Recovering lost magnetization: polarization enhancement in biomolecular NMR, *Journal of biomolecular NMR*, 49 (2011) 9-15.
- [120] L. Kay, P. Keifer, T. Saarinen, Pure absorption gradient enhanced heteronuclear single quantum correlation spectroscopy with improved sensitivity, *Journal of the American Chemical Society*, 114 (1992) 10663-10665.
- [121] M. Wittekind, L. Mueller, HNCACB, a High-Sensitivity 3D NMR Experiment to Correlate Amide-Proton and Nitrogen Resonances with the Alpha- and Beta-Carbon Resonances in Proteins, *Journal of Magnetic Resonance, Series B*, 101 (1993) 201-205.
- [122] M. Ikura, L.E. Kay, A. Bax, A novel approach for sequential assignment of ^1H , ^{13}C , and ^{15}N spectra of proteins: heteronuclear triple-resonance three-dimensional NMR spectroscopy. Application to calmodulin, *Biochemistry*, 29 (1990) 4659-4667.
- [123] G.W. Vuister, A. Bax, Quantitative J correlation: a new approach for measuring homonuclear three-bond J(HNH.alpha.) coupling constants in ^{15}N -enriched proteins, *Journal of the American Chemical Society*, 115 (1993) 7772-7777.
- [124] A.J. Shaka, J. Keeler, Broadband spin decoupling in isotropic-liquids, *Progress in Nuclear Magnetic Resonance Spectroscopy*, 19 (1987) 47-129.
- [125] D.S. Wishart, C.G. Bigam, J. Yao, F. Abildgaard, H.J. Dyson, E. Oldfield, J.L. Markley, B.D. Sykes, ^1H , ^{13}C and ^{15}N chemical shift referencing in biomolecular NMR, *Journal of biomolecular NMR*, 6 (1995) 135-140.

- [126] N.A. Farrow, R. Muhandiram, A.U. Singer, S.M. Pascal, C.M. Kay, G. Gish, S.E. Shoelson, T. Pawson, J.D. Forman-Kay, L.E. Kay, Backbone dynamics of a free and phosphopeptide-complexed Src homology 2 domain studied by ¹⁵N NMR relaxation, *Biochemistry*, 33 (1994) 5984-6003.
- [127] G. Lipari, A. Szabo, Model-free approach to the interpretation of nuclear magnetic resonance relaxation in macromolecules. 1. Theory and range of validity, *Journal of the American Chemical Society*, 104 (1982) 4546-4559.
- [128] L. Salmon, J.L. Ortega Roldan, E. Lescop, A. Licinio, N. van Nuland, M.R. Jensen, M. Blackledge, Structure, dynamics, and kinetics of weak protein-protein complexes from NMR spin relaxation measurements of titrated solutions, *Angewandte Chemie*, 50 (2011) 3755-3759.
- [129] M.V. Berjanskii, D.S. Wishart, A simple method to predict protein flexibility using secondary chemical shifts, *Journal of the American Chemical Society*, 127 (2005) 14970-14971.
- [130] M.V. Berjanskii, D.S. Wishart, Application of the random coil index to studying protein flexibility, *Journal of biomolecular NMR*, 40 (2008) 31-48.
- [131] L.E. Kay, D.A. Torchia, A. Bax, Backbone Dynamics of Proteins as Studied by N-15 Inverse Detected Heteronuclear Nmr-Spectroscopy - Application to Staphylococcal Nuclease, *Biochemistry*, 28 (1989) 8972-8979.

Acknowledgments

My most sincere gratitude to Prof. Dr. Dieter Willbold for providing such an excellent research environment and inspiring me with many ideas.

I am grateful for the guidance and support from PD Dr. Bernd König and Dr. Silke Hoffmann. Both have been patient teachers over the last few years, and without their support and advice some of the project goals would never have been achieved.

I am indebted to Prof. Ella H. Sklan, who provided the initial concepts of the project and shared her virology results with me. I would also like to thank Prof. Carsten Münk for giving me some valuable suggestion towards my research project.

I am grateful to Dr. Melanie Schwarten, Dr. Sven Schünke and Dr. Pallavi Thiagarajan-Rosenkranz for their help with recording NMR experiments, and Dr. Justin Lecher, Dr. Rudolf Hartmann, Christina Bösing and Dr. Luis Möckel for help with NMR data analysis. I like to thank Olga Valdau for her contribution with previous research. I would like to thank Dr. Julian Glück for help with the SPR measurements and Dr. Simone König for mass spectrometric analysis. I thank Axel Baumann from ICS-5 for the introduction to liposome preparation and acquisition of DLS experiments. I am grateful for the many exciting discussions with Dr. Pexing Ma, Dr. Sameer Singh, Dr. Karen Hänel and Dr. Jeannine Mohrlüder.

I would also like to thank the Molecules of Infection Graduate School programme for financial support and the stimulating lectures. Financial support from the Jürgen Manchot Foundation and administrative support from Dr. Inge Krümpelbeck are gratefully acknowledged. I am grateful for the wonderful experience with Dr. Katerina Krikoni and Dr. Sabrina Thomas during the lab rotation.

I like to thank Esther Jonas, Nicole Esser, Anne Cousin, Nicole Müller, Judith Fabig and Markus Tusche for the great support in the wet laboratory. I am indebted to the fantastic support and help from Dr. Lei Wang, Dr. Yeliz Cinar, Dr. Ellen Kammula, Dr. Hoa Do Quynh, Dr. Silke Dornieden, Dr. Amine Aladag, Dr. Marina Pavlidou, Susanne Mödder, Carsten Krichel, Alexandra Boeske, Claudia Börger, Kun Wang, Na Jiang and many others in the institute.

Finally, and most importantly, I would like to thank my wife, Yuan-Chi Chu. It is through her understanding and constant support with our son, Leon Hung that I have been able to focus fully on my research project. I thank my parents and my whole family in Taiwan for their encouragement and support. I am a lucky man, and I feel so blessed and content in your love that I find the courage to carry on.

Die hier vorgelegte Dissertation habe ich eigenständig und ohne unerlaubte Hilfe angefertigt.
Die Dissertation wurde in der vorgelegten oder in ähnlicher Form noch bei keiner anderen
Institution eingereicht. Ich habe bisher keine erfolglosen Promotionsversuche unternommen.



Yu-Fu Hung

Jülich, den 17.09.2013